Title
Insane in the Membrane: Modification of Polymeric Membranes for High Performance Water Separations

Author
McVerry, Brian

Publication Date
2016

Peer reviewed|Thesis/dissertation

UNIVERSITY OF CALIFORNIA

Los Angeles

Insane in the Membrane:

Modification of Polymeric Membranes for High Performance Water Separations

A dissertation submitted in satisfaction

of the requirements for the degree Doctor of Philosophy

in Chemistry

by

Brian McVerry

2016

ABSTRACT OF THE DISSERTATION

Insane in the Membrane:

Modification of Polymeric Membranes for High Performance Water Separations

by

Brian McVerry

Doctor of Philosophy in Chemistry

University of California, Los Angeles, 2016

Professor Richard B. Kaner, Chair

It is not unknown that the worldwide freshwater supply is dwindling and current freshwater sources are being contaminated. The total amount of freshwater, which makes up 2.5-3% of the total water on earth, is actually sufficient to sustain the growing population for many years. However, the disproportionate geographical distribution of freshwater raises issues, as many people occupy arid regions. The transport or piping of large volumes of water over long distances is typically prohibitively expensive and/or prevented by geopolitical interests. The drive to produce freshwater locally from non-traditional sources has advanced in recent years and current energy and production costs have fallen due to technological advances.

Filtration through polymeric materials has emerged as the leading technology for freshwater production from seawater, brackish water, and wastewater. Polymer membranes have surpassed ceramic membranes as the leading filtration medium because of their low-cost and

versatility. Large sheets of membranes can be cast using an in-line manufacturing process and pore sizes can be readily tuned for specific applications. However, membrane fouling severely limits the advantages and economics of polymeric membrane-based separations. This dissertation will examine methods to produce fouling-resistant membranes that maintain the low-cost and scalability of polymer membranes for ultrafiltration and reverse osmosis.

The first chapter presents a brief history and introduction to membrane technology and its current status. This chapter outlines membrane casting methods, the polymers used in casting films and their advantages, different configurations for membrane modules, the effects of fouling, and the cost of fouling.

The second chapter introduces a new hydrophilic, polyaniline-based additive that was synthesized to blend into polysulfone unltrafiltration membranes. Sulfonated polyaniline (SPANi) is a self-doped polyaniline derivative that is readily synthesized using fuming sulfuric acid. SPANi, when de-doped, is soluble in polar organic solvents and insoluble in water, making it an excellent candidate for blending into ultrafiltration membranes. When redoped at pH 7, the presence of pendant sulfonic acid groups creates a zwitterionic species. Zwitterionic moeities are known to possess super-hydrophilic and ultra-low fouling properties. When blended into polysulfone (PSf) ultrafiltration membranes at low concentrations, the SPANi-PSf membranes demonstrate greater hydrophilicity and anti-fouling properties when compared to pure PSf membranes with nominal changes in performance.

For reverse osmosis (RO) membranes, the active or “skin” layer that performs the separation is a dense, non-porous polymer. Thus, blending hydrophilic molecules into the active layer or modifying the chemistry of the active layer affects the separation properties of the resulting polymer blend. To address this issue, researchers have grafted hydrophilic polymers to

the surface of membranes to impart anti-fouling properties without significant changes in their performance. In Chapter 3, a new method is presented using photoactive hydrophilic polymer precursors to modify membrane surfaces. With this new method, commercial RO membranes can be modified rapidly under ambient conditions, maintaining the roll-to-roll scalability of RO membrane processing. The grafted commercial RO membranes exhibit enhanced hydrophilicity and anti-fouling properties when compared with unmodified RO membranes.

Chapter 4 investigates applying the same method of imparting anti-fouling properties to polymeric membranes as discussed in Chapter 3, except here this method is applied to ultrafiltration (UF) membranes used for membrane bioreactors. Membrane bioreactor technology has gained attention recently for its highly efficient ability to clean wastewater. However, the concentrated loading of organics and microorganisms into the reactor medium leads to high fouling rates. First, modeling data are presented that identifies specific acid-base interactions between different foulants and the membrane surface that accelerate membrane fouling. New photoactive small molecule precursors were then synthesized and covalently bound to the membrane surface to repel these interactions. The small molecule with the greatest repulsive interaction, a zwitterionic derivative, imparted the greatest anti-fouling properties to the commercial UF membranes. The modified membranes exhibited low fouling rates in both a short-term and a long-term study.

Chapter 5 summarizes the dissertation and outlines the key takeaways.

This dissertation of Brian McVerry is approved.

William M. Gelbart

Eric M.V. Hoek

Richard B. Kaner, Committee Chair

University of California, Los Angeles

2016

TABLE OF CONTENTS

LIST OF FIGURES

LIST OF TABLES AND SCHEMES

Tables

Schemes

ACKNOWLEDGMENTS

I would first like to thank my advisor, Prof. Richard Kaner, for his encouragement and guidance. Ric has an exceptional ability to measure the amount of guidance each student in his lab needs, identifies the potential in his students, and truly cares about his students on a personal level. When initially being rejected to the Material Science department at UCLA in spring of 2011, I was on campus at UCLA for the NSF-IGERT fellowship open house and met with Ric. After our meeting, Ric brought me to the UCLA Chemistry department and had the administration accept my application, changing my life forever. Ric, if you are reading this, never forget the huge role you have played in my growth, confidence, and success for which I will be forever grateful.

I would also like to thank the other faculty members, in my committee and outside of my committee, who have been involved in the course of my Ph.D. Special thanks to Dr. Eric Hoek who has helped immerse me in the world of water purification and separations and for his great resources and laboratory space at UCLA.

My current and former colleagues have been there for me every step of the way. I am particularly grateful to Dr. Dukwoo Jun, Chain Lee, Robert Jordan, Kris Marsh, William Huang, Dr. Ben Feinberg and Dr. Mavis Wong for helpful discussions and help with experiments. Many ideas have been bounced back and forth between us and our motivations are very much aligned. They all share the same passion to research new ideas and make an impact in their field and I will always have fond memories of the laughs and fun times during late nights in the laboratory.

Most of all, I'd like to thank my family for their love and support. I have been raised by two of the greatest parents, Robert and Marlene, who have spent the last 27 years constructing my moral foundation, fostering a strong sense of intellectual curiosity and independence in me.

My brother Michael, has given me constant encouragement and advice, and shares the same passion to make an impact that I do. And lastly, I'd like to thank my roommates, friends, and Santa Barbara family close and far. You know who you are. You guys have kept me young, sane, and always remind me that life is too short to be taken seriously, and for that, I will be forever grateful.

My financial support was provided by two scholarships from the National Science Foundation. During my first two years of graduate school, I was supported by the NSF Clean Energy for Green Industry (CGI) IGERT fellowship. Near the end of the 2-year IGERT scholarship, I was awarded the 3-year NSF GFRP fellowship that supported my research efforts for my remaining graduate career.

Within this document is content from currently published material and one recent article that is currently under review. I am the primary author on all of the publications. **Chapter 1** will present a general introduction to membrane separations, membrane fouling, and costs associated with fouling. **Chapters 2 and 3** are based on published, peer-review articles in high impact journals as follows, respectively: Brian T. McVerry, James A. T. Temple, Xinwei Huang, Kristofer L. Marsh, Eric M. V. Hoek and Richard B. Kaner, "Fabrication of Low-Fouling Ultrafiltration Membranes Using a Hydrophilic, Self-Doping Polyaniline Additive," *Chemistry of Materials*, **2013**, 25(18), pp 3597–3602 and Brian T. McVerry, Mavis C. Y. Wong, Kristofer L. Marsh, James A. T. Temple, Catalina Marambio-Jones, Eric M. V. Hoek, and Richard B. Kaner, "Scalable Antifouling Reverse Osmosis Membranes Utilizing Perfluorophenyl Azide Photochemistry," *Macromolecular Rapid Communications*, **2014**, 35, 1528−1533.

Chapter 4 is based on a manuscript that is currently under peer review. The document is titled: "Novel, Small Molecule Perfluorophenyl Azide Coatings for Fouling-resistant Membrane Bioreactors," with an author list as follows: Brian T. McVerry, Dukwoo Jun, Robert Jordan, Xinwei Huang, Kristofer L. Marsh, Ethan Rao, Yves Rubin, Eric M.V. Hoek, and Richard B. Kaner. The manuscript has been submitted to *Advanced Functional Materials*.

VITA

Education and Fellowships

2007-2011	B.S. Biochemistry and Molecular Biology University of California, Santa Barbara, USA
2010	Cooperative International Science and Engineering Internships Technische Universiteit Eindhoven, Netherlands
2010-2011	Research Internships in Science and Engineering University of California, Santa Barbara, USA
2012-2013	NSF Clean Energy for Green Industry, IGERT University of California, Los Angeles, USA
2013-2016	NSF Graduate Research Fellowship University of California, Los Angeles, USA

Publications

Brian T. McVerry, James A. T. Temple, Xinwei Huang, Kristofer L. Marsh, Eric M. V. Hoek and Richard B. Kaner, "Fabrication of Low-Fouling Ultrafiltration Membranes Using a Hydrophilic, Self-Doping Polyaniline Additive," *Chemistry of Materials,* 2013, 25(18), pp 3597–3602

Brian T. McVerry, Mavis C. Y. Wong, Kristofer L. Marsh, James A. T. Temple, Catalina Marambio-Jones, Eric M. V. Hoek, and Richard B. Kaner, "Scalable Antifouling Reverse Osmosis Membranes Utilizing Perfluorophenyl Azide Photochemistry," *Macromolecular Rapid Communications*, 2014, 35, 1528−1533

Brian T. McVerry, Dukwoo Jun, Robert Jordan, Xinwei Huang, Kristofer L. Marsh, Ethan Rao, Yves Rubin, Eric M.V. Hoek, and Richard B. Kaner. "Novel, Small Molecule Perfluorophenyl Azide Coatings for Fouling-resistant Membrane Bioreactors," *Advanced Functional Materials*, in review.

Lisa J Wang, Maher F El‐Kady, Sergey Dubin, Jee Youn Hwang, Yuanlong Shao, Kristofer Marsh, **Brian T. McVerry**, Matthew D Kowal, Mir F Mousavi, Richard B Kaner, "Flash Converted Graphene for Ultra‐High Power Supercapacitors," *Advanced Energy Materials*, 2015, 5, 1500786

Xinwei Huang, **Brian T. McVerry**, Catalina Marambio-Jones, Mavis CY Wong, Eric MV Hoek, Richard B Kaner, "Novel chlorine resistant low-fouling ultrafiltration membrane based on a hydrophilic polyaniline derivative," *Journal of Materials Chemistry A*, 2015, 3(16), 8725-8733

Gregory R. Guillen, **Brian T. McVerry**, Benjamin J. Feinberg, Mavis C.Y. Wong, Thomas P. Farrell, Qiang Wei, Benjamin R. Mattes, Richard B. Kaner, Eric M.V. Hoek, "Tuning the Properties of Polyaniline-based Ultrafiltration Membranes with Chemical Post-treatments," *in preparation.*

Chapter 1

Introduction

1.1 Polymeric Membrane Technology: Background and Current Status

The ability for a material to separate two or more things was necessary for life to begin, as the earliest organisms required lipid barriers to protect their genetic material from the primordial world. As evolution produced more complex beings, the lipid barriers evolved as well into a phospholipid bilayer. This bilayer separates the cell(s) of almost all living things (and many viruses) from the environment. Just as important, the dynamic membrane actively plays a role in signaling, diffusion, and endocytosis/exocytosis and possesses many pumps and channels embedded into the bilayer for further functionality.[1] On the macroscale, human skin acts as a membrane barrier that protects internal organs and responds to changes in body temperature and injury. For a materials scientist, producing a membrane material that even closely resembles the membranes that nature has provided, for their functionality and complexity, would be a dream.[2]

Although mimicking Mother Nature's work is likely impossible today, humans have been using materials to achieve separations for thousands of years. Depth filters made from sediment have been made dating back to 2000 BC in early India to purify water.[3] Polymer cellulosic fiber filters are still used today in laboratories to collect organic precipitate. Synthetic membrane films were not developed until 1865, when Adolf Fick produced nitrocellulose films to examine diffusion of gases.[4] In 1907, the first recorded filtration through a polymer film membrane occurred when Bechold impregnated filter paper with acetic acid collodion (named Bechold ultrafilters) and applied pressure, introducing the concept of ultrafiltration.[5] In the mid to late 20th century, researchers and engineers began producing polymer thin-film membranes out of new, synthetic polymers with enhanced mechanical, thermal, and chemical stability. New casting techniques were developed to fabricate asymmetric films with thin active layers or "skin" layers that produce membranes with much higher performance capabilities than the first generation,

dense polymer films. Additional form factors and fabrication methods have been engineered, such as spiral wound and hollow fiber modules, to maximize surface area and reduce manufacturing costs. Membranes are now used for dialysis, desalination, wastewater recycling, oil/gas separations and are implemented in the food, beverage, and pharmaceutical industries. By 2018, the global demand for membranes is estimated to reach $25 billion.[6]

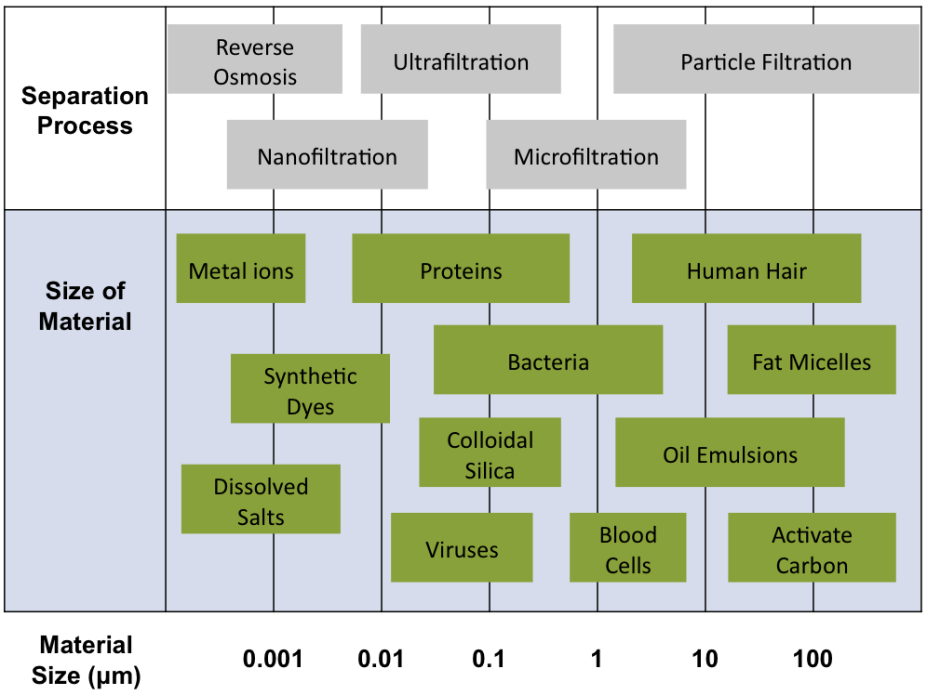

Figure 1.1. Filtration process classifications based on rejection of material and particle size.

Current, state-of-the-art membranes are specifically tailored for a wide variety of applications. Thus, pressure-driven separations are typically categorized by membrane pore size and rejection capabilities. Microfiltration (MF) is used to clarify solutions from suspended particles, with membrane pore sizes in the range of 0.1 – 5 micrometers. Ultrafiltration (UF) membranes have smaller pores than microfiltration, with pore sizes typically between 5 – 100 nanometers and are utilized to remove bacteria, viruses, and macromolecules from aqueous

solutions. Reverse osmosis (RO) membranes are capable of removing salts from solutions at high pressure. RO membranes are considered to be non-porous, although water (at high pressure) passes through the interstitial spaces in a dense polymer film. This dissertation will focus solely on UF and RO membranes.

1.2. How Membranes Are Made: Membrane Casting

Of the several methods that have been developed, non-solvent induced phase inversion is the most common casting technique used to fabricate UF membranes. Guillen *et al.*[7] provides an up-to-date comprehensive review on the phase inversion process and the different types of UF membranes formed with phase inversion. Briefly, a viscous polymer solution is created by dissolving a polymer in a water-miscible solvent. The solution is then cast onto a solid substrate or fabric using a casting blade and placed into a non-solvent bath, typically water. As the solvent and water exchange, the polymer precipitates into a porous architecture that is capable of filtration. By varying the polymer, solvent, non-solvent, temperature, humidity, and additives, the pore size and mechanical properties can be modified. Large areas of membranes are cast on an in-line manufacturing process and solutions can be wet-spun into narrow fibers utilizing the same technique to maximize surface area.

RO membranes are fabricated from a UF membrane "support" that can withstand the high pressures of operation. A flat sheet UF membrane is dipped into two sequential solutions of a multifunctional acyl chloride and a diamine to form a dense polyamide layer on the surface of the UF support. If two immiscible solvents are used, an interfacial polymerization proceeds that creates a very thin layer (~150 nm), enabling high permeability. The thin-film composite (TFC) membranes, capable of desalting seawater to produce drinkable water in a single pass, were first

invented in 1981.[8] Since then, nearly all membrane-based desalination is performed using TFC membranes.

1.3. Polymers Used for Membranes

Non-solvent induced phase inversion enables a number of polymers to be cast into UF membranes with narrow pore size distributions. The polymers are generally highly soluble in water-miscible solvents such as dimethylformamide, dimethylacetamide, *N*-methylpyrollidone, acetone, and/or tetrahydrofuran and insoluble in water. These polymers are listed in an exhaustive review by Ulbricht,[9] and typically possess strong chemical and thermal stability and are mechanically robust. However, the scale at which membranes are manufactured causes polymers to be selected for their cost over their physical properties. Thus, the most popular polymers used for UF tend to be commodity polymers that have sufficient physical properties for UF, such as polysulfone (PSf), polyethersulfone (PES), polyvinylidenefluoride (PVDF), and polyacrylonitrile (PAN).

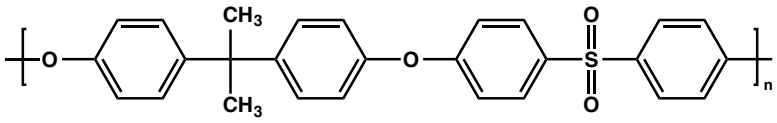

Polysulfone

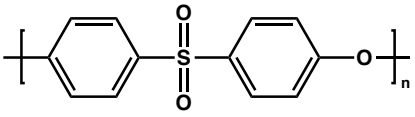

Polyethersulfone

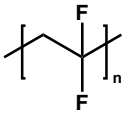

Polyvinylidene Fluoride

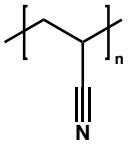

Polyacrylonitrile

Figure 1.2. Repeating units of the chemical structure of the most common polymers used in ultrafiltration.

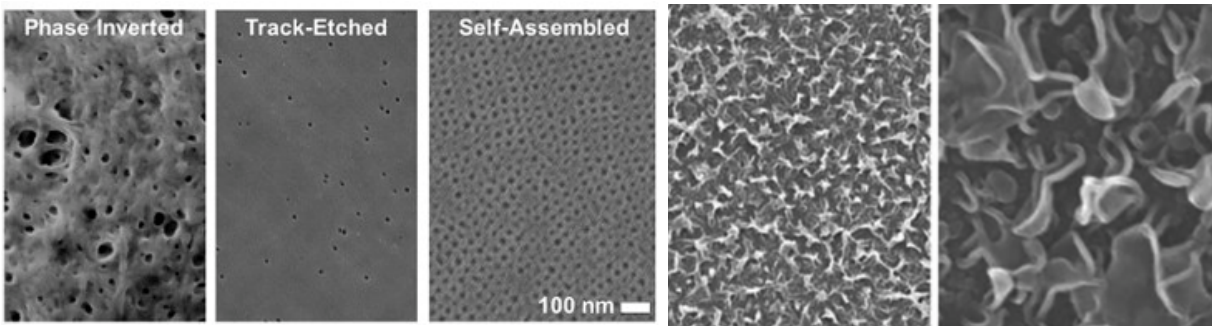

Figure 1.3. Scanning electron microscopy surface images of ultrafiltration and reverse osmosis membranes. The left three images are surface images of ultrafiltration membranes produced by different processes with visible pores.[10] The right two images show the dense, rough polyamide polymer formed on the surface produced as a result of interfacial polymerization.[11]

For materials used as the RO membrane active or selective layer, the choice of polymer is quite limited in comparison to UF membranes. For UF membranes, microscopic pores (observed under scanning electron microscopy, Figure 1.3) are formed during the phase inversion process

that separates material in the feed based on size-exclusion. This is referred to as the pore-flow model. For polymers that are used for reverse osmosis membranes, a thin-dense polymer film is used as the selective layer. The polymer must swell in saline solutions[12,13] and enable water and salts to dissolve into the polymer matrix, a phenomena known as solution-diffusion.[14-17] Polymers that possess high water diffusivity and low salt diffusivity[18] are excellent candidates for RO membrane selective layers, and although many have been screened,[19] only a few classes of polymers provide water permeability and salt rejection properties sufficient for real-world applications.[20,21] In addition, the polymers must be readily polymerized under conditions that do not destroy the underlying UF support membrane. Thus, the aforementioned interfacial polymerization of polyamide active layers has been dominant in producing state-of-the-art RO membranes.[22]

1.4 Membrane Form Factors

Because membranes are solution processed, they can be cast and formed into several configurations, also known as form factors. The different configurations offer distinct benefits and, like the polymeric material used, are selected for specific applications. For example, wet-spun, unsupported hollow fiber UF membranes are often used in membrane bioreactors for their high surface area and low-pressure operation. Standard modules and cartridges can fit into existing low-pressure cross-flow systems or self-standing modules that can then be submerged directly into feed solutions.

Seawater RO membranes are typically operated above 600 psi, pressures too high for hollow fibers, therefore, flat sheets that are fabric-supported are used for desalination purposes. The flat sheets are fit into a spiral wound configuration that compiles multiple flat sheets, feed

spacers, and permeate collection sheets into a cylindrical package that can be fit into standard pressurized systems (Figure 1.4).

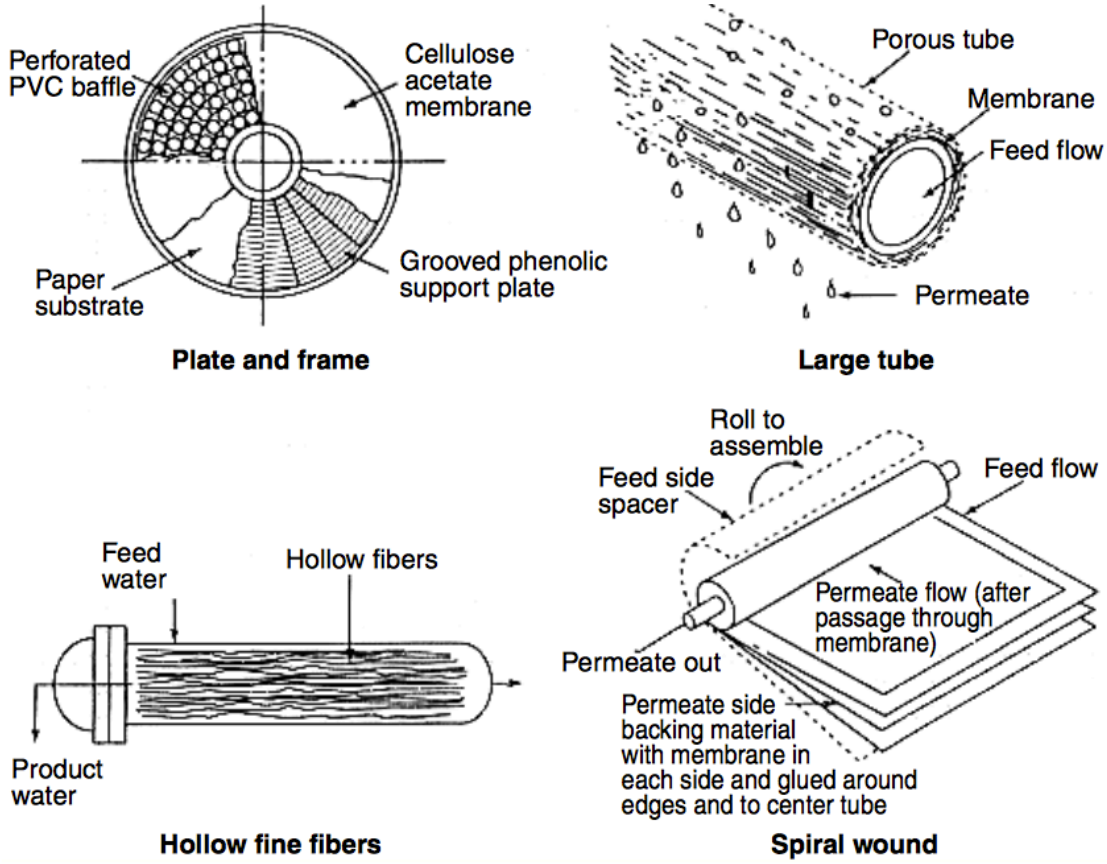

Figure 1.4. The different configurations of UF and RO membranes.[23]

1.5 Membrane Fouling and Cleaning

Often referred to as the "Achilles heel" of polymeric membrane separations, membrane fouling leads to losses in performance. Broadly, membrane fouling occurs when rejected particles and/or dissolved solids adhere to the surface of the microporous material. Several foulants exist, such as inorganic minerals and colloids, organic cellulosics, biopolymers, microorganisms, and oils.[24-28] These foulants often aid in the attachment of other foulants, as

cellulosic materials facilitate binding of microorganisms that lead to biofilm growth. The dense fouling layer increases the resistance of water as it passes through the membrane and often hurts the quality of the effluent. To address the detrimental effects of fouling, operators must perform rigorous cleaning steps frequently to regain performance losses.[29] Rarely do the cleaning steps fully recover the initial performance, a phenomena known as irreversible or irrecoverable fouling.

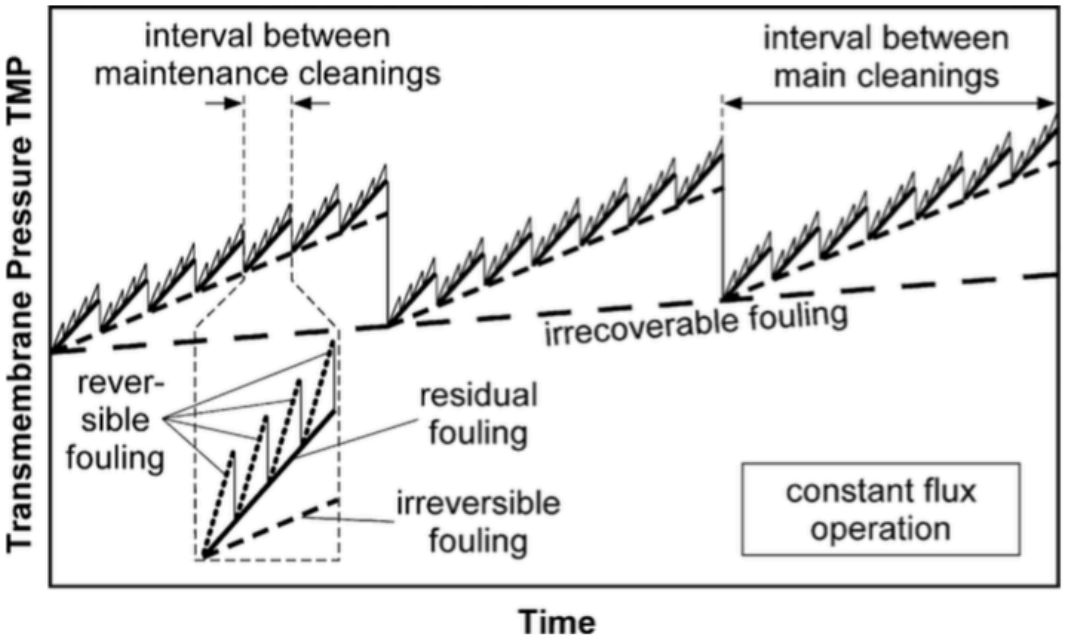

Figure 1.5. Representation of different fouling rates for a membrane bioreactor.[29] The transmembrane pressure is an indicator of the fouling rate, as fouling causes an increase in the pressure difference between the two sides of the membrane. Over long-term operation, the initial permeability cannot be regained.

1.6 The Costs of Fouling

Fouling, and the measures to reduce it, form the basis for increased operational, and maintenance expenses in water treatment. Due to flux decline, greater energy is needed to meet demands. Constant cleaning steps that require aggressive cleaning agents, and the additional labor involved, drive up maintenance costs. These chemicals often degrade the membranes and

cause the membranes to be replaced creating additional expenses. Furthermore, extra equipment for cleaning the modules in-place or out-of-place introduces higher capital expenditures. In a 2012 international survey of academics, contractors, operators, and membrane suppliers, 34% of the respondents identified fouling related issues to be the key challenge for MBR operation (fouling, cleaning, and clogging).[30]

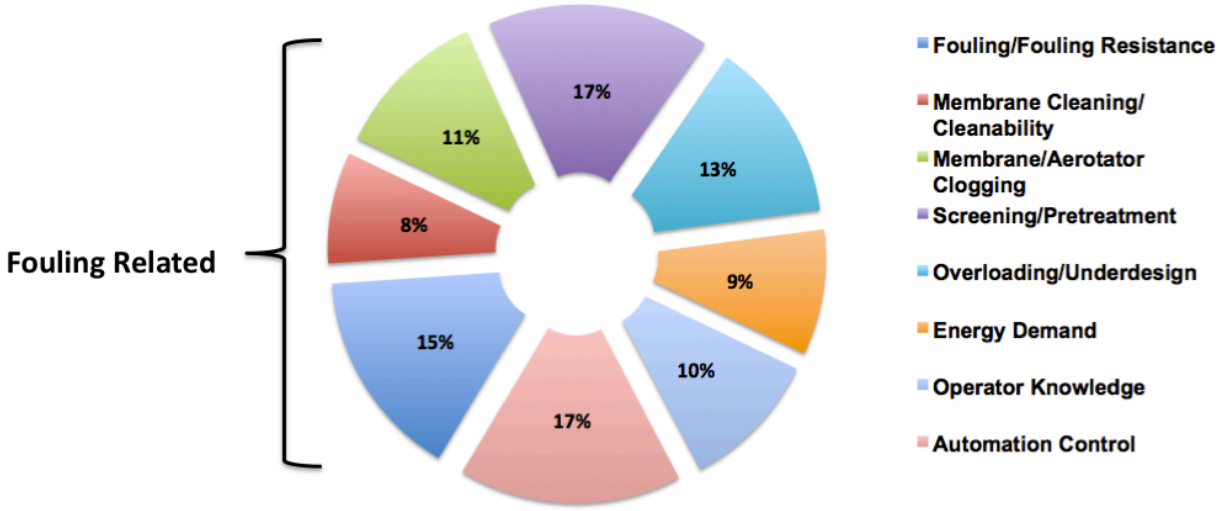

Figure 1.6. Survey results: Respondents were asked to identify the key factors challenging MBR operation. Figure adapted from Ref. 30.

The goal of this research is to investigate novel methods to fabricate new membranes or modifying existing membranes to produce fouling-resistant UF and RO membranes, using scalable processes. In the ensuing chapters, you will read about many previous physical and chemical methods to impart anti-fouling properties to membrane surfaces. By changing the surface properties of a material, the ability for a foulant to adhere to the material is also altered. In my opinion, many of the previous techniques work very well in the laboratory. However, I believe that for a new technology to be applied in the real world, it must be scalable, safe, and

cost-effective. The following dissertation will present two different techniques to modify polymeric membranes for water treatment that meet these requirements.

References

(1) Alberts B, Johnson A, Lewis J; et al. Molecular Biology of the Cell, Garland Science, New York, 4th ed., **2002**

(2) J. C. Crittenden, R. R. Trussel, D. W. Hand, K. J. Howe and G. Tchobanoglous, Water Treatment: Principles and Design, John Wiley & Sons, Inc., Hoboken, New Jersey, 2nd ed., **2005**

(3) Budin, I.; Devaraj, N. K. Membrane Assembly Driven by a Biomimetic Coupling Reaction. *J. Am. Chem. Soc.* **2012**, *134*, 751–753.

(4) Fick, A. Ueber Diffusion. *Ann. Phys.* **1855**, *170*, 59–86.

(5) Bechhold, H. Kolloidstudien mit der Filtrationsmethode, *Z. Phys. Chem.* **1907**, *60*, 257

(6) *Global Membrane Technology Market.* Acmite Market Intelligence. November **2015**. [Online][Accessed on April 14, 2016]

(7) Guillen, G. R.; Pan, Y.; Li, M.; Hoek, E. M. V. Preparation and Characterization of Membranes Formed by Nonsolvent Induced Phase Separation: A Review. *Ind. Eng. Chem. Res.* **2011**, *50*, 3798–3817.

(8) Cadotte, J. E. Interfacially synthesized reverse osmosis membrane, US Patent 4,277,344, **1981**.

(9) Ulbricht, M. Advanced functional polymer membranes. *Polymer*. **2006**, *47*, 2217–2262.

(10) Pendergast, M. M.; Mika Dorin, R.; Phillip, W. A.; Wiesner, U.; Hoek, E. M. V. Understanding the structure and performance of self-assembled triblock terpolymer membranes. *J. Memb. Sci.* **2013**, *444*, 461–468.

(11) Kim, H. J.; Baek, Y.; Choi, K.; Kim, D.-G.; Kang, H.; Choi, Y.-S.; Yoon, J.; Lee, J.-C. The improvement of antibiofouling properties of a reverse osmosis membrane by oxidized CNTs. *RSC Adv.* **2014**, *4*, 32802–32810.

(12) Freger, V. Swelling and Morphology of the Skin Layer of Polyamide Composite Membranes: An Atomic Force Microscopy Study. *Environ. Sci. Technol.* **2004**, *38*, 3168–3175.

(13) Chan, E. P.; Young, A. P.; Lee, J.H.; Stafford, C. M. Swelling of Ultrathin Molecular Layer-by-Layer Polyamide Water Desalination Membranes. *J. Polym. Sci. Part B Polym. Phys.* **2013**, *51*, 1647–1655.

(14) Podall, H. E. Permeability Requirements of Membranes for Use In Desalination by Reverse Osmosis. Washington, D.C.: U.S. Govt. Print. Off. , **1957**

(15) Reid, C. E. and Breton, E. J., Water and ion flow across cellulosic membranes. J. *Appl. Polym. Sci.,* **1959**, *1*, 133–143.

(16) Loeb, S. *Synthetic Membranes*. ACS Symposium Series; American Chemical Society, **1981**; Vol. 153, p. 1.

(17) Banks, W.; Sharples, A.; Water, U. S. O. of S. *The mechanism of desalination by reverse osmosis, and its relation to membrane structure*; Research and development progress report; U.S. Dept. of the Interior, **1965**.

(18) Geise, G. M.; Paul, D. R.; Freeman, B. D. Fundamental water and salt transport properties of polymeric materials. *Prog. Polym. Sci.* **2014**, *39*, 1–42.

(19) Strathmann, H.; Michaels, A. S. Polymer-water interaction and its relation to reverse osmosis desalination efficiency. *Desalination* **1977**, *21*, 195–202.

(20) Beasley, J. K. The evaluation and selection of polymeric materials for reverse osmosis membranes. *Desalination* **1977**, *22*, 181–189.

(21) Lee, K. P.; Arnot, T. C.; Mattia, D. A review of reverse osmosis membrane materials for desalination—Development to date and future potential. *J. Memb. Sci.* **2011**, *370*, 1–22.

(22) Petersen, R. J. Composite reverse osmosis and nanofiltration membranes. *J. Memb. Sci.* **1993**, *83*, 81–150.

(23) Sincero, A. P.; Sincero, G. A. Physical-chemical treatment of water and wastewater, **2003**.

(24) Shi, X.; Tal, G.; Hankins, N. P.; Gitis, V. Fouling and cleaning of ultrafiltration membranes: A review. *J. Water Process Eng.* **2014**, *1*, 121–138.

(25) Gao, W.; Liang, H.; Ma, J.; Han, M.; Chen, Z.; Han, Z.; Li, G. Membrane fouling control in ultrafiltration technology for drinking water production: A review. *Desalination* **2011**, *272*, 1–8.

(26) Potts, D. E.; Ahlert, R. C.; Wang, S. S. A critical review of fouling of reverse osmosis membranes. *Desalination* **1981**, *36*, 235–264.

(27) Howe, K. J.; Clark, M. M. Fouling of Microfiltration and Ultrafiltration Membranes by Natural Waters. *Environ. Sci. Technol.* **2002**, *36*, 3571–3576.

(28) Pandey, S. R.; Jegatheesan, V.; Baskaran, K.; Shu, L. Fouling in reverse osmosis (RO) membrane in water recovery from secondary effluent: a review. *Rev. Environ. Sci. Bio/Technology* **2012**, *11*, 125–145.

(29) Drews, A. Membrane fouling in membrane bioreactors—Characterisation, contradictions, cause and cures. *J. Memb. Sci.* **2010**, *363*, 1–28.

(30) Judd, S.; Judd, C. The 2012 MBR Survey – the results; **2012**.

CHAPTER 2

Fabrication of Low-Fouling Ultrafiltration Membranes Using a Hydrophilic, Self-Doping Polyaniline Additive

2.1 Background

With a rising demand for clean water and declining availability from traditional freshwater sources, water must be treated effectively to meet future demands.[1] Pressure-driven ultrafiltration (UF) membranes made from polysulfone (PSf) provide an efficient, cost-effective method for removing pathogens, macromolecular natural organic matter, and inorganic colloidal particles from water[2] and serve as a pretreatment filter before the desalination of water through reverse osmosis membranes.[3] Unfortunately, PSf membranes suffer from irreversible fouling that significantly reduces membrane permeability during their operation. To regain part of the lost performance, PSf films are exposed to hydraulic backwashes and aggressive cleaning agents that degrade the membranes, increase operating costs, and shorten membrane life.[4,5] In this study, we are motivated to produce a less fouling prone and easier to clean UF membrane that can resist irreversible fouling, thus preventing the need for destructive or harsh cleaning agents.

Previous studies have shown that PSf membrane irreversible fouling is a result of hydrophobic interactions between the foulant and the membrane polymer.[6] Many attempts have been made to reduce the hydrophobicity of PSf to improve fouling resistance via grafting reactions with hydrophilic polymers,[7-13] the addition of water-soluble[14-18] or nanomaterial additives to the casting solution,[19-21] or plasma oxidative post-treatments.[13,22,23] Despite increasing the hydrophilicity in the membranes, these treatments are often detrimental to the flux and rejection properties of the membrane, produce only short-term effects, or require complex steps that do not scale to the manufacturing level.

Recently, the conjugated polymer polyaniline (PANi) has been incorporated into PSf membranes as a hydrophilic modifier.[24-26] PANi is known for its facile synthesis, electrical conductivity, environmental stability, and ability to be processed in polar aprotic solvents such as

those used to cast UF membranes. PANi's hydrophilic nature and water insolubility make it an exceptional candidate to be a hydrophilic modifier in UF membranes. However, blended PANi/PSf membranes lose their ability for high-molecular weight protein rejection when increasing amounts of PANi are incorporated into a PSf polymer matrix.[24] Additionally, even at low concentrations, PANi solutions eventually gel because of intermolecular hydrogen bonding with adjacent polymer chains[27] as illustrated in Figure 2.1. Organic cosolvents have been added to inhibit gelation,[28,29] but their addition results in a loss of hydrophilicity in the final product.[30]

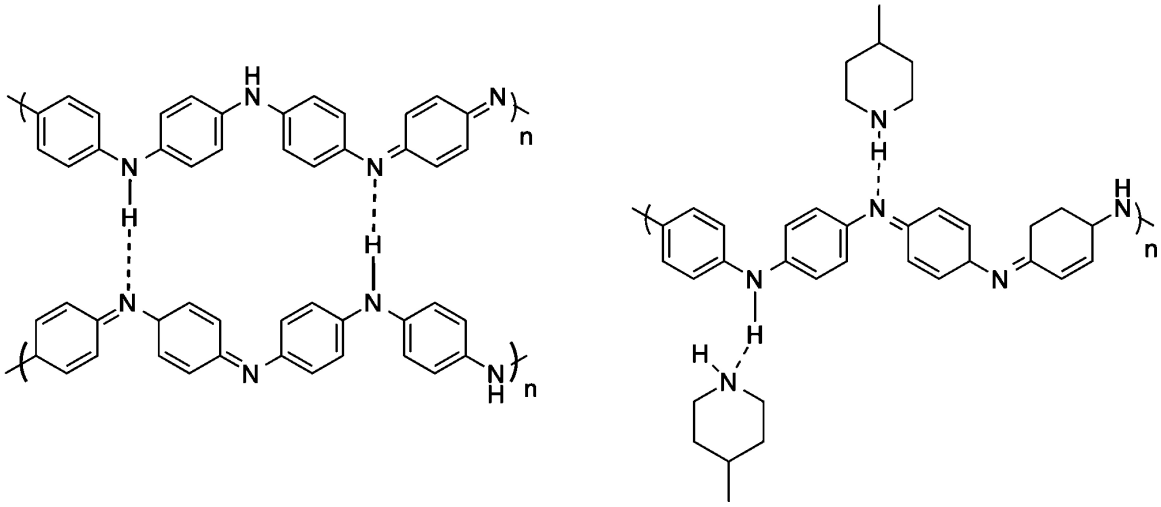

Figure 2.1. Intermolecular hydrogen bonding can cause the PANi solution to gel (left). Gel inhibitors such as 4-methylpiperidine can be used to prevent gelation by competing for hydrogen bonding sites (right).

Sulfonated polyaniline (SPANi) is a unique conducting polymer known for its self-doping characteristics.[31] Typically, PANi is doped with organic and/or inorganic acids to form the emeraldine salt form (PANi-ES), thus becoming more hydrophilic because of the formation of charged groups along the polymer backbone (Figure 2.2).[32] However, in neutral solutions (e.g., water), PANi-ES dedopes and reverts back to its base form. In the case of SPANi, the sulfonic acid groups covalently bound to the polymer backbone form a stable six-membered ring with the imine nitrogen that allows the conducting polymer to remain doped at neutral pH.[33]

With a sulfonation degree near 0.5 (sulfur:nitrogen ratio), SPANi is a dark green powder that is insoluble in both organic and aqueous solutions.[34] In this state, SPANi is zwitterionic, possessing both positive and negative charges along the polymer chain. Zwitterionic species are known to be superhydrophilic[35] and possess ultralow fouling characteristics.[36] To process SPANi in solution, the six-membered ring must be broken with a strong base.[37] When broken, the SPANi is dedoped and dissolves to form a deep violet solution, in aqueous or polar organic environments.

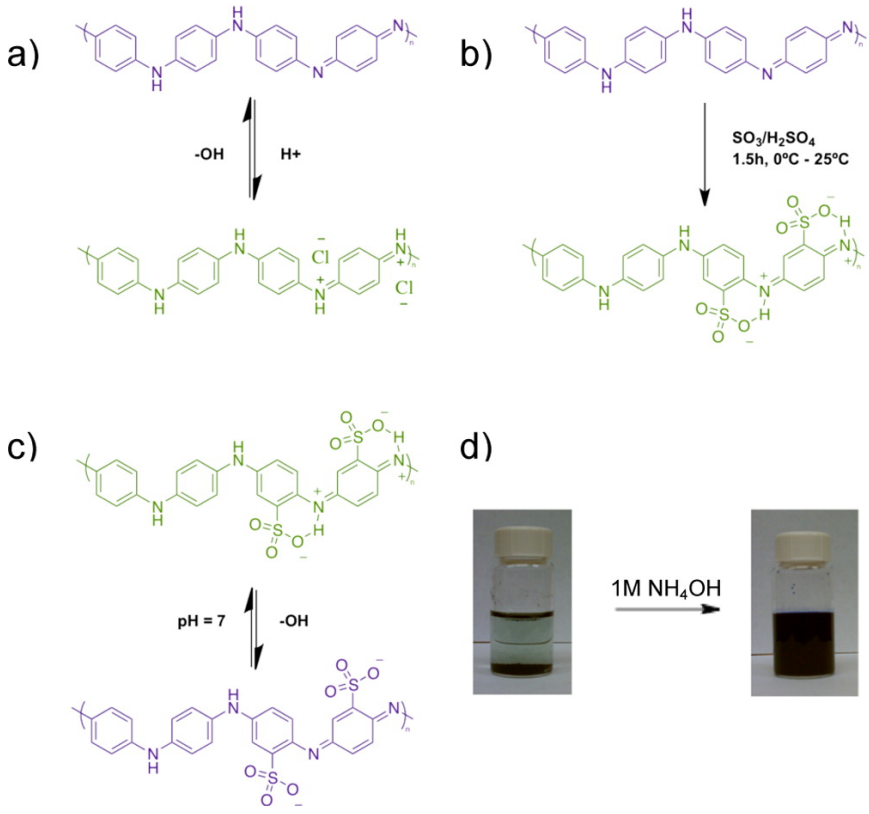

Figure 2.2. (a) PANi can be doped and dedoped with acids and bases. (b) The covalent addition of a sulfonic acid group to the polymer produces a self-doping effect. (c) SPANi is dedoped with a base to process the polymer in solution. (d) The solubility and color of the SPANi polymer change in its doped and dedoped state.

Here, we introduce SPANi as a hydrophilic modifier for PSf membranes. SPANi is a superhydrophilic, ionic polymer that does not gel *in situ*. Thus, the polymer can be dissolved

directly into UF membrane precast solutions and precipitated during the phase inversion process, a highly scalable method for hydrophilic UF membranes. The enhanced hydrophilicity prevents bovine serum albumin, a representative protein, from irreversibly binding to the membrane surface and pores, resulting in a decreased flux and increased flux recovery with only a water wash. Furthermore, the incorporation of SPANi does not hinder its separation performance compared to that of a pure PSf membrane and maintains rejection characteristics of typical UF membranes.

2.2 Materials

PANi-EB (20 kDa), PSf (22 kDa), bovine serum albumin (BSA), *N*-methylpyrollidone (NMP), and methanol were purchased from Sigma-Aldrich (Milwaukee, WI). Ammonium hydroxide (NH_4OH, 14.8 M) and acetone were purchased from Fisher Scientific (Pittsburgh, PA). Fuming sulfuric acid (20% SO_3) was purchased from Spectrum Chemical Manufacturing Corp. (Gardena, CA). All materials were used as received.

2.3 SPANi Synthesis

SPANi was synthesized as described by Yue et al.[34] using fuming sulfuric acid. This method yields a degree of sulfonation of ~0.5 (sulfur:nitrogen ratio). In a 500 mL round-bottom flask in an ice bath was dissolved 0.75 g of 20 kDa MW PANi-EB in 90 mL of fuming sulfuric acid (20%), and the mixture was stirred. After 10 min, the ice bath was removed and the reaction was allowed to continue for 1.5 hours. Upon completion, the reaction products were poured slowly over a fresh ice bath to precipitate the polymer. After the ice had melted, the green suspension was centrifuged at 3000 rpm for 10 minutes three times in deionized water, each time

decanting the supernatant and resuspending in solution to break up the agglomerates and to remove the acid. After centrifugation, the powder was further dialyzed in a fresh deionized (DI) water bath until the pH of the water bath reached 7. The resulting green SPANi suspension was dried *in vacuo* at 50 °C overnight and stored in a desiccator (66% yield). The sulfonation of PANi was confirmed via Fourier transform infrared (FT-IR) spectroscopy, and the degree of sulfonation, i.e., the sulfur:nitrogen ratio, was 0.48 as confirmed by XPS (see the Supporting Information, Appendix A).

2.4 Membrane Fabrication

Composite PSf membrane films containing 0, 1, 5, and 10% SPANi (relative to the mass of PSf in the solution) were fabricated via an immersion precipitation method. Using the 1% SPANi/PSf film as an example, 22 mg of SPANi was added to 10 g of a 0.25 M NH_4OH/NMP solution and the mixture stirred overnight at room temperature. The blue solution was filtered through a 0.45 μm PTFE filter into a new vial and weighed. The amount of SPANi was calculated by the weight ratio of the initial solution; PSf beads were added accordingly to create an 18 wt % SPANi/PSf solution, and the mixture was stirred overnight. The pure PSf membrane was made from an 18 wt % PSf solution in a 0.25 M NH_4OH/NMP solution. The deep violet solutions containing dedoped SPANi were cast at 152 μm using an adjustable doctor blade on a nonwoven polyester support (from NanoH_2O Inc., Los Angeles, CA) taped to a glass plate. Samples used for scanning electron microscopy (SEM) were cast unsupported on a glass plate. After being cast, the glass plate was immediately immersed in a coagulation bath containing 3 L of a 0.1 M H_2SO_4 solution to precipitate the films, which immediately turned green (redoping). The temperature of the coagulation bath was 25 °C with 57 ± 3% humidity as measured by a

digital thermometer and humidimeter. After 30 min, the membrane films were transferred to a clean DI water bath to remove any residual solvent and acid. Each film was stored in 18 MΩ water purified by an in-house reverse osmosis membrane at room temperature for the duration of the testing.

2.5 Membrane Characterization

The hand-cast membranes were used for pure water permeability and flux decline and recovery testing. To determine pure water permeability values, a 19 cm^2 cutout of each supported membrane film was placed in an in-house cross-flow system shown in the Supporting Information (Appendix A). A computer connected to a scale recorded the dynamic mass change of the filtrate and calculated the active flux. Because there were instantaneous fluctuations in the flux recorded by the computer, the average values for each time point were plotted. The membranes were compacted with DI water at 20 psi with a cross-flow rate of 7.2 L/h until the decaying flux stabilized. The stable flux was recorded as the pure water permeability. The flux was then normalized to 68 L/m^2 per day (LMH) by manually reducing the pressure with a pressure control valve (68 LMH corresponds to 40 gallons/ft^2 per day, a typical operational flux). Once stable at 68 LMH, a 1.5 g/L BSA feed solution was introduced to observe the flux decline caused by BSA fouling. After obtaining a stable flux for at least 10 min, DI water was introduced to wash the membrane surface. During the washing step, the cross-flow rate was increased to 9.5 L/h and flux recovery was recorded when a stable flux was reached. The flux recovery percentage (FR%) was calculated via Equation 2.1:

$$F_r = J_f/J_i \times 100\% \quad \textbf{(2.1)}$$

where J_f is the final flux (LMH) after the DI water wash step and J_i is the initial 68 LMH flux.

BSA rejection tests were conducted using an HP4750 Sterlitech dead-end filtration cell holding membranes 4 cm in diameter. Water (18 MΩ) was pressurized via nitrogen gas in a stainless steel vessel with an adjustable pressure valve. The filtrate passed through a flowmeter (GJC Instruments Ltd., model 5025000) to record flux. A coupon of each supported membrane was compacted at 20 psi until a stable flux was reached. The pressure was adjusted to record flux values at 5, 10, and 20 psi. From a linear curve fit, corresponding pressures were selected to perform the rejection testing at 68 LMH for each membrane. Ten milliliters of a 1.0 g/L BSA solution was placed into the dead-end cell and pushed through the membrane with nitrogen gas. The permeate solution was collected and analyzed using UV–vis spectroscopy (Perkin-Elmer Lambda 20). The BSA rejection was calculated from Equation 2.2.

$$R = 1 - A_p/A_f \quad \textbf{(2.2)}$$

where A_p is the absorbance of the permeate solution at 278 nm (λ) and A_f is the absorbance of the feed solution at 278 nm (λ).

Cross-sectional morphologies were determined using a JEOL JSM-6701F scanning electron microscope. Images were observed at 650X magnification using a 10 kV accelerating voltage. Unsupported membrane samples were cut out, air-dried overnight, and then dried in a desiccator for at least 24 h. The dried samples were frozen in liquid nitrogen, fractured, and then sputter-coated with gold before being observed under an electron microscope.

Membrane surface contact angle measurements were obtained using the captive bubble technique on a Krüss DSA 10 goniometer. Membrane samples of approximately 1 cm × 3 cm were carefully mounted on a glass slide using double-sided tape and submerged surface down in DI water. Twelve air bubbles were then placed manually on each surface for software angle fitting. Reported contact angle data were averaged over 10 measurements after elimination of the highest and lowest values.

Dried samples were also used for atomic force microscopy (AFM) to investigate surface topography. The topography was investigated using a Bruker Dimension 5000 scanning probe microscope (in tapping mode). The average surface roughness and surface area difference percentage were determined from the surface topography for each sample.

In this study, we synthesized SPANi and incorporated increasing amounts of the polymer into PSf UF membranes to enhance membrane hydrophilicity, thus inducing antifouling properties. Because solution additives often affect membrane performance, pure water permeability and rejection measurements were taken. Additionally, cross-sectional SEM images and AFM images were observed for the investigation of morphological differences induced by the addition of SPANi. To confirm changes in the hydrophilicity of the membrane surface compared with the PSf membrane, a series of contact angle measurements were recorded for each composite membrane. Fouling flux decline and flux recovery studies were then conducted to explore the performance and antifouling characteristics of the SPANi/PSf membrane composites.

2.6 Performance Testing

Figure 2.3 presents the performance and rejection characteristics of the SPANi/PSf composite membranes. Compared with the PSf control, the SPANI/PSf composites possess similar permeability values with increasing amounts of SPANi. The differences in flux are within experimental error of that of the cross-flow system. The rejection of BSA remains the same for each membrane (~95%), which suggests that the pore size has not increased significantly because of the inclusion of SPANi.

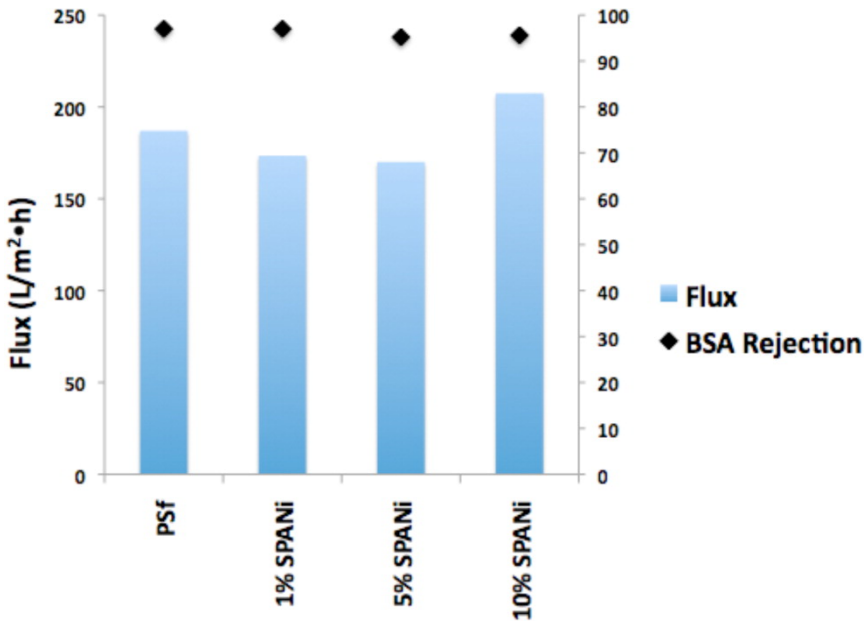

Figure 2.3. Pure water permeability (bars, left axis) and BSA rejection (diamonds, right axis).

2.7 Film Morphology

To examine the membrane film morphology, cross sections of the membrane samples were observed under SEM, as displayed in Figure 2.4. PSf membranes (cast from an NMP solvent) typically produce a thick skin layer at the surface supported by fingerlike voids during

the phase inversion process.[38] The PSf membrane cast from the 0.25 M NH_4OH solution in an NMP solution is consistent with this model (Figure 2.4, top left). In the top layer of the membrane film, vertical microvoids are seen, while horizontally angled macrovoids form in the bottom layer. Subsequently, with the 1 and 5% SPANi membranes, the vertical microvoids extend through a larger span of the membrane film, while the horizontally angled macrovoids are less pronounced. In the 10% SPANi membrane cross section, the vertical void structures completely span the height of the membrane. Vertically aligned pores allow water to permeate with a more direct path through the membrane with less internal resistance, increasing the flux in comparison to those of the three other membranes, thus accounting for the increase in permeability. Additionally, the thick skin layer is preserved at the top of each of the SPANi/PSf membrane composites, supporting the rejection characteristics comparable to those of the pure PSf membrane.

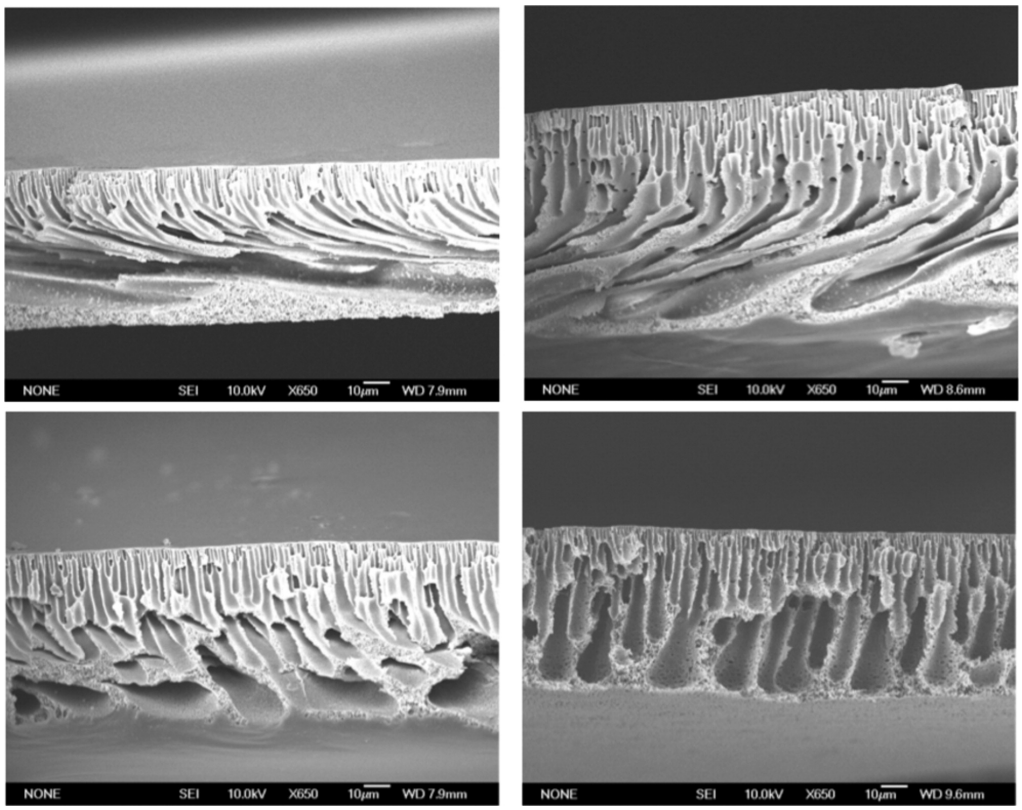

Figure 2.4. Cross-sectional morphologies of the pure PSf membrane (top left), the 1% SPANi membrane (top right), the 5% SPANi membrane (bottom left), and the 10% SPANi membrane (bottom right).

2.8 Hydrophilicity

Figure 2.5 presents the results of captive bubble measurements for comparing the hydrophilicity of each membrane film. The captive bubble technique is advantageous relative to the sessile drop technique for determining the contact angle because UF membranes remain in their wet state; thus, there is no change in morphology caused by drying.[39] Relative to that of the pure PSf membrane, there was a small change in the apparent contact angle for the 1% SPANi and 5% SPANi membranes, with 0° and 6° reductions in the contact angle, respectively. The 10% SPANi membrane apparent contact angle is significantly smaller (25°), exhibiting a large increase in hydrophilicity when compared with those of the other membrane films. During the

10% SPANi measurement, it was difficult to obtain an image because the bubble did not contact the surface (no surface dewetting) and often "rolled" off the membrane film. It is also observed in Figure 2.5d that the spherical shape of the air bubble is compressed because of the lack of surface contact and buoyant force of the bubble. This leads us to believe that the 10% SPANi/PSf composite membrane retains a thin film of water on its surface that the air bubble cannot pervade.

Similar to hydrophilicity, surface roughness plays a role in fouling properties; i.e., rougher surfaces tend to trap particles within valleys leading to increased surface fouling.[40] AFM was utilized to analyze the surface topography of the PSf and SPANi composite membranes, shown in Figure 2.6.

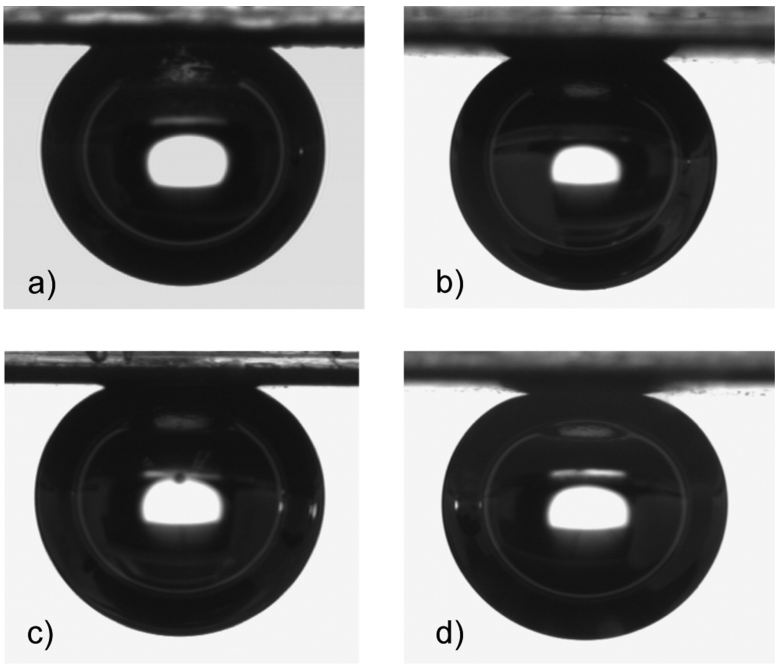

Figure 2.5. Captive bubble contact angle images of (a) the PSf membrane film, (b) the 1% SPANi membrane film, (c) the 5% SPANi membrane film, and (d) the 10% SPANi membrane film.

With increasing amounts of SPANi, there is an increase in surface roughness, with root-mean-square roughness values of 12.6, 17.3, 25.1, and 38.1 nm for the PSf membrane and 1, 5, and 10% SPANi membranes, respectively (Table 2.1).

Table 2.1. Summary of Membrane Performance Properties

Membrane Composition	Pure Water Permeability at 20 psi (LMH)	Rejection of BSA (%)	Contact Angle (°)	RMS Surface Roughness (nm)	Flux Decline (%)	Flux Recovery (%)
Polysulfone (PSF)	187.0	97.0	50	12.6	50	62
1 wt% SPANi/PSF	173.4	97.0	50	17.3	41	75
5 wt% SPANi/PSF	170.0	95.2	44	25.1	32	85
10 wt% SPANi/PSF	207.4	95.6	25	38.1	16	95

Also shown in Table 2.1 is the surface area difference percentage (SAD%) for each membrane, which is defined as the difference between the image's three-dimensional surface area and the projected two-dimensional surface area. Wenzel's equation[41,42] is used to normalize the measured contact angle with surface roughness (Equation 2.3):

$$Cos(\theta_A) = Cos(\theta_M)/ r \qquad \textbf{(2.3)}$$

where θ_A is the apparent contact angle, θ_M is the measured contact angle, and r is the roughness ratio and is equal to 1 + SAD%. When the apparent contact angle is normalized using Wenzel's equation to account for surface roughness, the apparent contact angle of the membrane is roughly the same as the measured contact angle (Table 2.1). Thus, the large decrease in the contact angle

is largely attributed to the change in surface chemistry and is only nominally affected by changes in surface roughness.

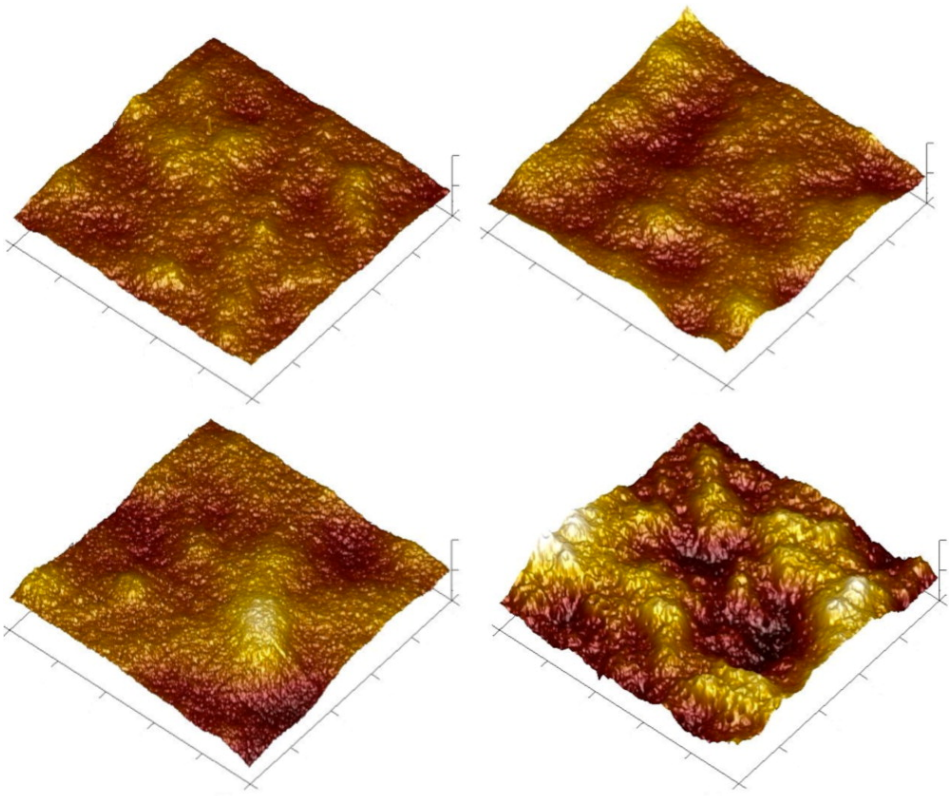

Figure 2.6. AFM surface images of the pure PSf membrane (top left), the 1% SPANi membrane (top right), the 5% SPANi membrane (bottom left), and the 10% SPANi membrane (bottom right). Scale bars represent 10 μm on the horizontal axis and 150 nm on the vertical axis.

The Cassie equation[43] is used to describe the apparent contact angle on the surface of binary composite materials (Equation 2.4):

$$Cos(\theta_A) = \zeta_{SPANi}\, Cos(\theta_{SPANi}) + \zeta_{PSf}\, Cos(\theta_{PSf}) \qquad \textbf{(2.4)}$$

where θ_A is the apparent contact angle, ζ_{SPANi} is the weight percent of SPANi within the membrane, θ_{SPANi} is the contact angle of pure SPANi, ζ_{PSf} is the weight percent of PSf within the membrane, and θ_{PSf} is the contact angle of pure PSf. From this equation, we can predict ζ_{SPANi} for each measured contact angle when we assume that θ_{SPANi} is 0° and θ_{PSf} is 50°. When this model is employed for the 5 and 10% SPANi/PSf composite membranes, ζ_{SPANi} is predicted to be 21.4 and 73.8%, respectively. The large discrepancy can be described by the migration of hydrophilic additives to the surface of the polymer matrix during phase inversion.[44,45] To lower the interfacial energy between the polymer blend solution and the coagulation bath during phase inversion, the hydrophilic SPANi polymer migrates to the surface of the composite polymer matrix. This results in a higher density of SPANi at the pore surfaces and on the surface of the membrane and a much lower density of SPANi in the bulk polymer. This phenomenon is further manifested by a visual difference in the top and bottom of the unsupported membranes (shown in the Supporting Information, Appendix A).

2.9 Flux Decline and Recovery

To evaluate the effects of the enhanced hydrophilicity and increased surface roughness on fouling properties, flux decline and recovery testing was performed using BSA as a model organic foulant in a cross-flow system (Figure 2.7). When the membranes are exposed to a BSA solution, the flux decreases immediately due to membrane fouling. The pure PSf membrane loses approximately 50% of its original flux when exposed to the BSA solution. The 1, 5, and 10% SPANi/PSf composite membranes exhibit a reduced flux decline, with the 10% SPANi/PSf membrane losing only 16% of its original flux. The decrease in flux decline is most likely due to

the enhanced hydrophilicity from the incorporation of SPANi and is directly related to the amount of SPANi contained within the membrane composites.

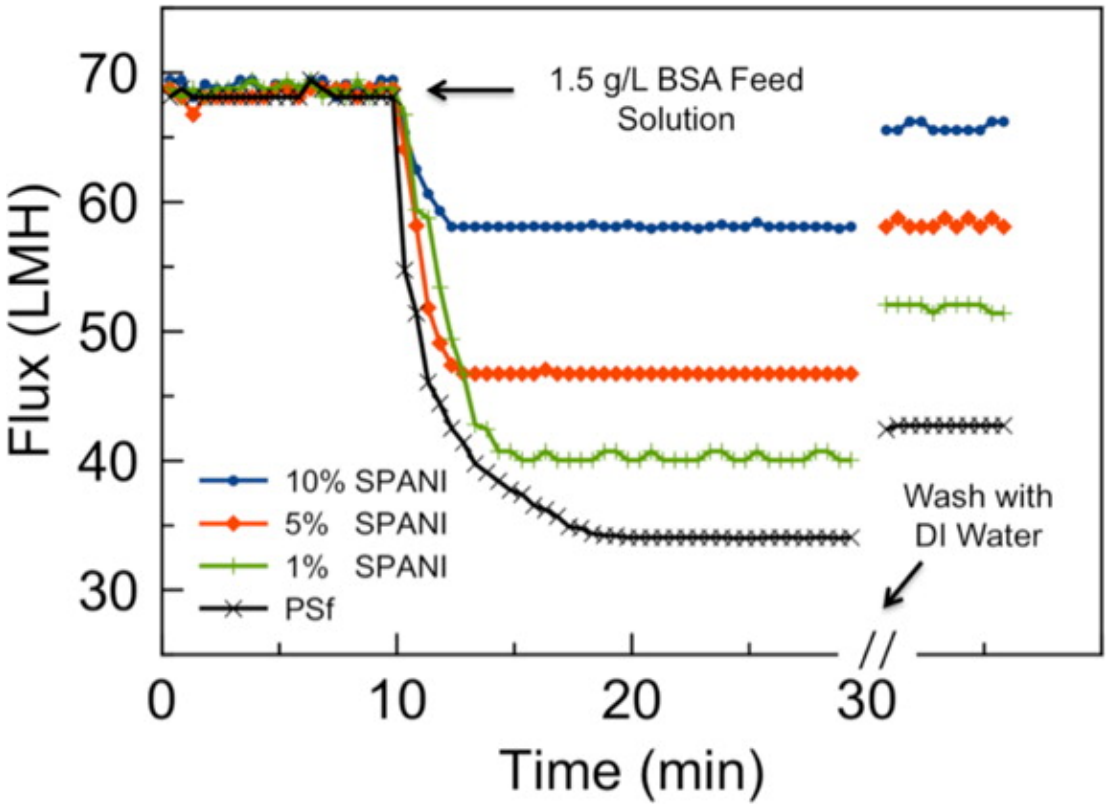

Figure 2.7. Flux decline and recovery results for PSf membranes containing 0, 1, 5, and 10% SPANi after being exposed to BSA and then washed.

The degree of irreversible membrane fouling is evident during the flux recovery stage of the experiment (Figure 2.7). During the DI water wash, the membranes recovered a fraction of their initial flux. The PSf membrane has a percent flux recovery (FR%) of 62, losing approximately 38% of its initial performance to irreversible fouling. With the addition of the SPANi additive, FR% increased to 75, 85, and 95 for the 1, 5, and 10% SPANi membranes, respectively.

A schematic illustration of the irreversible fouling mechanism of PSf membranes and the low-fouling properties of the SPANi membrane composites are presented in Figure 2.8. When the pure water feed solution is switched to a BSA feed solution (a), the hydraulic pressure forces the BSA into the pores and across the surface of the PSf membrane (b). This phenomenon causes the pore volume to decrease, and free particles are trapped within the pores, leading to a large flux decline. During the wash step with pure water (c), the concentration gradient removes only unattached particles. Thus, irreversibly bound particles remain in the pores, leading to a low flux recovery. Throughout operation of the SPANi composite membranes, the hydraulic pressure again forces BSA particles into the pores (d). In contrast to the PSf UF membrane, the enhanced hydrophilicity prevents BSA particles from irreversibly binding to the walls of the pores (e). This causes the pore volume to remain the same, and the membrane experiences a smaller flux decline. When the membrane is washed with pure water, the concentration gradient removes a greater amount of free BSA particles (f), and in the case of the 10% SPANi/PSf membrane, 95% of the initial flux is recovered. A summary of performance characteristics for each membrane is given in Table 2.1.

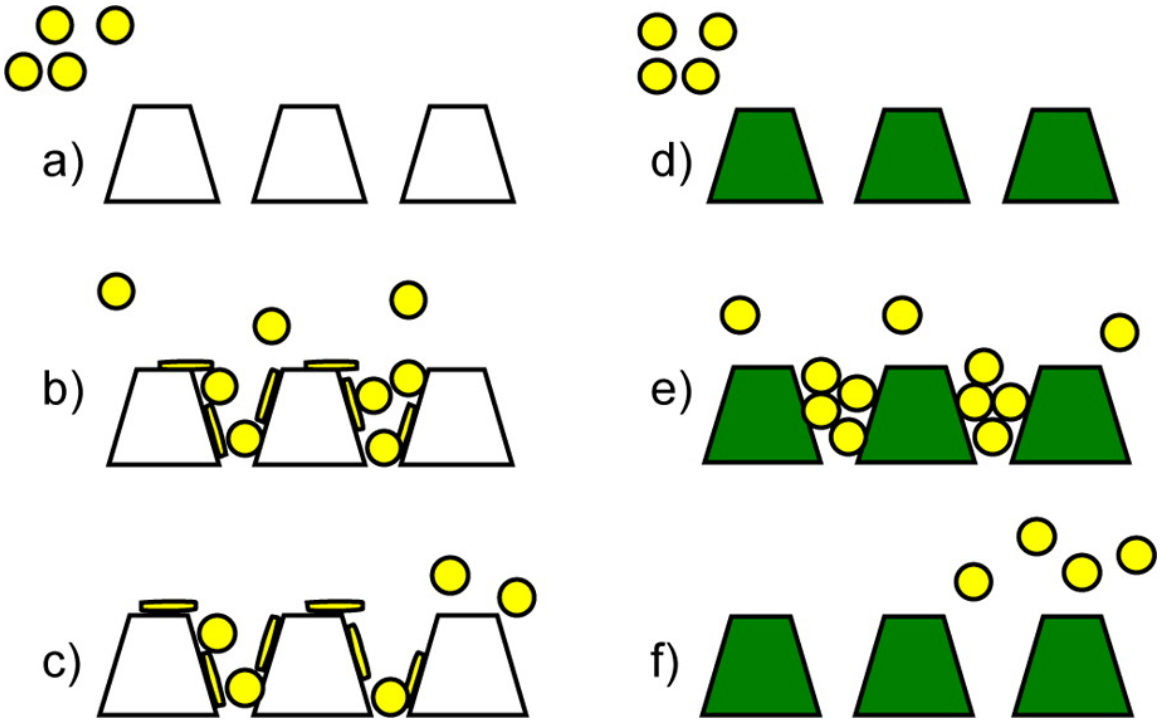

Figure 2.8. Schematic diagram illustrating irreversible fouling of a PSf membrane surface (left) and the reversible fouling of a SPANi/PSf composite membrane surface (right). The spheres represent BSA proteins in solution, and the plates represent conformational changes due to hydrophobic interactions with the PSf surfaces.

2.10 Conclusions

We have demonstrated the fabrication of a low-fouling UF membrane with the addition of a superhydrophilic sulfonated polyaniline additive. The solution additive maintains the scalability and cost-effectiveness of current UF membrane manufacture processing without complex steps or post-treatments. The incorporation of self-doped SPANi enhances the morphology and hydrophilicity of the UF membranes, achieving performances superior to that of the pure PSf membrane. Because relatively small amounts of SPANi are added, the rejection properties of the composite membranes remain consistent with those of current UF membranes. With only a DI water wash, SPANi/PSf composite membranes regain up to 95% of their initial flux, highlighting

their antifouling characteristics. We believe that antifouling membranes could eliminate the need for strong cleaning agents and processes, thus reducing the costs and energy for next-generation UF membranes.

2.11 Acknowledgments

We thank NanoH_2O for the generous donation of materials and NantWorks for use of their facilities and instrumentation. We also thank J. Shaw and Prof. H. Potsma for help with AFM measurements and data workup with the use of the SPM facility at the Nano and Pico Characterization Lab at the California NanoSystems Institute. This work was supported by National Science Foundation Grant 0903720 to B.T.M. and Grant CBET 1337065 E.M.V.H. and R.B.K.

References

(1) Service, R. F. Desalination Freshens Up. *Science*. **2006**, *313*, 1088–1090.

(2) Cheryan, M. Ultrafiltration and Microfiltration Handbook; Technomic: Lancaster, PA, **1998**.

(3) Rosberg, R. Ultrafiltration (new technology), a viable cost-saving pretreatment for reverse osmosis and nanofiltration — A new approach to reduce costs. *Desalination* **1997**, *110*, 107–113.

(4) Eykamp, W. Microfiltration and ultrafiltration. In Membrane Separation Technology: Principles and Applications; Noble, R. D.; Stern, S. A., Eds.; Elsevier Science: Amsterdam, **1995.**

(5) Kuzmenko, D.; Arkhangelsky, E.; Belfer, S.; Freger, V.; Gitis, V. Chemical cleaning of UF membranes fouled by BSA. *Desalination* **2005**, *179*, 323–333.

(6) Hilal, N.; Ogunbiyi, O. O.; Miles, N. J.; Nigmatullin, R. Methods Employed for Control of Fouling in MF and UF Membranes: A Comprehensive Review. *Sep. Sci. Technol.* **2005**, *40*, 1957–2005.

(7) Yu, H.; Cao, Y.; Kang, G.; Liu, J.; Li, M.; Yuan, Q. Enhancing antifouling property of polysulfone ultrafiltration membrane by grafting zwitterionic copolymer via UV-initiated polymerization. *J. Memb. Sci.* **2009**, *342*, 6–13.

(8) Kaeselev, B.; Pieracci, J.; Belfort, G. Photoinduced grafting of ultrafiltration membranes: comparison of poly(ether sulfone) and poly(sulfone). *J. Memb. Sci.* **2001**, *194*, 245–261.

(9) Hua, H.; Li, N.; Wu, L.; Zhong, H.; Wu, G.; Yuan, Z.; Lin, X.; Tang, L. Anti-fouling ultrafiltration membrane prepared from polysulfone-graft-methyl acrylate copolymers by UV-induced grafting method. *J. Environ. Sci.* **2008**, *20*, 565–570.

(10) Akbari, A.; Homayonfal, M.; Jabbari, V. Synthesis and characterization of composite polysulfone membranes for desalination in nanofiltration technique. *Water Sci. Technol.* **2010**, *62*, 2655–2663.

(11) Park, J. Y.; Acar, M. H.; Akthakul, A.; Kuhlman, W.; Mayes, A. M. Polysulfone-graft-poly(ethylene glycol) graft copolymers for surface modification of polysulfone membranes. *Biomaterials* **2006**, *27*, 856–865.

(12) Liu, G.; Lu, Z.; Duncan, S. Porous Membranes of Polysulfone-graft-poly(tert-butyl acrylate) and Polysulfone-graft-poly(acrylic acid): Morphology, pH-Gated Water Flow, Size Selectivity, and Ion Selectivity. *Macromolecules* **2004**, *37*, 4218–4226.

(13) Ulbricht, M.; Belfort, G. Surface modification of ultrafiltration membranes by low temperature plasma II. Graft polymerization onto polyacrylonitrile and polysulfone. *J. Memb. Sci.* **1996**, *111*, 193–215.

(14) Matsuyama, H.; Maki, T.; Teramoto, M.; Kobayashi, K. *Sep. Sci. Technol.* Effect of PVP Additive on Porous Polysulfone Membrane Formation by Immersion Precipitation Method. **2003**, *38*, 3449–3458.

(15) Han, M.-J.; Nam, S.-T. Thermodynamic and rheological variation in polysulfone solution by PVP and its effect in the preparation of phase inversion membrane. *J. Memb. Sci.* **2002**, *202*, 55–61.

(16) Chakrabarty, B.; Ghoshal, A. K.; Purkait, M. K. Preparation, characterization and performance studies of polysulfone membranes using PVP as an additive. *J. Memb. Sci.* **2008**, *315*, 36–47.

(17) Kim, J.-H.; Lee, K.-H. Effect of PEG additive on membrane formation by phase inversion. *J. Memb. Sci.* **1998**, *138*, 153–163.

(18) Chakrabarty, B.; Ghoshal, A. K.; Purkait, M. K. Effect of molecular weight of PEG on membrane morphology and transport properties. *J. Memb. Sci.* **2008**, *309*, 209–221.

(19) Bae, T.-H.; Tak, T.-M. Effect of TiO2 nanoparticles on fouling mitigation of ultrafiltration membranes for activated sludge filtration. *J. Memb. Sci.* **2005**, *249*, 1–8.

(20) Yang, Y.; Zhang, H.; Wang, P.; Zheng, Q.; Li, J. The influence of nano-sized TiO2 fillers on the morphologies and properties of PSF UF membrane. *J. Memb. Sci.* **2007**, *288*, 231–238.

(21) Qiu, S.; Wu, L.; Pan, X.; Zhang, L.; Chen, H.; Gao, C. Preparation and properties of functionalized carbon nanotube/PSF blend ultrafiltration membranes. *J. Memb. Sci.* **2009**, *342*, 165–172.

(22) Kim, K. S.; Lee, K. H.; Cho, K.; Park, C. E. Surface modification of polysulfone ultrafiltration membrane by oxygen plasma treatment. *J. Memb. Sci.* **2002**, *199*, 135–145.

(23) Steen, M. L.; Hymas, L.; Havey, E. D.; Capps, N. E.; Castner, D. G.; Fisher, E. R. Low temperature plasma treatment of asymmetric polysulfone membranes for permanent hydrophilic surface modification. *J. Memb. Sci.* **2001**, *188*, 97–114.

(24) Guillen, G. R.; Farrell, T. P.; Kaner, R. B.; Hoek, E. M. V. Pore-structure, hydrophilicity, and particle filtration characteristics of polyaniline-polysulfone ultrafiltration membranes. *J. Mater. Chem.* **2010**, *20*, 4621–4628.

(25) Zhao, S.; Wang, Z.; Wei, X.; Zhao, B.; Wang, J.; Yang, S.; Wang, S. Performance improvement of polysulfone ultrafiltration membrane using PANiEB as both pore forming agent and hydrophilic modifier. *J. Memb. Sci.* **2011**, *385–386*, 251–262.

(26) Fan, Z.; Wang, Z.; Sun, N.; Wang, J.; Wang, S. Performance improvement of polysulfone ultrafiltration membrane by blending with polyaniline nanofibers. *J. Memb. Sci.* **2008**, *320*, 363–371.

(27) Yang, D.; Mattes, B. R. Polyaniline emeraldine base in N-methyl-2-pyrrolidinone containing secondary amine additives: A rheological investigation of solutions. *J. Polym. Sci. Part B Polym. Phys.* **2002**, *40*, 2702–2713.

(28) Yang, D.; Mattes, B. R. Investigation of gel inhibitor assisted dissolution of polyaniline: A case study for emeraldine base, 2-methyl-aziridine, and N-methyl-pyrrolidone. *Synth. Met.* **1999**, *101*, 746–749.

(29) Yang, D.; Zuccarello, G.; Mattes, B. R. Physical Stabilization or Chemical Degradation of Concentrated Solutions of Polyaniline Emeraldine Base Containing Secondary Amine Additives. *Macromolecules* **2002**, *35*, 5304–5313.

(30) Guillen, G. R.; McVerry, B. T.; Farrell, T. P.; Kaner, R. B.; Hoek, E. M. V. Tuning the properties of polyaniline-based ultrafiltration membranes with chemical post-treatments. Manuscript in progress.

(31) Yue, J.; Epstein, A. J. Synthesis of self-doped conducting polyaniline. *J. Am. Chem. Soc.* **1990**, *112*, 2800–2801.

(32) Huang, J.; Kaner, R. B. A General Chemical Route to Polyaniline Nanofibers. *J. Am. Chem. Soc.* **2004**, *126*, 851–855.

(33) Yue, J.; Wang, Z. H.; Cromack, K. R.; Epstein, A. J.; MacDiarmid, A. G. Effect of sulfonic acid group on polyaniline backbone. *J. Am. Chem. Soc.* **1991**, *113*, 2665–2671.

(34) Yue, J.; Gordon, G.; Epstein, A. J. Comparison of different synthetic routes for sulphonation of polyaniline. *Polymer*. **1992**, *33*, 4410–4418.

(35) Kobayashi, M.; Terayama, Y.; Yamaguchi, H.; Terada, M.; Murakami, D.; Ishihara, K.; Takahara, A. Wettability and Antifouling Behavior on the Surfaces of Superhydrophilic Polymer Brushes. *Langmuir* **2012**, *28*, 7212–7222.

(36) Jiang, S.; Cao, Z. Ultralow-fouling, functionalizable, and hydrolyzable zwitterionic materials and their derivatives for biological applications.. *Adv. Mater.* **2010**, *22*, 920–932.

(37) Wu, Q.; Qi, Z.; Wang, F. The six-member ring self-doping structure in sulfonated polyaniline. *Synth. Met.* **1999**, *105*, 191–194.

(38) Guillen, G. R.; Pan, Y.; Li, M.; Hoek, E. M. V. Preparation and Characterization of Membranes Formed by Nonsolvent Induced Phase Separation: A Review. *Ind. Eng. Chem. Res.* **2011**, *50*, 3798–3817.

(39) Zhang, W.; Wahlgren, M.; Sivik, B. Membrane Characterization by the Contact Angle Technique. *Desalination* **1989**, *72*, 263–273.

(40) Vrijenhoek, E. M.; Hong, S.; Elimelech, M. Influence of membrane surface properties on initial rate of colloidal fouling of reverse osmosis and nanofiltration membranes. *J. Memb. Sci.* **2001**, *188*, 115–128.

(41) Wenzel, R. N. Resistance of Solid Surfaces to Wetting by Water. *Ind. Eng. Chem.* **1936**, *28*, 988–994.

(42) Wenzel, R. N. Surface Roughness and Contact Angle. *J. Phys. Colloid Chem.* **1949**, *53*, 1466–1467.

(43) Cassie, A. B. D.; Baxter, S. Wettability of porous surfaces. *Trans. Faraday Soc.* **1944**, *40*, 546–551.

(44) Kajiyama, T.; Tanaka, K.; Takahara, A. Surface Segregation of the Higher Surface Free Energy Component in Symmetric Polymer Blend Films. *Macromolecules* **1998**, *31*, 3746–3749.

(45) Zhu, L.-P.; Xu, L.; Zhu, B.-K.; Feng, Y.-X.; Xu, Y.-Y. Preparation and characterization of improved fouling-resistant PPESK ultrafiltration membranes with amphiphilic PPESK-graft-PEG copolymers as additives. *J. Memb. Sci.* **2007**, *294*, 196–206.

CHAPTER 3

Scalable Antifouling Reverse Osmosis Membranes Utilizing

Perfluorophenyl Azide Photochemistry

3.1 Introduction

The World Health Organization provided a plan this past year to ensure that the world's population has access to a basic clean water supply by 2030.[1] Presently, over one billion people do not have access to clean water and dwindling freshwater supplies are leading to new health, environmental, and geopolitical implications in the 21st century.[2,3] Unfortunately, natural purification of water, i.e., through sedimentation and aquifers, cannot sustain these future demands.[4] New technologies must be developed to treat water effectively from traditional and nontraditional sources to adequately supply global needs.

Reverse osmosis (RO) has emerged as a leading technology in water treatment for its ability to efficiently convert seawater and brackish water into high purity water for potable and high tech applications. The polymeric thin-film membranes used for RO exhibit high flux, high selectivity, low cost, and relatively low energy expenditure compared with alternative desalination technologies.[3,5] Acting as a physical barrier, RO membranes allow water molecules to permeate through a dense, microporous film and reject small dissolved solutes. Among numerous polymeric materials used to fabricate RO membranes, aromatic polyamide membranes are the most widely used because of their superior transport and separation properties. Thin-film composite membranes are produced on an industrial scale using roll-to-roll processing and are packaged into spiral wound elements to achieve optimal performance.

Although polyamide membranes have approached theoretical limits on performance, they are highly susceptible to biological surface fouling that significantly reduces intrinsic operational and economic advantages.[2,3,6] Microorganisms in the feed water adsorb onto the surface via hydrophobic interactions and block the flow of water through the membrane. Harsh chemical disinfectants used to prevent the growth of biofilms on the surface, such as chlorine and base

treatments, prevent and remove biofilms from the surface, but also attack the chemical bonds within the polyamide layer and degrade the high selectivity of the membranes.[7,8] Thus, biogrowth inhibition and cleaning agents that are commonly used in water treatment cannot be used with RO membranes, increasing the pretreatment, operating and maintenance costs of desalination plants.[9-11]

Recently, researchers have attempted to reduce or prevent RO membrane biofouling by developing antifouling membrane surface treatments.[12,13] By covalently modifying the surface with hydrophilic brush polymers,[14-19] hydrophobic interactions between the foulant and the membrane surface are obstructed. In addition, initial attachment of biological cells and dissolved organics, a key step in biofilm formation, is impeded. A hydrophilic surface forms a layer of hydration[20] that prevents foulants from adsorbing onto the surface of the membrane film and allows water to pass freely through the membrane.

Unfortunately, the designed chemical stability of polyamide membranes makes surface manipulations a difficult task. Previous studies have utilized reactive epoxide terminal groups,[15] carbodiimide activation,[16] or radical-initiated graft polymerizations that chemically attach the hydrophilic polymers to the polyamide surface.[13,16-19] However, these modifications require long reaction times, exotic reaction conditions, and are performed *in situ*, preventing them from being easily translated into commercial roll-to-roll manufacturing processes for thin-film composite membranes.

The need for a scalable method to produce antifouling RO membranes has led us to investigate the use of perfluorophenyl azide (PFPA) as a chemical modifier. PFPAs are known for their highly reactive azide group that allows PFPA derivatives[21,22] to make chemical bonds with rather unreactive targets, such as graphene,[23,24] carbon nanotubes,[25] fullerenes,[26] and

organic polymers.[27] The azide functionality is activated by photoexcitation that expels nitrogen gas and affords a reactive singlet nitrene that inserts into −NH− and C=C bonds.[28,29] The surface layer of RO membranes is comprised of cross-linked polyamide networks that contain these groups, thus providing a target for modification. Our goal is to develop a dip-coating technique using PFPA derivatives that confers antifouling properties to RO membranes and maintains the roll-to-roll manufacturing process.

3.2 Objective

Because PFPAs can be prepared with a functional ester group in the para-position relative to the azide moiety, PFPAs can be readily coupled to molecules containing free amino or hydroxyl groups to form corresponding amide or ester linkages (Figure 3.1). In this chapter, we have synthesized three hydrophilic polyethyleneglycol (PEG) brush polymers of different molecular weights (MW = 550, 1000, 5000 Daltons) with a terminal PFPA group. PFPA-PEG_{550}, PFPA-PEG_{1000}, and PFPA-PEG_{5000} are used to denote the respective PFPA-terminated PEG derivatives according to their molecular weight. The water solubility of the PFPA-PEGs allows the product to be isolated in high purity from the starting material by using an aqueous phase extraction. More importantly, the water solubility enables RO membranes to be dipped into an aqueous solution containing the dissolved PFPA-PEG derivatives. This is attractive commercially, as many common organic solvents dissolve the underlying polysulfone layer supporting the thin-film composite membrane.

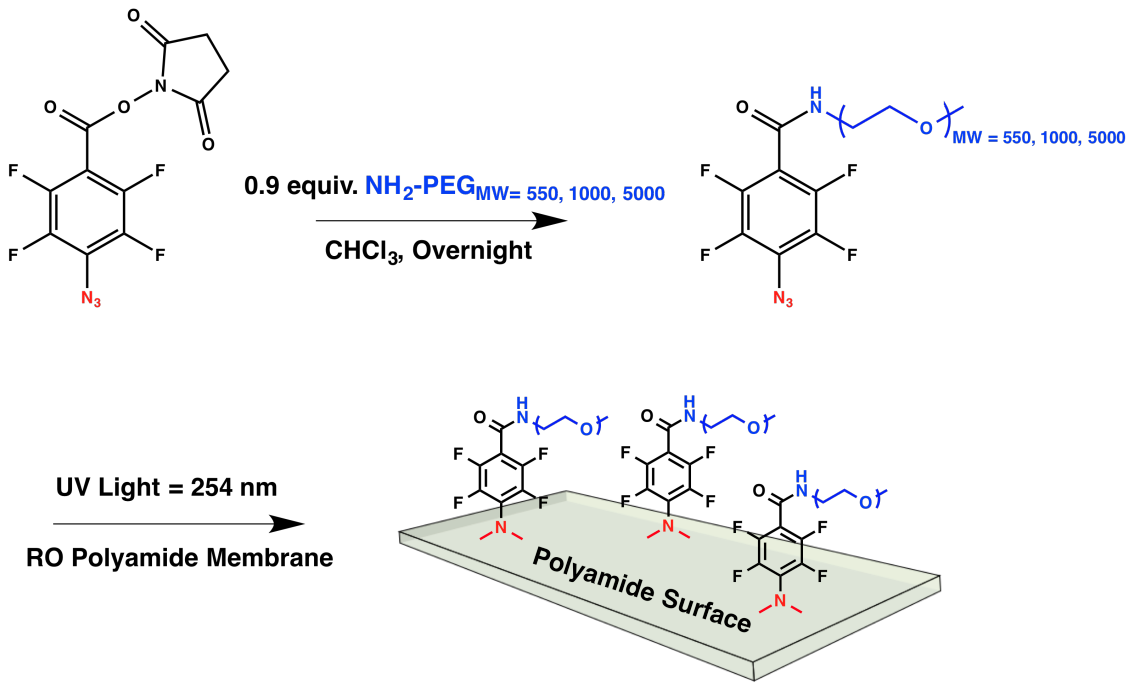

Figure 3.1. Synthesis of PFPA terminated PEG brush polymers and attachment to RO membrane surface.

3.3 PFPA Modification and Characterization

To test if PFPA photochemical reactions can covalently modify RO membranes, commercial PA membrane cutouts were dipped into aqueous solutions containing PFPA-PEG_{550}, PFPA-PEG_{1000}, and PFPA-PEG_{5000} and allowed to air dry under ambient conditions. Once dried, the coupons were irradiated with low-power UV light (254 nm, 585 μW cm^{-2} average intensity) from a handheld UV lamp. The cutouts were rinsed in a water bath to remove any unreacted azide and dimerized by-products from the surface and dried before surface analysis (see Supporting Information, Appendix B). The membranes were then characterized with attenuated total reflectance infrared (ATR-IR) spectroscopy. The presence of alkane groups within the PEG polymer brushes is discernible in the ATR-IR spectrum when compared with a bare PA

membrane (Figure 3.2). A broad C−H stretch is observed at 2860 cm^{-1} and becomes stronger when PFPA-PEG of higher molecular weight is used for the modification.

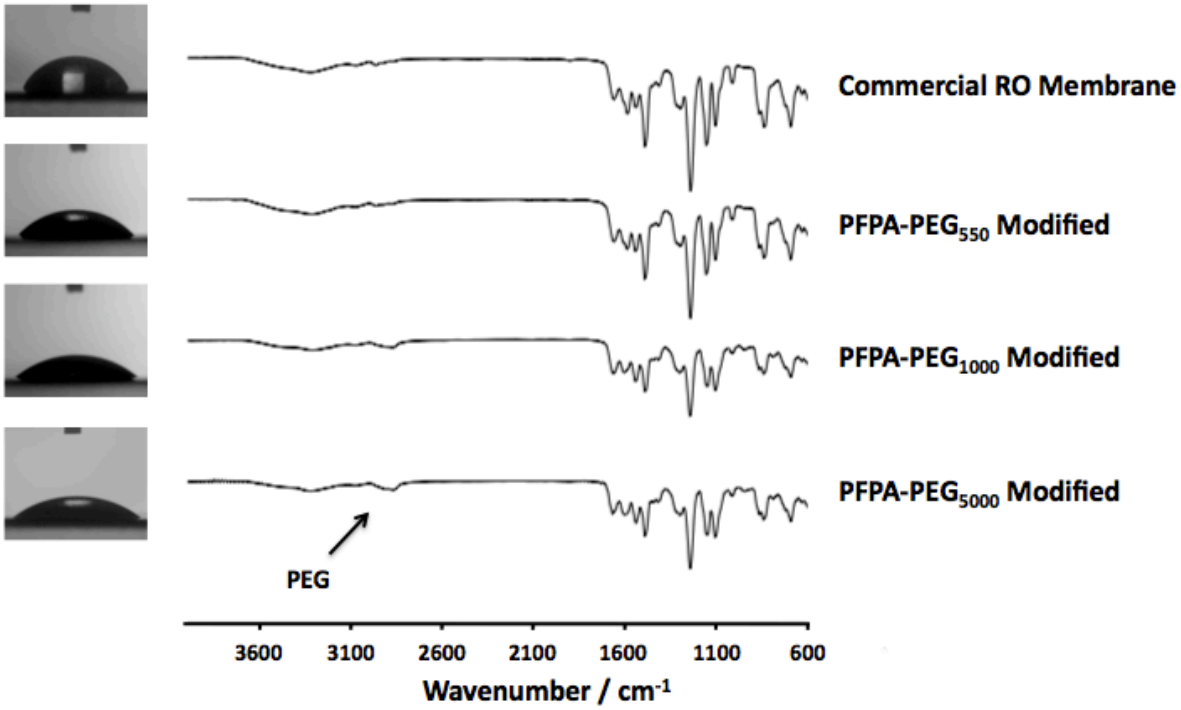

Figure 3.2. ATR-IR spectroscopy of the commercial polyamide RO membrane and modified membranes. Apparent contact angle images are shown in the photos on the left.

3.4 Contact Angle Measurements

The modification is further manifested through contact angle measurements shown in the photos in Figure 3.3. The introduction of hydrophilic brush polymers to the surface of the membrane reduces the liquid/solid interfacial energy between a drop of water and the top PA layer. The hydrophilic surface has a stronger interaction with water than the bare membrane, resulting in a decreased contact angle. A bare commercial membrane was also dried and exposed to UV light (no dip-coating) to confirm that the decreased contact angle was not caused by UV irradiation.

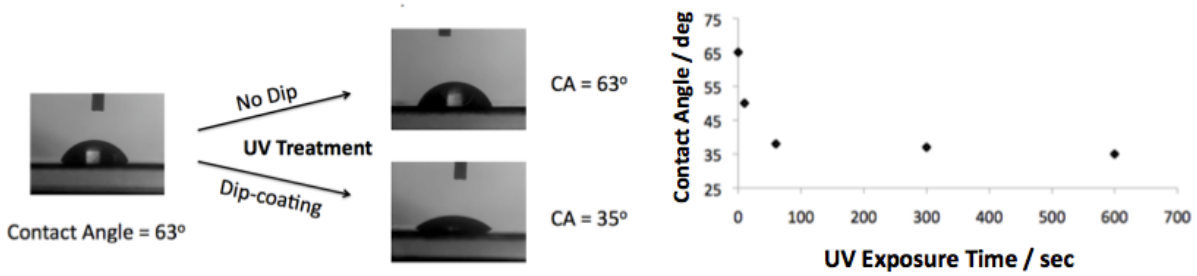

Figure 3.3. Effect of UV exposure on a bare membrane and PFPA-PEG_{5000} coated membrane (left) and contact angle vs. UV exposure time for a PFPA-PEG_{5000} coated membrane (right).

The contact angle was also measured as a function of UV exposure time to investigate modification completion (Figure 3.3). Several 4 cm^2 membrane cutouts were dip coated in PFPA-PEG_{5000}, exposed to UV light for different lengths of time, and rinsed. The results shown in Figure 3.3 indicate that the modification is complete after ~60 seconds of UV exposure time. It is also important to note that with zero UV exposure time, the contact angle of the bare commercial membrane is restored at 63°. This indicates that the wash step removes essentially all the physically adsorbed PFPA-PEG from the surface of the membrane. Thus, UV exposure is necessary to generate covalent interactions between the RO membrane surface and the PFPA functionality.

3.5 XPS Characterization

X-ray photoelectron spectroscopy (XPS) was employed to further elucidate the nature of the covalent attachment of PFPA to the surface of the RO membrane. Because the long PEG polymer chains dominate the XPS spectra, the small molecule 4-azidotetrafluorobenzoic acid (PFPA-COOH) was prepared and used to modify analytical samples (Supporting Information, Appendix B) for XPS measurements, shown in Figure 3.4. When compared with the unmodified

membrane, the N 1s spectrum for the modified membrane exhibits an additional peak at 402.2 eV, attributed to the newly formed aziridine linkage between the PFPA and the aromatic rings on the membrane surface.[24] Furthermore, the absence of signal above 403 eV indicates that N_2 is expelled from Ar−N=N^+=N^- during irradiation, as Ar−N=N^+=N^- exhibits a distinct peak at 406.5 eV. Additionally, the modified membrane survey spectrum reveals the presence of fluorine at 687.6 eV (Figure 3.4).

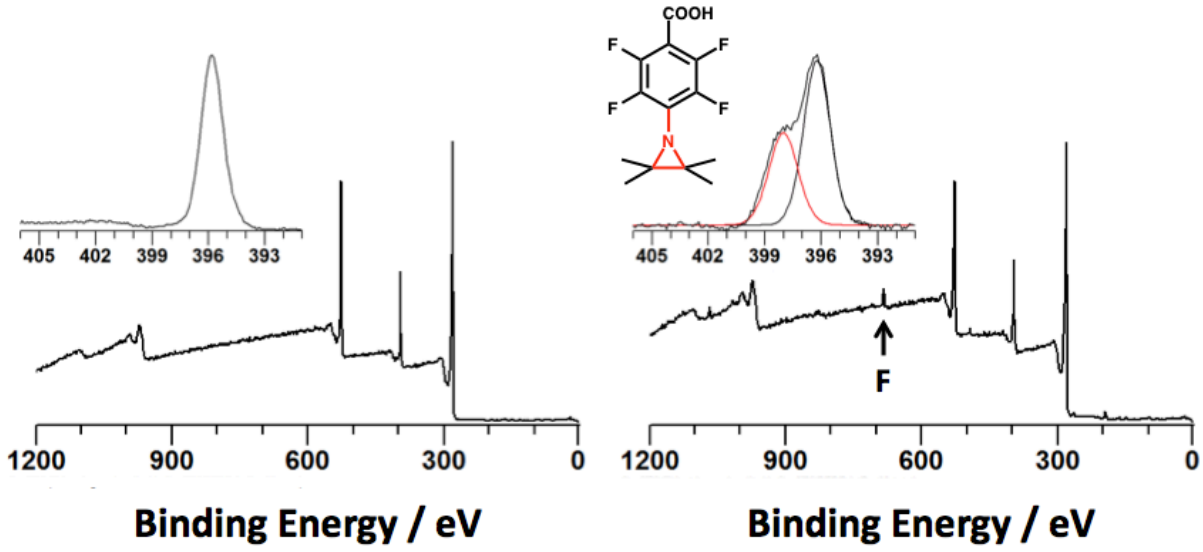

Figure 3.4. XPS survey spectra and N 1S spectra (inset) of the unmodified (left) and modified (right) RO membrane surfaces.

3.6 Performance of Modified and Unmodified Membranes

To determine the effect of the surface modification on the performance of commercial RO membranes, pure water permeability tests and NaCl rejection tests of the modified membranes were conducted. As shown in Figure 3.5, the addition of hydrophilic polymers to the membrane surface reduces the pure water permeability and increases NaCl rejection due to steric hindrance.[30] Moreover, systematically increasing the molecular weight of the brush polymer has

a greater effect on the permeability and rejection, presumably caused by larger flexible polymer chains. Although the initial permeability is reduced by the attachment of hydrophilic polymers, the PFPA-PEG-modified membranes exhibit higher fluxes than many commercially available RO membranes with comparable monovalent salt rejection.[31]

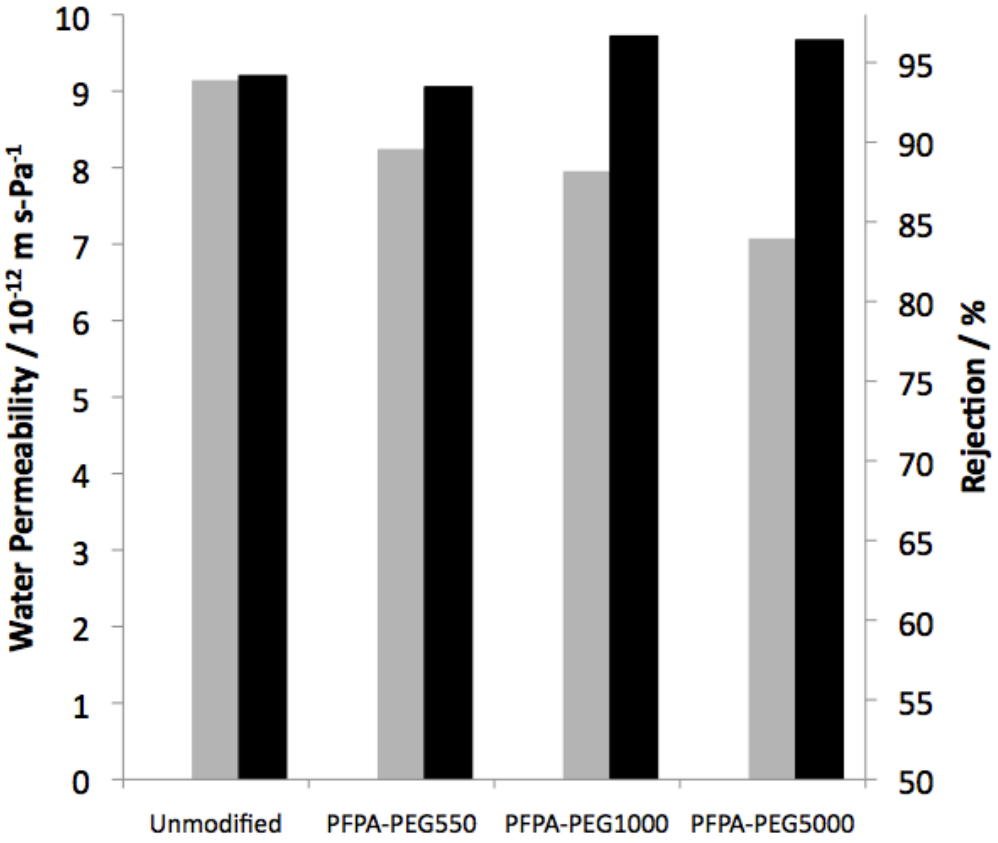

Figure 3.5. Pure water permeability (left axis) and rejection of NaCl (right axis).

3.7 Static Adhesion Testing

The ability of the modified membrane to resist cell adhesion was challenged using *Escherichia coli*, a gram-negative bacterium that is commonly used in antifouling experiments.[19,32-34] Because initial attachment of bacteria is crucial in biofilm formation, inhibiting bacterial adhesion prevents the growth and spreads of bacteria across a surface. In this

study, we measured *E. coli* adhesion on the modified and unmodified RO membranes by fluorescent microscopy, following a modified procedure described by Rong and Gleason.[19] Using ImageJ software,[35] we estimated the surface coverage percentage of the adhered bacteria and compared these values to the unmodified RO membrane.

Figure 3.6 presents the surface coverage analysis and fluorescent microscopy images (inset). Regarding the unmodified RO membrane, ~22% of the membrane surface is covered with irreversibly attached *E. coli*. When modified with PFPA-PEGn derivatives, notably less attachment is observed for the membranes. The membranes modified with PFPA-PEG_{550} and PFPA-PEG_{1000} showed less adhered bacteria and <1% of the surface is covered with *E. coli* on the membranes modified with PFPA-PEG_{5000}. Clearly, increased PEG molecular weight (chain length) is directly related to the antifouling ability of the modified membrane.

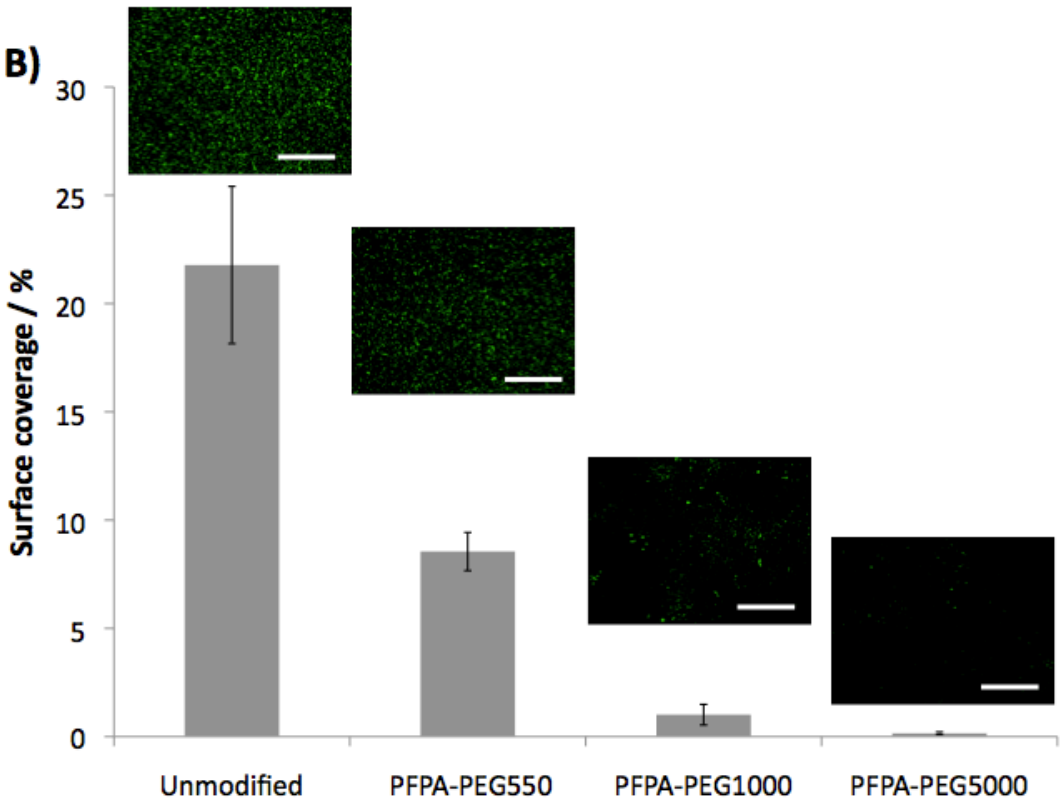

Figure 3.6. Observed adhesion of *E. coli* onto PFPA-PEG modified membranes with fluorescence microscopy, converted with ImageJ software. Scale bar = 50 μm.

3.8 Conclusions

Here, we have demonstrated the scalable surface modification of a commercial RO membrane consistent with the roll-to-roll processing of RO membranes. Utilizing the photochemistry of PFPAs as a platform, our system modifies RO membranes under ambient conditions, with minute modification times, using a dip-coating technique in environmentally benign solvents. By modifying a commercial RO membrane with our method, we prevent initial bacterial adhesion that leads to biofilm formation. We believe that the production of antifouling RO membranes will reduce or eliminate biofouling on RO membranes, thus reducing the high maintenance and energy costs associated with current RO desalination. In the future, we will

examine the modification of RO membranes with PFPAs bearing small molecule functionalities with our process.

3.9 Synthesis of PFPA-PEG$_n$

PFPA-PEG Synthesis: PFPA-PEG derivatives were synthesized by a modified procedure originally described by Yan.[36] Briefly, 1 equiv. of *N*-hydroxysuccinimidyl 2,3,5,6-tetrafluorobenzoate and 0.9 equiv. of the H_2N-PEG were dissolved in $CHCl_3$. The solution was stirred overnight in the dark at room temperature. The reaction mixture was then poured into diethyl ether and extracted three times with DI water. After evaporation under reduced pressure, the product was collected and used without further purification. Detailed syntheses and characterization (^{1}H NMR, ^{19}F NMR, and ATR-IR) of the three PFPA-PEG derivatives are provided in Appendix B.

3.10 Surface Modification Procedure

The 2×10^{-3} M PFPA-PEG$_n$ solutions were prepared by dissolving PFPA-PEG$_n$ in 18 MΩ water and shaking vigorously until the PFPA-PEG was fully dissolved. All dip-coating solutions were used the same day as prepared. The commercial reverse osmosis membrane coupons (2×2 cm^2) were dipped into the solutions for ~5 seconds and allowed to air dry on a flat surface. Larger 110 cm^2 samples were used for performance testing. Once dried, the coupons were placed under a 6 W Spectroline ENF-260C handheld UV lamp using a 254 nm wavelength for 3 min. The lamp was held 5 inches above the surface of the membrane using a ring stand. The average UV intensity was determined using a UV-C light meter (Sper Scientific). After UV exposure, the membrane cutouts were placed in a 10% ethanol/water bath stream to remove by-

products and any unreacted azide. The ethanolic solution also helped to restore permeability to the membranes that was lost during the drying step.[37] The membrane coupons were then placed in a DI water bath overnight. Membrane coupons used for ATR-IR and contact angle measurements were stored in a dessicator. Detailed protocols for membrane performance and cell adhesion testing can be found in Appendix B.

3.11 Acknowledgments

This work was supported by the NSF SUSchem grant CBET 1337065 (E.M.V and R.B.K.) and a National Science Foundation—Graduate Research fellowship (B.M.). The authors would also like to thank Dow Water Process and Solutions for their generous donation of RO XLE flat sheet membranes.

References

(1) World Health Organization, Progress on Sanitation and Drinking-Water, WHO Press, Geneva **2013**.

(2) Shannon, M. A.; Bohn, P. W.; Elimelech, M.; Georgiadis, J. G.; Marinas, B. J.; Mayes, A. M. Science and technology for water purification in the coming decades. *Nature* **2008**, *452*, 301–310.

(3) Elimelech, M.; Phillip, W. A. The Future of Seawater Desalination: Energy, Technology, and the Environment. *Science* **2011**, *333*, 712–717.

(4) Service, R. F. Desalination freshens up. *Science* **2006**, *313*, 1088–1090.

(5) Lee, K. P.; Arnot, T. C.; Mattia, D. A review of reverse osmosis membrane materials for desalination—Development to date and future potential. *J. Memb. Sci.* **2011**, *370*, 1–22.

(6) Herzberg, M.; Elimelech, M. Biofouling of reverse osmosis membranes: Role of biofilm-enhanced osmotic pressure. *J. Memb. Sci.* **2007**, *295*, 11–20.

(7) Glater, J.; Hong, S.; Elimelech, M. The search for a chlorine-resistant reverse osmosis membrane. *Desalination* **1994**, *95*, 325–345.

(8) Kawaguchi, T.; Tamura, H. Chlorine-resistant membrane for reverse osmosis. I. Correlation between chemical structures and chlorine resistance of polyamides. *J. Appl. Polym. Sci.* **1984**, *29*, 3359–3367.

(9) Isaias, N. P. Experience in reverse osmosis pretreatment. *Desalination* **2001**, *139*, 57–64.

(10) Redondo, J. A. Brackish-, sea- and wastewater desalination. *Desalination* **2001**, *138*, 29–40.

(11) Kang, G.-D.; Gao, C.-J.; Chen, W.-D.; Jie, X.-M.; Cao, Y.-M.; Yuan, Q. Study on hypochlorite degradation of aromatic polyamide reverse osmosis membrane. *J. Memb. Sci.* **2007**, *300*, 165–171.

(12) Rana, D.; Matsuura, T. Surface modifications for antifouling membranes. *Chem. Rev.* **2010**, *110*, 2448–2471.

(13) Kang, G.; Cao, Y. Development of antifouling reverse osmosis membranes for water treatment: A review. *Water Res.* **2012**, *46*, 584–600.

(14) Belfer, S.; Purinson, Y.; Fainshtein, R.; Radchenko, Y.; Kedem, O. Surface modification of commercial composite polyamide reverse osmosis membranes. *J. Memb. Sci.* **1998**, *139*, 175–181.

(15) Van Wagner, E. M.; Sagle, A. C.; Sharma, M. M.; La, Y.-H.; Freeman, B. D. Surface modification of commercial polyamide desalination membranes using poly(ethylene glycol) diglycidyl ether to enhance membrane fouling resistance. *J. Memb. Sci.* **2011**, *367*, 273–287.

(16) Kang, G.; Yu, H.; Liu, Z.; Cao, Y. Surface modification of a commercial thin film composite polyamide reverse osmosis membrane by carbodiimide-induced grafting with poly(ethylene glycol) derivatives. *Desalination* **2011**, *275*, 252–259.

(17) Zou, L.; Vidalis, I.; Steele, D.; Michelmore, A.; Low, S. P.; Verberk, J. Q. J. C. Surface hydrophilic modification of RO membranes by plasma polymerization for low organic fouling. *J. Memb. Sci.* **2011**, *369*, 420–428.

(18) Lin, N. H.; Kim, M.; Lewis, G. T.; Cohen, Y. Polymer surface nano-structuring of reverse osmosis membranes for fouling resistance and improved flux performance. *J. Mater. Chem.* **2010**, *20*, 4642.

(19) Yang, R.; Xu, J.; Ozaydin-Ince, G.; Wong, S. Y.; Gleason, K. K. Surface-Tethered Zwitterionic Ultrathin Antifouling Coatings on Reverse Osmosis Membranes by Initiated Chemical Vapor Deposition. *Chem. Mater.* **2011**, *23*, 1263–1272.

(20) Banerjee, I.; Pangule, R. C.; Kane, R. S. Antifouling Coatings: Recent Developments in the Design of Surfaces That Prevent Fouling by Proteins, Bacteria, and Marine Organisms. *Adv. Mater.* **2011**, *23*, 690–718.

(21) Leyva, E.; Young, M. J. T.; Platz, M. S. High yields of formal CH insertion products in the reactions of polyfluorinated aromatic nitrenes. *J. Am. Chem. Soc.* **1986**, *108*, 8307–8309.

(22) Liu, L.-H.; Yan, M. Perfluorophenyl Azides: New Applications in Surface Functionalization and Nanomaterial Synthesis. *Acc. Chem. Res.* **2010**, *43*, 1434–1443.

(23) Liu, L.-H.; Yan, M. Simple Method for the Covalent Immobilization of Graphene. *Nano Lett.* **2009**, *9*, 3375–3378.

(24) Liu, L.-H.; Zorn, G.; Castner, D. G.; Solanki, R.; Lerner, M. M.; Yan., M. A simple and scalable route to wafer-size patterned graphene. *J. Mater. Chem.* **2010**, *20*, 5041–5046.

(25) Pastine, S. J.; Okawa, D.; Kessler, B.; Rolandi, M.; Llorente, M.; Zettl, A.; Fréchet, J. M. J. A Facile and Patternable Method for the Surface Modification of Carbon Nanotube Forests Using Perfluoroarylazides. *J. Am. Chem. Soc.* **2008**, *130*, 4238–4239.

(26) Yan, M.; Cai, S. X.; Keana, J. F. W. Photochemical and Thermal Reactions of C60 with N-Succinimidyl 4-Azido-2,3,5,6-tetrafluorobenzoate: A New Method for Functionalization of C60. *J. Org. Chem.* **1994**, *59*, 5951–5954.

(27) Bartlett, M. A.; Yan, M. Fabrication of Polymer Thin Films and Arrays with Spatial and Topographical Controls. *Adv. Mater.* **2001**, *13*, 1449–1451.

(28) Morawietz, J.; Sander, W. Photochemistry of Fluorinated Phenyl Nitrenes: Matrix Isolation of Fluorinated Azirines. *J. Org. Chem.* **1996**, *61*, 4351–4354.

(29) Poe, R.; Schnapp, K.; Young, M. J. T.; Grayzar, J.; Platz, M. S. Chemistry and kinetics of singlet pentafluorophenylnitrene. *J. Am. Chem. Soc.* **1992**, *114*, 5054–5067.

(30) Y. Cohen, N. Lin, K. J. Varin, D. Chien, R. F. Hicks, Membrane Surface Nanostructuring with Terminally Anchored Polymer Chains, in *Functional Nanostructured Materials and Membranes for Water Treatment* (Eds: M. Duke, D. Zhao, R. Semiat), Wiley-VCH Verlag GmbH & Co. KGaA, Weinheim, Germany **2013**, p. 85.

(31) Jeong, B.-H.; Hoek, E. M. V; Yan, Y.; Subramani, A.; Huang, X.; Hurwitz, G.; Ghosh, A. K.; Jawor, A. Interfacial polymerization of thin film nanocomposites: A new concept for reverse osmosis membranes. *J. Memb. Sci.* **2007**, *294*, 1–7.

(32) Adout, A.; Kang, S.; Asatekin, A.; Mayes, A. M.; Elimelech, M. Ultrafiltration Membranes Incorporating Amphiphilic Comb Copolymer Additives Prevent Irreversible Adhesion of Bacteria. *Environ. Sci. Technol.* **2010**, *44*, 2406–2411.

(33) Kim, S. H.; Kwak, S.-Y.; Sohn, B.-H.; Park, T. H. Design of TiO2 nanoparticle self-assembled aromatic polyamide thin-film-composite (TFC) membrane as an approach to solve biofouling problem*J. Memb. Sci.* **2003**, *211*, 157–165.

(34) Tan, K.; Obendorf, S. K. Fabrication and evaluation of electrospun nanofibrous antimicrobial nylon 6 membranes. *J. Memb. Sci.* **2007**, *305*, 287–298.

(35) M. D. Abramoff, P. J. Magalhaes, S. J. Ram, Image Processing with ImageJ. *Biophotonics Int.* **2004**, 11, 36

(36) Yan, M. Covalent functionalization of natural rubber latex. *React. Funct. Polym.* **2000**, *45*, 137–144.

(37) Louie, J. S.; Pinnau, I.; Reinhard, M. Effects of surface coating process conditions on the water permeation and salt rejection properties of composite polyamide reverse osmosis membranes. *J. Memb. Sci.* **2011**, *367*, 249–255.

CHAPTER 4

Novel, Small Molecule Perfluorophenyl Azide Coatings for Fouling-resistant Membrane Bioreactors

4.1 Introduction

The lack of access to clean water worldwide is one of the greatest challenges the world must address in the 21st century.[1] The rising population, and the agriculture to support it, requires greater volumes of freshwater than ever before. The Middle East—the region most deprived of water—already consumes more than 40% of its freshwater availability.[2] In the US, legislation is currently being passed to confront California's historic drought.[3] Because of the large cost associated with water transport, communities must seek efficient systems to locally treat wastewater for re-use for a sustainable future.

Membrane bioreactors (MBRs) have emerged as an efficient technology that can produce high quality water from wastewater, with a relatively small footprint compared to traditional treatment processes.[4] Conventional treatment, such as the activated sludge process, utilizes aerobic bacteria in a controlled system to treat industrial or municipal wastewater. Bioreactor technology employs the same phenomena, but eliminates multiple treatment steps through the use of membrane technology. Micro- or ultrafiltration membranes can be submerged directly into the bioreactor to effectively separate the treated water from the mixed liquor to produce effluent that can be safely reused. Applying MBR technology provides higher effluent quality, enables higher volumetric loading rates, and requires less space in comparison to traditional wastewater treatment processes.[5]

Despite the advantages of MBR technology, membrane fouling remains the operational challenge that limits the widespread use of MBR for wastewater treatment.[6,7,8] Because the membranes are immersed in mixed liquor containing high concentrations of biomass, the membranes quickly foul, greatly reducing the production efficiency of treated water that can be separated by the membrane. Traditionally, membranes are cleaned during operation with

chemical agents to remove foulants and then regain their performance. Due to sensitivity of the microorganisms to chemicals, the membranes used in MBRs can generally only be treated with mild, ineffectual reagents during operation and must be removed completely from the system for more aggressive cleaning. These operating and maintenance costs drive up the total cost of MBR, diminishing its appeal over conventional treatment methods.

4.1 Prior Research

Recently, research has focused on developing new membrane materials that resist or reduce the rate of fouling.[9-22] Materials that repel foulants will inherently foul less quickly and are easier to clean with milder cleaning treatments. Because the major part of the fouling occurs at the surface of the polymer membranes, it is essential to understand the influence of the key interfacial factors between the interface of liquid media and the solid surfaces and how they affect adhesion of foulants. Early studies have indicated that hydrophobic interactions between biological media and polymeric membrane surfaces largely impact membrane fouling. A more hydrophilic membrane will repel hydrophobic forces from occurring. Thus, past studies have attempted to impart membranes with hydrophilic properties by grafting hydrophilic polymers to the surface. Water soluble, hydrophilic polymers have been covalently polymerized from or covalently attached to the membranes' surface via plasma grafting[9,10] or radical initiated polymerizations.[11,13] The modified membranes exhibit antifouling properties, but have only been demonstrated on a laboratory scale. Additionally, the presence of a thick gel layer on the surface of the membrane often adds mass transfer resistance to the membranes' interior and surfaces, decreasing permeability.[19-21] Many of the surface modifications require exotic reaction

conditions, long reaction times, and expensive reagents that are not compatible with the roll-to-roll manufacturing of state-of-the-art commercial membranes.

4.3 Objective

Previously, we have developed a novel photochemical surface modification of polymeric reverse osmosis membranes.[22] Photoactive perfluorophenyl azides (PFPAs) were utilized to generate highly reactive nitrenes (when exposed to UV light) that can covalently bind to the membranes' surfaces. Therefore, the membrane surfaces can be modified under ambient conditions and be completed within minutes, maintaining the roll-to-roll scalability of membrane manufacturing. Herein, we present a scalable process to functionalize the surface of commercial UF membrane with small molecule PFPA derivatives to impart anti-fouling properties. Modeling data are reported that indicate that specific components of surface energy plays an essential role in foulant adhesion forces. The data directed us to modify the UF membrane surfaces with water-soluble small molecules to maintain the membranes' high permeability, while achieving anti-fouling properties. The target species were readily synthesized from commercially available precursors without the use of hazardous and/or expensive materials and synthetic conditions. Commercial UF membranes were then photochemically modified and their properties compared to the unmodified membranes. The modified polyethersulfone membrane displays increased permeability and hydrophilicity relative to an unmodified membrane. Furthermore, the modified membrane exhibits outstanding foul-resistance against sodium alginate, a model foulant, during operation.

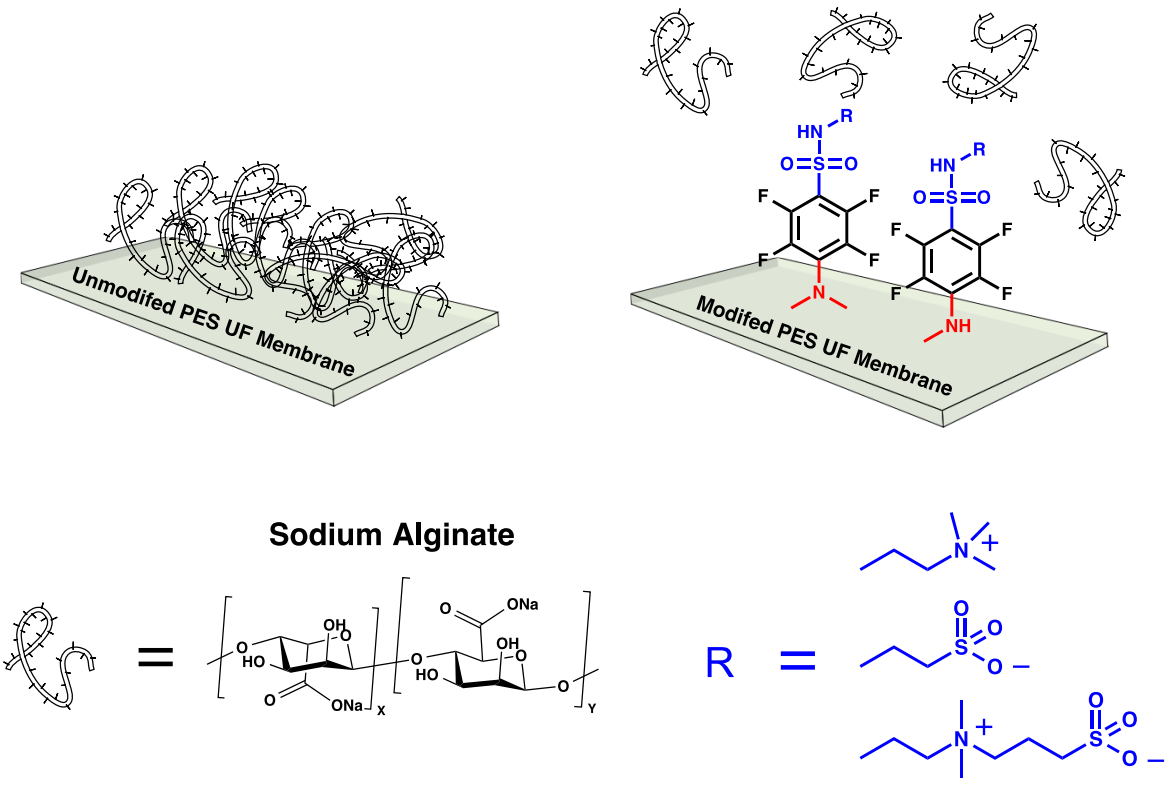

Figure 4.1. Schematic diagram illustrating sodium alginate adhesion to polyethersulfone ultrafiltration membranes unmodified (left) and modified with perfluorophenyl azide derivatives (right).

4.4 Adhesion Interaction Modeling

The transport and deposition of foulants are dictated by hydrodynamic and interfacial forces when a foulants contacts a membrane surface in solution.[23] Because hydrodynamic forces are theoretically identical, interfacial forces determine the affinities of foulants to a polymer's surface for the same foulants in solution. Kim *et al*.[23] defines these interfacial forces as the sum of the Lifshitz-van der Waals force, the acid-base force, and the electrostatic force, which excludes hydrodynamic forces. These forces are summarized by mathematical expressions in Equations 4.1, 4.2, and 4.3 below:[24,25]

$$F_{LW} = 2\pi h_0^2 \Delta G_{132}^{LW} a_p \left(\frac{1}{h^2}\right)\left(1 + \frac{5.32h}{\lambda_{LW}}\right)^{-1} \quad \textbf{(4.1)}$$

$$F_{AB} = 2\pi \Delta G_{132}^{AB} a_p \exp\left(-\frac{h_0 - h}{\lambda_{AB}}\right) \quad \textbf{(4.2)}$$

$$F_{EL} = 4\pi\varepsilon\left(\frac{zF}{RT}\right)^2 \left(\frac{\gamma_c \gamma_m}{\lambda_{EL}}\right) a_p \exp\left(-\frac{h}{\lambda_{EL}}\right) \quad \textbf{(4.3)}$$

where a_p is the radius of particle, h is the interfacial separation distance, h_0 is the minimum separation distance (0.157 nm), ΔG_{132}^{LW} and ΔG_{132}^{AB} the Lifshitz-van der Waals and Lewis acid-base interfacial energies, λ_{LW} (= 100 nm), λ_{AB} (≅ 0.6 nm), and λ_{EL} (= $[3.28\times10^9\sqrt{C_{NaCl}}]^{-1}$) are characteristic decay lengths for LW, AB, and EL interactions in water, ε the dielectric permittivity of water (= $78.5\times8.854\times10^{-12}CV^{-1}m^{-1}$), Υ_c and Υ_m are dimensionless surface (zeta) potentials $(\tanh[zF\zeta_{c/m}/4RT])$ and ζc and ζm are the zeta potentials of the particle and the membrane surface.[25]

In order to calculate the interfacial free energies (ΔG_{132}^{LW}, ΔG_{132}^{AB}, ΔG_{132}^{Tot}), the surface tension components of the membranes were determined with contact angles (θ) measured by using three different probe liquids that have known values of surface tension components.[26] The surface tension components (γ^{LW}, γ^+, γ^-) that were used have been reported elsewhere.[27-30] The extended Young-Dupré equation[31] (Equation 4.4) was used to calculate the surface tension components:

$$(1+\cos\theta)\gamma_l^{TOT} = 2\left(\sqrt{\gamma_s^{LW}\gamma_l^{LW}} + \sqrt{\gamma_s^{+}\gamma_l^{-}} + \sqrt{\gamma_s^{-}\gamma_l^{+}}\right) \quad \textbf{(4.4)}$$

where θ is the ideal contact angle formed between a droplet of liquid L and the smooth membrane surface, γ_S^{LW} and $\gamma_L^{LW}$are the apolar (Lifshitz-van der Waals) components of the surface tension of solid, S (membrane or particle) and liquid L, γ_S^+, γ_L^+, γ_S^-, γ_L^- and are the polar (electron-acceptor and electron donor) components of the surface tension of solid (*s*) and liquid (*l*), respectively.[32]

We denote the interfacial free energy at contact, ΔG_{132}^{Tot}, as a thermodynamic value that indicates the inherent affinity of a solid foulant (1) that interacts through a liquid media (3) with a solid membrane surface (2). ΔG_{132}^{Tot} was determined from Equation 4.5 below:

$$\Delta G_{132}^{Tot} = \Delta G_{132}^{LW} + \Delta G_{132}^{AB} \quad \textbf{(4.5)}$$

where ΔG_{132}^{LW} and $\Delta G_{132}^{AB}$are the Lifshitz–van der Waals and Lewis acid–base interfacial free energies, respectively. They can be calculated from Equation 4.6 and 4.7:[33]

$$\Delta G_{132}^{LW} = 2\left(\sqrt{\gamma_3^{LW}} - \sqrt{\gamma_1^{LW}}\right)\left(\sqrt{\gamma_2^{LW}} - \sqrt{\gamma_3^{LW}}\right) \quad \textbf{(4.6)}$$

$$\Delta G_{132}^{AB} = 2\sqrt{\gamma_3^{+}}\left(\sqrt{\gamma_1^{-}} + \sqrt{\gamma_2^{-}} - \sqrt{\gamma_3^{-}}\right) + 2\sqrt{\gamma_3^{-}}\left(\sqrt{\gamma_1^{+}} + \sqrt{\gamma_2^{+}} - \sqrt{\gamma_3^{+}}\right) - 2\sqrt{\gamma_1^{+}\gamma_2^{-}} - 2\sqrt{\gamma_1^{-}\gamma_2^{+}} \quad \textbf{(4.7)}$$

An electrokinetic analyzer (SurPASS Electrokinetic Analyzer, Anton-Paar GmbH) was used to calculate the membrane zeta potential (ζ_M). The analysis provides a slope of the streaming current versus pressure (*dI*/*dp*) from which the membrane zeta potential is derived.

The zeta potential was measured at pH 7±0.1 and 1 mM KCl was used as the electrolyte. The membrane zeta potential was calculated using the Helmholtz-Smoluchowski equation (Equation 4.8):

$$\zeta_M = \frac{dI}{dp} \cdot \frac{\mu}{\varepsilon \cdot \varepsilon_0} \cdot \frac{L}{A} \qquad \textbf{(4.8)}$$

where ε is the dielectric constant of the solution, ε_0 is the permittivity of vacuum, L is the length of the streaming channel and A is the cross-section of the streaming channel. The zeta potential was assumed to be constant at -54.5 mV, as measured for the unmodified PES membrane. The zeta potential for the unmodified and modified membranes varied slightly (within error of the experiment) and it was found that these nominal variations in the zeta potential produced negligible contributions to the total interfacial force.

4.5 Modification Procedure and Experimental

Commercial PES membranes were modified using a revised procedure from a previous publication.[22] Flat sheet membrane samples were cut into 4x10 cm^2 rectangular sheets. The membrane samples were dipped into a 0.1 mM solution containing the selected small molecule PFPA. The sheets were immediately placed under a 6 W UV lamp (254 nm) and irradiated for 60 seconds with an intensity of 1200 mW/cm^2. The membrane samples were then rinsed with a stream of deionized (DI) water and stored in a DI water bath. For contact angle measurements, thin strips of the membrane were cut out and attached to microscope glass slides using double sided tape. The slides were placed onto the sample platform of a KRÜSS DSA 10 goniometer used for the measurement. A series of drops of the corresponding liquid were placed manually

onto each membrane surface with a syringe before taking the angle measurement using software fitting. For XPS experiment samples, 1x1 cm^2 boron-doped (P-type) silicon wafers (0.002-0.0005 ohms/meter resistivity) were spin-coated at 2500 rpm for 30 seconds with polyethyleneimine. The top polyethersulfone layer was deposited on top of the polyethyleneimine layer by spin-coating from a 5 wt% *N*,*N*-dimethylformamide solution at 2500 rpm for 30 seconds. The samples were dried in a vacuum oven at 75 ºC overnight before modification. To modify the PES thin films, PES coated wafers were dipped in 0.1 mM PFPA solutions and irradiated under the same conditions as the membrane sheets mentioned above.

In order to evaluate the fouling resistance of the modified membranes, a lab-built cross-flow apparatus (Appendix C) was used to monitor the dynamic change of transmembrane pressure (TMP) in the presence of sodium alginate solution. A 19 cm^2 cutout of each membrane was compacted first using DI water at 16 psi for 2 hours. A balance connected to a computer was used to record and calculate the active flux. Once stable, permeate flux was then adjusted manually to 3.2 mL/min using a peristaltic pump. After 10 minutes of stable flux at 3.2 mL/min, the feed was switched to 200 ppm sodium alginate solution while maintaining the same flux until 300 mL of permeate was collected (first fouling stage). The feed was then switched back to DI water. Membranes were flushed with DI water for 5 min before changing the feed to sodium alginate solution again until 300 mL of permeate was collected at the same flux (second fouling stage). Pressure gauges were placed at both the feed side and the permeate side and connected to the computer. The TMP was calculated automatically throughout the cross-flow fouling test via Equation 4.9:

$$TMP = (P_{in} - P_{ret})/2 - P_{perm} \quad \textbf{(4.9)}$$

where P_{in} is the inlet pressure and P_{ret} are the pressure at the feed side and the retentate side of the membrane, respectively, and P_{perm} is the pressure on the permeate side of the film. The TMP increase of the modified membranes can then be compared with the control membranes. It's worth noting that in addition to the blank PES membrane as a control, the UV control membrane (same modification method without the PFPA solution) membrane was also analyzed to observe the impact of UV light exposure alone on the PES membrane.

Membrane rejection properties were tested by collecting the permeate during the first fouling stage and measuring the permeate's sodium alginate concentration using total organic compound (TOC) analysis. The sodium alginate rejection can be calculated from Equation 4.10:

$$R = [1- (C_p / C_f)] \times 100\% \quad \textbf{(4.10)}$$

where C_p and C_f are the concentration of sodium alginate in the permeate and feed, respectively.

4.6 Modeling Results

Figure 4.2a illustrates the results from modeling the interfacial forces for several foulants found in MBRs. Sodium alginate (SA), which has a strong attractive force to the polyethersulfone membrane surface, is a common polysaccharide-based extracellular polymeric substance (EPS) secreted by microorganisms that facilitates initial attachment of microbe to

membrane surfaces and provides the framework in biofilm formation.[34] Once the SA is anchored to the membrane surface, other foulants can readily attach to the polysaccharide and rapidly foul the membrane. In Figure 4.2b and 4.2c, the interfacial forces of *E. coli* and SA, respectively, have been broken down into their three components, electrostatic force (F_{EL}), acid-base force (F_{AB}), and Lifshitz-van der Waals force (F_{LW}). The greatest impact to the overall repulsive interfacial force of *E. coli* is the strong repulsion by the F_{AB} (Fig. 4.2b), outweighing the small F_{LW}, which is attractive, and the nominal FEL. For the overall attractive interfacial force of the SA, the attraction by the FAB again plays the dominant role (Fig. 4.2c). Since we cannot control the chemistry of the foulant exterior, these modeling results imply that varying the acid-base functionality of the membrane surface can make a dramatic impact in the interfacial forces of the membrane, drastically reducing membrane fouling.

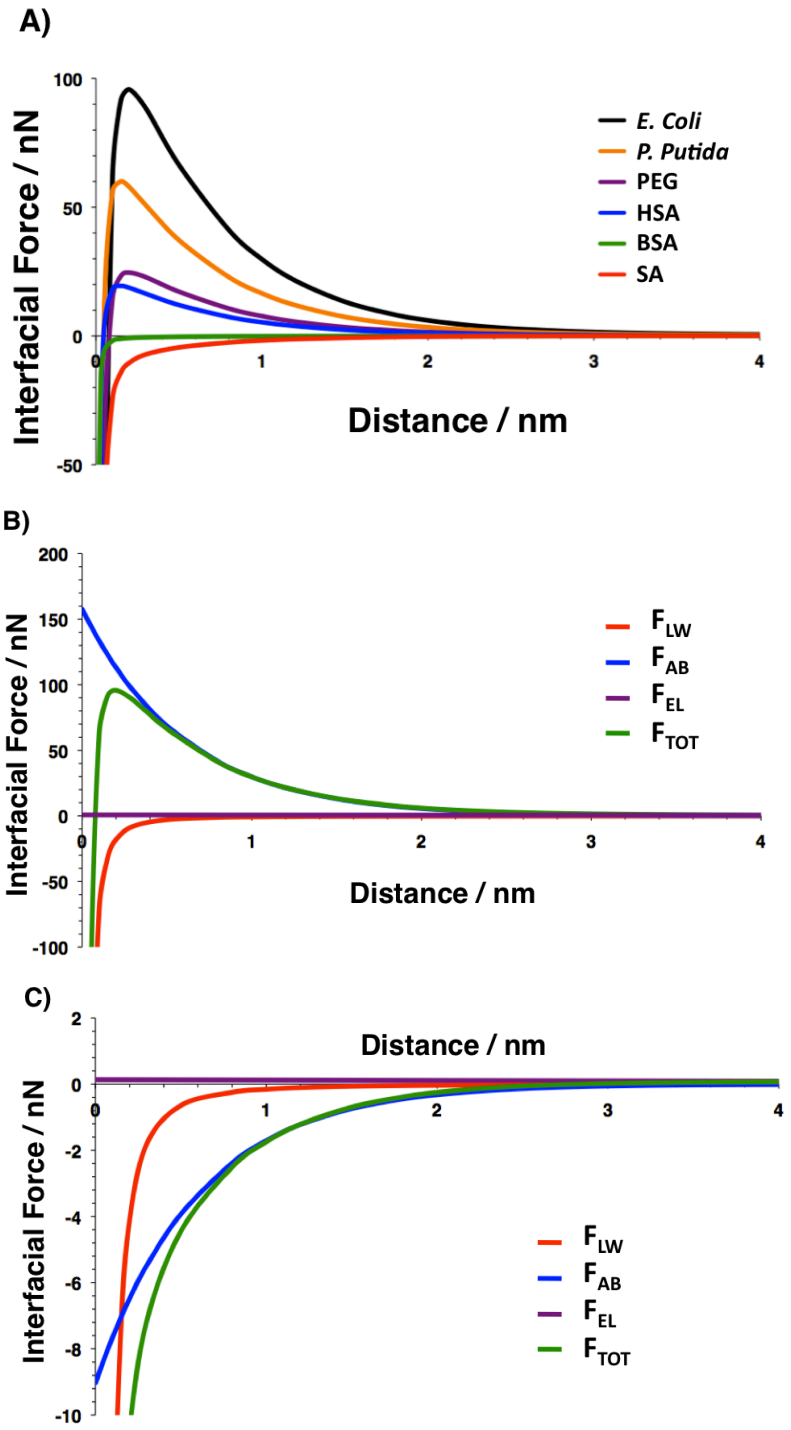

Figure 4.2. a) Interfacial forces between selected foulants in MBRs and PES. *E. coli* = *Escherichia coli*, *P. putida* = *Pseudomonas putida*, PEG = polyethylene glycol, HSA = human serum albumin, BSA = bovine serum albumin, SA = sodium alginate b) The interfacial forces of *E. coli* and PES broken down into their components c) The interfacial forces between sodium alginate and PES broken down into their components. F_{LW} = Lifshitz-van der Waals force, F_{AB} = acid-base force, F_{EL} = electrostatic force, F_{TOT} = total force

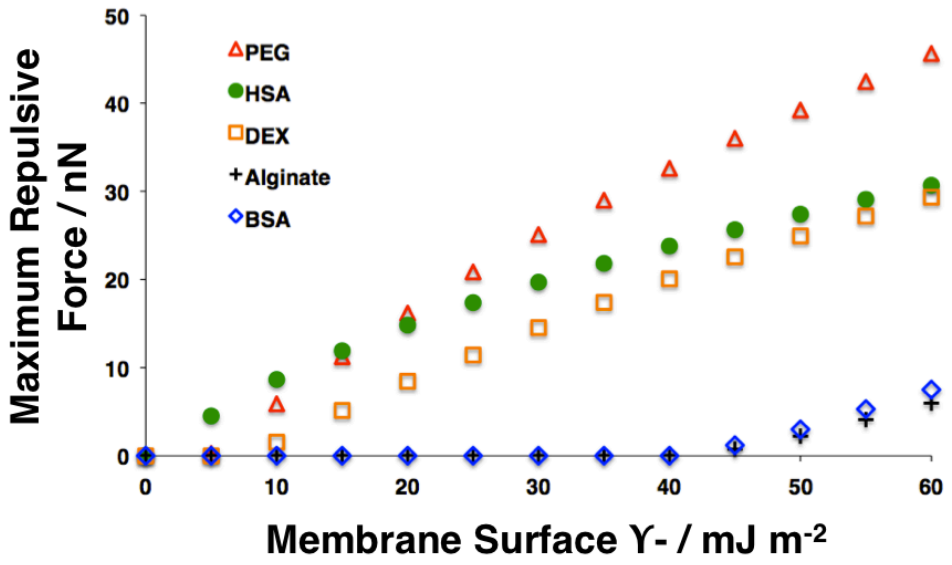

Figure 4.3. The effect of high γ- on repulsive forces between several foulants and a polyethersulfone membrane. PEG = polyethylene glycol, HSA = human serum albumin, DEX = dextran, BSA = bovine serum albumin

The F_{AB} can be quantified through contact angle measurements with different liquids, and can be further simplified into their interfacial tension components, electron-acceptors (γ+) and electron-donors (γ-). In work by Strathmann and coworkers,[27] these components for several polymers used to fabricate UF membranes were reported. Interestingly, there were relatively large changes to the γ- component compared with the small changes in the γ+ component across a wide spectrum of polymers. Thus, we were motivated to investigate the relationship between the γ- component of a surface and the repulsive force between several foulants, as shown in Figure 4.3. A fairly linear relationship exists between the maximum repulsive force and γ- for the foulants that possess high γ- values of their own. However, the foulants that have low γ- values (BSA and SA) require a membrane surface with high γ- values to achieve repulsion between the foulant and the membrane surface (Fig. 4.3). Our goal is to increase the γ- character of the membrane surface to achieve anti-fouling properties, without losses to membrane selectivity or permeability.

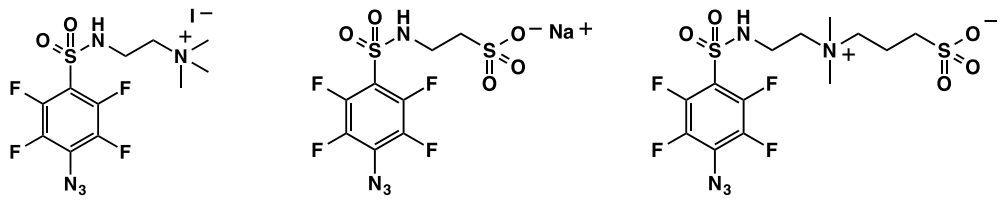

Figure 4.4. Target PFPA-derivatives.

4.7 Novel Synthesis of PFPA Small Molecules

In order to modify the membrane surface, three small molecule PFPA-derivatives were synthesized (Appendix C) that contain ionic groups to impart water solubility, as presented in Figure 4.4. Typically, PFPA target compounds are produced through an activated *N*-hydroxysuccinimide intermediate, which is synthesized via carbodiimide-mediated coupling.[35] Despite forming a stable compound that is able to perform solid-state surface modifications,[36] the synthesis of PFPA-NHS involves several steps and requires numerous protecting group manipulations. Additionally, the esterification necessitates the use of *N,N'*-dicyclohexylcarbodiimide—a potent allergen that is difficult to remove from the product—prohibiting the large scale synthesis of PFPA derivatives. Thus, we have developed a concise, facile synthesis of *para*-azido perfluorophenylsulfonamides (Scheme 4.1). Our approach utilizes commercially available pentafluorophenyl sulfonyl chloride **1**, which produces the desired derivative in two or three steps. This approach has the advantages of a short step count, mild reaction conditions, and scalability.

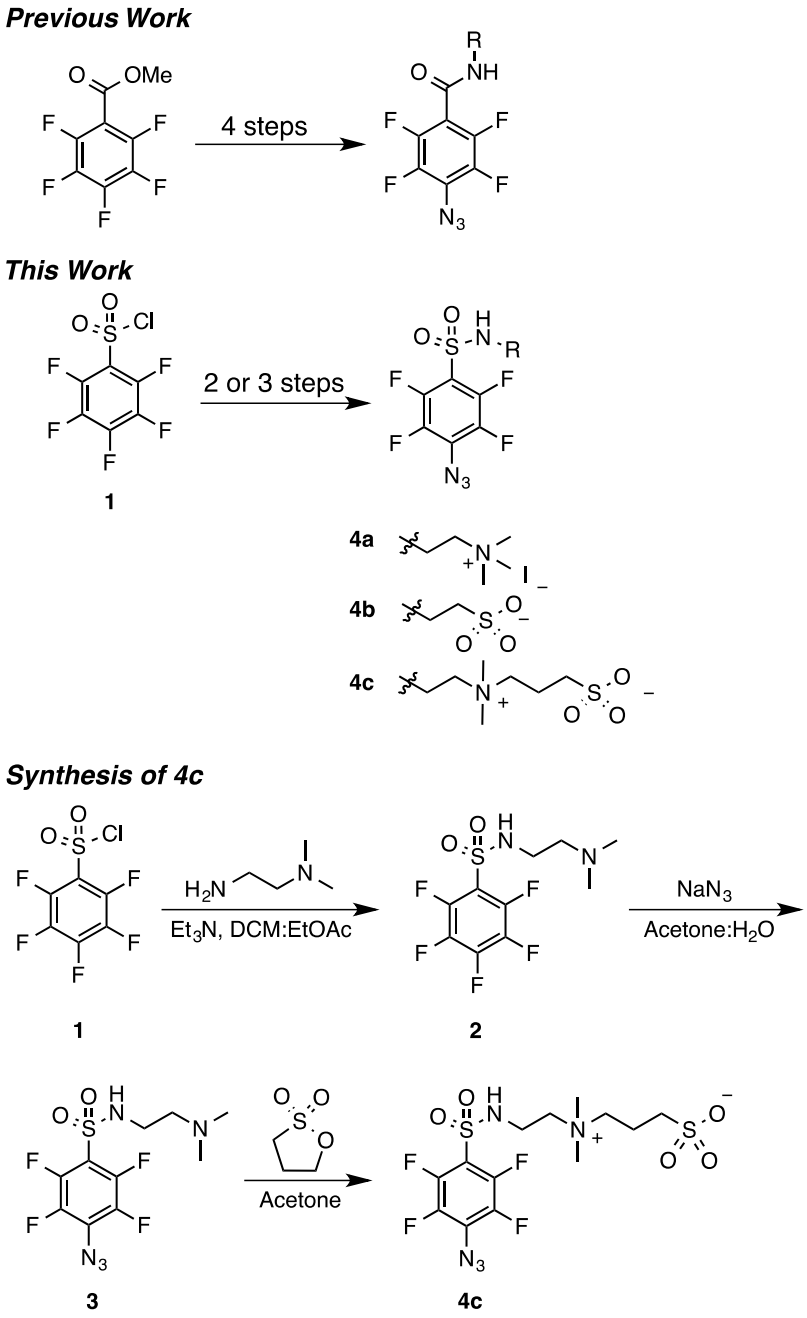

Scheme 4.1. Synthesis of PFPA small molecules from pentafluorophenyl sulfonyl chloride.

Our strategy utilizes an initial reaction of **1** with an amine to form sulfonamide **2**. The strong electron-withdrawing effect of the sulfonamide activates the para position to subsequent nucleophilic substitution by an azide ion producing compound **3**. It is important to note that in an

analogous series utilizing pentaflourophenyl amides, the nucleophilic substitution reaction fails to occur, even under forcing conditions. Compound **3** can be elaborated to the desired PFPA in a single operation, with the synthesis of **4c** given as an example. Additionally, we predict that the presence of a sulfonamide will add electron-donating functionality to the final products that ultimately impart higher γ- character to the modified membranes.

Table 4.1 Surface Properties of Unmodified and Modified PES Membranes

Membrane	Fluorine Content (atomic %)	CA (DI water)	CA (Ethylene Glycol)	CA (Diiodomethane)	ΔG^{lw} (mJ/m^2)	ΔG^{Y+} (mJ/m^2)	ΔG^{Y-} (mJ/m^2)	ΔG^{mlm}
PES	-	49.8	28.9	17.7	48.4	4E-07	29.4	-3.0
PES UV	-	48.8	29.9	23.3	46.8	1E-03	31.3	1.6
PES PFPA(-)	0.5%	46.8	25.3	21.6	47.3	1E-02	32.1	2.3
PES PFPA(+)	0.4%	45.7	23.2	23.7	46.6	4E-02	32.8	3.9
PES PFPA(+-)	0.7%	40.4	20.1	19.2	48.0	9E-03	38.4	12.5

4.8 Membrane Characterization

After commercial PES membranes were modified with the three PFPA derivatives, X-ray photoelectron spectroscopy (XPS) and sessile drop contact angle (CA) measurements with different liquids were conducted to analyze chemical and physical changes to the surface of the membranes (Table 4.1). The results from the XPS experiment performed directly on the surface of the commercial membranes (PES on a non-woven polyester support) showed too much noise in the spectra to make any conclusions. Therefore, representative samples were made by spin-

coating thin films of PES onto a doped silicon wafer and modifying the spin-coated samples with the PFPA precursors under the same conditions as the commercial membranes. After conducting contact angle measurements on modified membrane samples with multiple liquids, the surface tension components were quantified.

As shown in Table 4.1, the fluorine content of the samples confirm the grafting of the small molecule PFPA derivatives to the surface. To determine the effect of UV light on the membrane, a sample was included that was exposed to the same UV intensity as the modified samples, without exposure to the PFPA-derivatives. Upon modification, there is a slight decrease in the apparent contact angle of the modified membrane when polar liquids are used (DI water, ethylene glycol) and an increase in the corresponding Gibbs free energy (ΔG^{mwm}). Conventionally, a surface is considered hydrophilic when its contact angle is <90º. We enlist the use of ΔG^{mwm} to describe surface hydrophilicity as a method to quantify the amount of energy required to expel the adsorbed water layer when two identical membrane surfaces are brought into contact. Therefore, a positive ΔG^{mwm} requires energy to expel water when the two membrane surfaces unite, deeming those surfaces "hydrophilic." Figure 4.5 illustrates the effect of changes in apparent contact angle of water and ethylene glycol on ΔG^{mwm} of the modified and unmodified membrane samples. The contact angle of the membranes using diidomethane showed little change, highlighting the insignificant role on the ΔG^{mwm} of the membrane, and thus was held at 20º. Under our definition of hydrophilicity, the zwitterionic PFPA(+-) modified membrane surface exhibits the greatest hydrophilicity compared to the other modified and unmodified membrane surfaces.[36] Furthermore, as shown in Table 4.1, there is an overall increase in the γ- components of the membranes, when compared to the unmodified membrane samples.

It is important to note that there are slight changes in the ΔG^{lwl} and $\gamma+$ values, but these negligible changes have minimal effect on the attractive/repulsion forces compared to the difference $\gamma-$ as mentioned above.

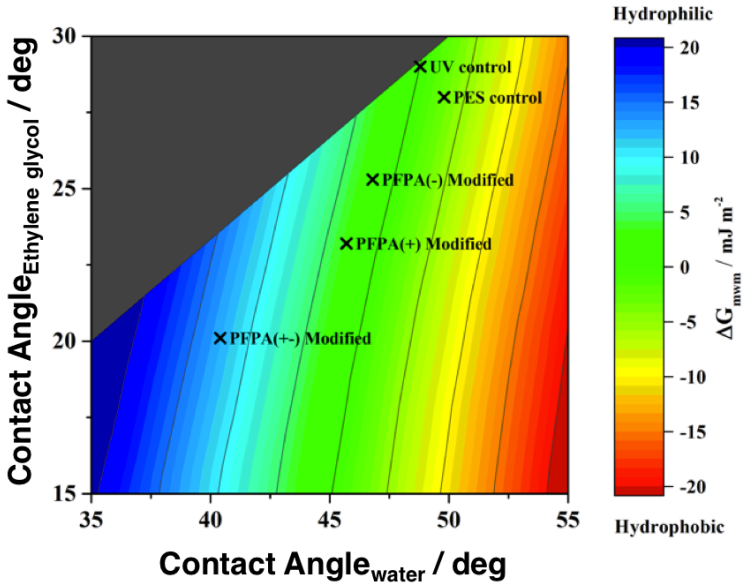

Figure 4.5. Hydrophilicity of unmodified and modified membranes based on the ΔG^{mwm} surface energy.

From the surface energy data listed in Table 4.1, the total interfacial forces between sodium alginate and the modified and unmodified membranes were plotted, as shown in Figure 4.6. In comparison to the commercial, unmodified PES membrane, there is an apparent decrease in attraction at the interface of the modified membranes and SA. The UV treated, PFPA(-), and PFPA(+) membranes possess similar $\gamma-$ values (31.3, 32.1, and 32.8 mJ/m^2, respectively) and demonstrate similar interfacial forces. The PFPA(+-) modified surface stands out with the least attractive force with SA, exemplifying the significance of a high $\gamma-$ (38.4 mJ/m^2).

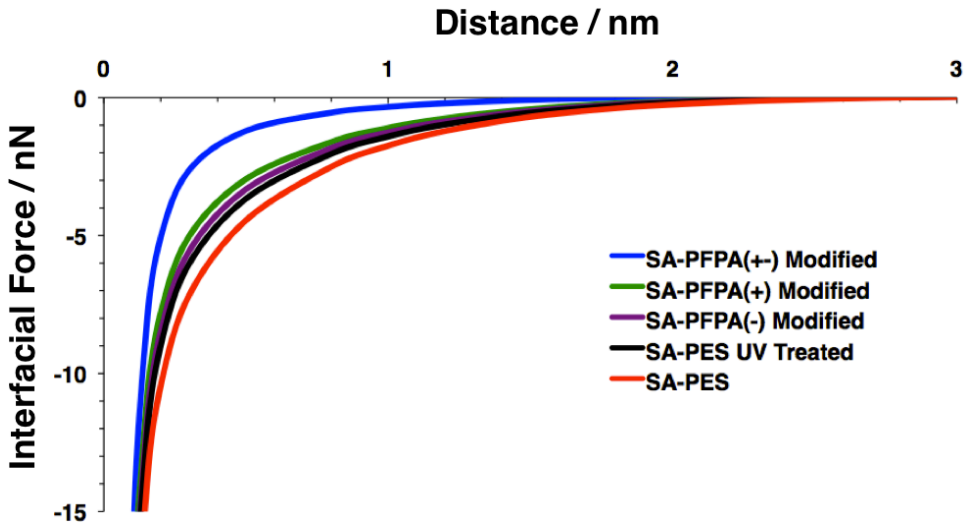

Figure 4.6. Overall interfacial force between sodium alginate and the unmodified and modified membrane surfaces.

4.9 Membrane Performance

To experimentally compare the effect of the increased electron donor moieties on the surface of the membrane with membrane fouling rate, membrane samples were placed in a cross-flow system (Appendix C). Pressure transducers were used to record a live feed of the TMP during operation, and membrane fouling was directly correlated to the change in TMP over the duration of the experiment. The results of the experiments are shown in a short-term study (Figure 4.7). Two fouling rates were recorded, before and after a 5-minute rinse by switching the feed solution to DI water, then resuming the experiments with the SA feed solution.

The commercial PES membrane possessed the greater initial and second stage-fouling rate compared to the modified membranes. The second stage fouling is presumably higher than the initial stage due to unsuccessful rinsing of the SA layer from the surface of the membrane,

enabling additional SA particles to attach. Among the modified membranes, the PFPA(+-) coated

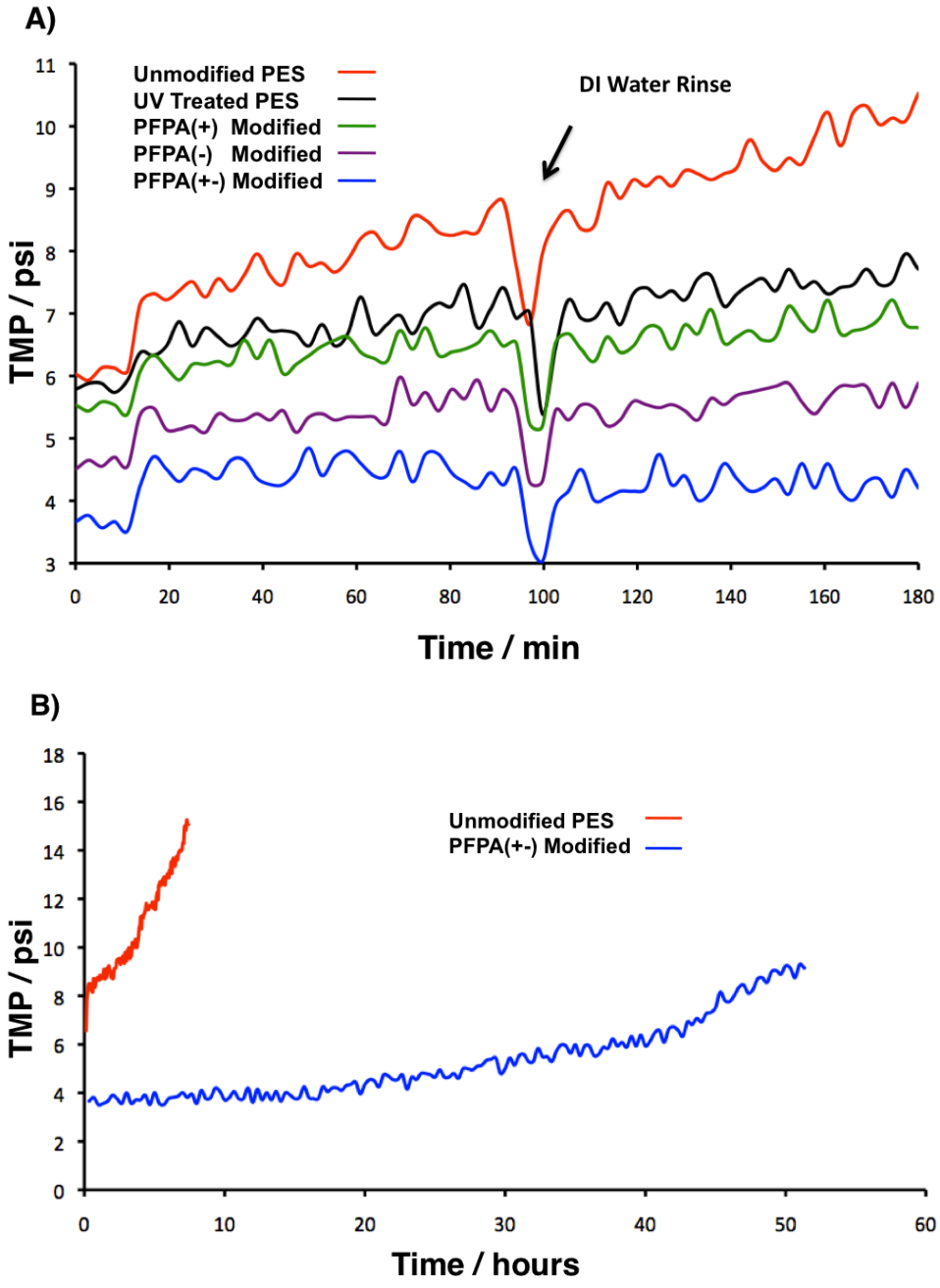

Figure 4.7. (A) A short and (B) a long term fouling study of the unmodified and modified membranes.

membrane demonstrates the greatest γ- and greatest anti-fouling ability, with a negative fouling rate for the 3-hour comparative study. Zwitterionic surface monolayers[38] and polymers[11,39,40] are

shown to have ultra-low fouling properties under static conditions. Furthermore, the PFPA(+-) modified membrane surface approaches the ~40 mJ/m^2 threshold required to produce repulsive forces between SA and a surface (Figure 4.3). When the sodium alginate solution is initially introduced, the TMP immediately increases due to the rapid change in concentration of SA. However, due to the contribution of repulsion of the membrane surface and the cross-flow velocity of the retentate, the particles are removed at a faster rate than the membrane is fouled. Over a longer duration of time, the modified membrane begins to foul, as observed in a long term fouling study shown in Figure 4.3, right. When running the cross-flow experiment for >2 days, there is only a ~4 psi change in the TMP. In comparison, the same long-term cross-flow experiment was conducted with the unmodified PES membrane. Because the TMP reaches the inlet pressure, there is no permeation through the membrane and the experiment is stopped.

Table 4.2 Performance Properties of Unmodified and Modified Membranes

Membrane	1st Stage Fouling Rate (psi/h)	2nd Stage Fouling Rate (psi/h)	Pure Water Permeability (LMH/bar)	Rejection of SA
Unmodified PES	0.85	1.28	1.069	98.0 %
PES UV Treated	0.54	0.54	1.136	98.8 %
PES-PFPA(+)	0.32	0.41	1.202	98.3 %
PES-PFPA(-)	0.22	0.22	1.603	97.7 %
PES-PFPA(+-)	-0.04	-0.06	1.804	98.7 %

In addition to imparting anti-fouling ability to the membrane surfaces, the PFPA grafting treatment also increases the permeability of the membrane. The modified membranes all demonstrate greater permeability than the unmodified membrane, with the PES-PFPA(+-) modified membrane exhibiting a water permeability 69% greater than the unmodified PES membrane. We believe that the increased permeability is caused by a decrease in molecular weight (chain scission) of the PES polymer at the membrane surface. Aromatic polyethersulfones are known to undergo photolysis into lower molecular species when exposed to UV irradiation.[41] Additionally, the covalent grafting of water-soluble analogs to the backbone of water insoluble polymers can impart water solubility to the top layer of PES polymeric chains. When increasing the concentration of a PFPA-derivative coating solution to increase graft density, visible degradation is observed under an optical microscope and bovine serum albumin rejection decreases (Appendix C). When a 0.1 mMol solution is used, the membrane surface is successfully modified with increased water permeability and negligible changes in SA rejection. Typically, higher permeability causes higher fouling rates, due to greater permeation drag forces and a more compressed cake layer.[23] Although the PFPA-PES membranes possess higher permeability, they maintain lower fouling rates, exemplifying the anti-fouling properties of the modified membranes.

4.10 Conclusions

In this chapter, our modeling data highlights the importance of controlling the γ- of the membrane surface to enhance the repulsion of foulants from a membrane surface. On the basis of this modeling result, we have synthesized novel PFPA small molecules to increase the γ- of commercial PES membranes, demonstrating a scalable synthesis to produce photoactive PFPA

small molecules in large quantities. The target compounds were easily prepared and readily grafted to the membrane surface utilizing a modified photochemical procedure that we have previously developed. In comparison to an unmodified, commercial membrane, the modified membranes exhibited enhanced γ- and hydrophilicity. The antifouling ability of the modified membranes was investigated, with the zwitterionic PFPA derivative demonstrating the greatest antifouling ability. When challenged against a solution of sodium alginate, the zwitterionic PFPA modified membrane possessing ultralow fouling properties was allowed to operate for 50+ hours with only a 5 psi increase in TMP. We believe that fouling-resistant UF membranes will decrease the cost of MBR technology, making use of MBRs more widespread for wastewater treatment.

4.11 Acknowledgments

This work was supported by the National Science Foundation SUSchem grant CBET 1337065 (E.M.V and R.B.K.) and a National Science Foundation—Graduate Research fellowship (B.M.). Additional support was provided by the National Science Foundation under Grant CHE 1125054 (R.J. and Y.R.). Mass Spectrometry Instrumentation was made available through the support of Greg Khitrov and was collected through a project described and supported by Grant Number S10-RR025631 from the National Center for Research Resources. The content is solely the responsibility of the authors and does not necessarily represent the official views of the National Center for Research Resources or the National Institutes of Health. The authors would also like to thank Soomin Kim for supplying spin-coated PES on silicon wafers.

References

(1) Shannon, M. a; Bohn, P. W.; Elimelech, M.; Georgiadis, J. G.; Mariñas, B. J.; Mayes, A. M. Science and technology for water purification in the coming decades. *Nature* **2008**, *452*, 301–310.

(2) Service, R. F. Desalination freshens up. *Science* **2006**, *313*, 1088–1090.

(3) California: Governor Signs $1 Billion Water Package. *The New York Times*. The New York Times, 27 Mar. 2015. Web access. 21 Apr. 2015.

(4) Ng, A. N. L.; Kim, A. S. A mini-review of modeling studies on membrane bioreactor (MBR) treatment for municipal wastewaters. *Desalination* **2007**, *212*, 261–281.

(5) Tchobanoglous, G.; Burton, F. L.; Stensel, H. D.; Eddy, M. &. *Wastewater Engineering: Treatment and Reuse*; McGraw-Hill higher education; McGraw-Hill Education, **2003**.

(6) Le-Clech, P.; Chen, V.; Fane, T. A. G. Fouling in membrane bioreactors used in wastewater treatment. *J. Memb. Sci.* **2006**, *284*, 17–53.

(7) Pollice, A.; Brookes, A.; Jefferson, B.; Judd, S. Sub-critical flux fouling in membrane bioreactors — a review of recent literature. *Desalination* **2005**, *174*, 221–230.

(8) Judd, S. The status of membrane bioreactor technology. *Trends Biotechnol.* **2008**, *26*, 109–116.

(9) Zhao, Z.-P.; Li, J.; Chen, J.; Chen, C.-X. Nanofiltration membrane prepared from polyacrylonitrile ultrafiltration membrane by low-temperature plasma: 2. Grafting of styrene in vapor phase. *J. Memb. Sci.* **2005**, *251*, 239–245.

(10) Mauter, M. S.; Wang, Y.; Okemgbo, K. C.; Osuji, C. O.; Giannelis, E. P.; Elimelech, M. Antifouling Ultrafiltration Membranes via Post-Fabrication Grafting of Biocidal Nanomaterials. *ACS Appl. Mater. Interfaces* **2011**, *3*, 2861–2868.

(11) Yang, R.; Jang, H.; Stocker, R.; Gleason, K. K. Synergistic Prevention of Biofouling in Seawater Desalination by Zwitterionic Surfaces and Low-Level Chlorination. *Adv. Mater.* **2014**, *26*, 1711–1718.

(12) Zou, L.; Vidalis, I.; Steele, D.; Michelmore, A.; Low, S. P.; Verberk, J. Q. J. C. Surface hydrophilic modification of RO membranes by plasma polymerization for low organic fouling. *J. Memb. Sci.* **2011**, *369*, 420–428.

(13) Van Wagner, E. M.; Sagle, A. C.; Sharma, M. M.; La, Y.-H.; Freeman, B. D. Surface modification of commercial polyamide desalination membranes using poly(ethylene glycol) diglycidyl ether to enhance membrane fouling resistance. *J. Memb. Sci.* **2011**, *367*, 273–287.

(14) Kang, G.; Yu, H.; Liu, Z.; Cao, Y. Surface modification of a commercial thin film composite polyamide reverse osmosis membrane by carbodiimide-induced grafting with poly(ethylene glycol) derivatives. *Desalination* **2011**, *275*, 252–259.

(15) Rana, D.; Matsuura, T. Surface modifications for antifouling membranes.. *Chem. Rev.* **2010**, *110*, 2448–2471.

(16) Adout, A.; Kang, S.; Asatekin, A.; Mayes, A. M.; Elimelech, M. Ultrafiltration Membranes Incorporating Amphiphilic Comb Copolymer Additives Prevent Irreversible Adhesion of Bacteria. *Environ. Sci. Technol.* **2010**, *44*, 2406–2411.

(17) McVerry, B. T.; Temple, J. A. T.; Huang, X.; Marsh, K. L.; Hoek, E. M. V; Kaner, R. B. Fabrication of Low-Fouling Ultrafiltration Membranes Using a Hydrophilic, Self-Doping Polyaniline Additive. *Chem. Mater.* **2013**, *25*, 3597–3602.

(18) Huang, X.; McVerry, B. T.; Marambio-Jones, C.; Wong, M. C. Y.; Hoek, E. M. V; Kaner, R. B. Novel chlorine resistant low-fouling ultrafiltration membrane based on a hydrophilic polyaniline derivative. *J. Mater. Chem. A* **2015**, *3*, 8725–8733.

(19) Louie, J. S.; Pinnau, I.; Ciobanu, I.; Ishida, K. P.; Ng, A.; Reinhard, M. Effects of polyether–polyamide block copolymer coating on performance and fouling of reverse osmosis membranes. *J. Memb. Sci.* **2006**, *280*, 762–770.

(20) Sagle, A. C.; Van Wagner, E. M.; Ju, H.; McCloskey, B. D.; Freeman, B. D.; Sharma, M. M. PEG-coated reverse osmosis membranes: Desalination properties and fouling resistance. *J. Memb. Sci.* **2009**, *340*, 92–108.

(21) Gilron, J.; Belfer, S.; Väisänen, P.; Nyström, M. Effects of surface modification on antifouling and performance properties of reverse osmosis membranes. *Desalination* **2001**, *140*, 167–179.

(22) McVerry, B. T.; Wong, M. C. Y.; Marsh, K. L.; Temple, J. A. T.; Marambio-Jones, C.; Hoek, E. M. V; Kaner, R. B. Scalable Antifouling Reverse Osmosis Membranes Utilizing Perfluorophenyl Azide Photochemistry. *Macromol. Rapid Commun.* **2014**, *35*, 1528–1533.

(23) Kim, S.; Marion, M.; Jeong, B.-H.; Hoek, E. M. V. Crossflow membrane filtration of interacting nanoparticle suspensions. *J. Memb. Sci.* **2006**, *284*, 361–372.

(24) Kang, S.-T.; Subramani, A.; Hoek, E. M. V; Deshusses, M. A.; Matsumoto, M. R. Direct observation of biofouling in cross-flow microfiltration: mechanisms of deposition and release. *J. Memb. Sci.* **2004**, *244*, 151–165.

(25) Subramani, A.; Hoek, E. M. V. Direct observation of initial microbial deposition onto reverse osmosis and nanofiltration membranes. *J. Memb. Sci.* **2008**, *319*, 111–125.

(26) Kim, S.; Hoek, E. M. V. Interactions controlling biopolymer fouling of reverse osmosis membranes. *Desalination* **2007**, *202*, 333–342.

(27) Cornelissen, E. R.; van den Boomgaard, T.; Strathmann, H. Physicochemical aspects of polymer selection for ultrafiltration and microfiltration membranes. *Colloids Surfaces A Physicochem. Eng. Asp.* **1998**, *138*, 283–289.

(28) Hong, H.; Peng, W.; Zhang, M.; Chen, J.; He, Y.; Wang, F.; Weng, X.; Yu, H.; Lin, H. Thermodynamic analysis of membrane fouling in a submerged membrane bioreactor and its implications. *Bioresour. Technol.* **2013**, *146*, 7–14.

(29) Guillen, G. R., McVerry, B. T., Farrell, T., Kaner, R. B., Hoek, E. M. V., Tuning the properties of polyaniline-based ultrafiltration membranes with chemical post-treatments. J. Membr. Sci., **2016**. *Resubmitted*.

(30) Jin, X.; Huang, X.; Hoek, E. M. V. Role of Specific Ion Interactions in Seawater RO Membrane Fouling by Alginic Acid. *Environ. Sci. Technol.* **2009**, *43*, 3580–3587.

(31) van Oss, C. J. Development and applications of the interfacial tension between water and organic or biological surfaces. *Colloids Surfaces B Biointerfaces* **2007**, *54*, 2–9.

(32) Wang, J.; Mo, Y.; Mahendra, S.; Hoek, E. M. V. Effects of water chemistry on structure and performance of polyamide composite membranes. *J. Memb. Sci.* **2014**, *452*, 415–425.

(33) van Oss, C. J. Acid—base interfacial interactions in aqueous media. *Colloids Surfaces A Physicochem. Eng. Asp.* **1993**, *78*, 1–49.

(34) Sheng, G.-P.; Yu, H.-Q.; Li, X.-Y. Extracellular polymeric substances (EPS) of microbial aggregates in biological wastewater treatment systems: A review. *Biotechnol. Adv.* **2010**, *28*, 882–894.

(35) Keana, J. F. W.; Cai, S. X. New reagents for photoaffinity labeling: synthesis and photolysis of functionalized perfluorophenyl azides. *J. Org. Chem.* **1990**, *55*, 3640–3647.

(36) Liu, L.-H.; Yan, M. Perfluorophenyl Azides: New Applications in SurfaceFunctionalization and Nanomaterial Synthesis. *Acc. Chem. Res.* **2010**, *43*, 1434–1443.

(37) Subramani, A.; Hoek, E. M. V. Biofilm formation, cleaning, re-formation on polyamide composite membranes. *Desalination* **2010**, *257*, 73–79.

(38) Holmlin, R. E.; Chen, X.; Chapman, R. G.; Takayama, S.; Whitesides, G. M. Zwitterionic SAMs that Resist Nonspecific Adsorption of Protein from Aqueous Buffer. *Langmuir* **2001**, *17*, 2841–2850.

(39) Jiang, S.; Cao, Z. Ultralow-Fouling, Functionalizable, and Hydrolyzable Zwitterionic Materials and Their Derivatives for Biological Applications. *Adv. Mater.* **2010**, *22*, 920–932.

(40) Mi, L.; Jiang, S. Integrated Antimicrobial and Nonfouling Zwitterionic Polymers. *Angew. Chemie Int. Ed.* **2014**, *53*, 1746–1754.

(41) Yamagishi, H.; Crivello, J. V.; Belfort, G. Development of a novel photochemical technique for modifying poly (arylsulfone) ultrafiltration membranes*J. Memb. Sci.* **1995**, *105*, 237–247.

Chapter 5

Conclusions and Summary

In Chapter 1, a brief history and current status of membrane technology is described, specifically for UF and RO membranes. Large areas of ultrafiltration membranes are cast using commodity polymers, utilizing the phase inversion method to create thin, porous films. Reverse osmosis membranes are made from UF membranes by forming a thin, dense polymer layer on the surface of the UF membrane by interfacial polymerization. UF membranes can be formed into several different configurations; RO membranes are limited to spiral wound configurations due to the high pressure of operation. Membrane fouling drastically affects both UF and RO, causing reduction in performance and increased operation, energy, and maintenance costs.

Chapter 2 investigates a new polyaniline-based additive for UF membranes. Membrane hydrophilicity is directly linked to fouling; a more hydrophilic membrane will reduce the hydrophobic interactions between the membrane surface and foulants.

- Sulfonated polyaniline (SPANi) is a water-insoluble, superhydrophilic, and zwitterionic polymer that can be processed at elevated pH. SPANi was blended into polysulfone membranes at different wt% to determine its effect on membrane performance, hydrophilicity, morphology, and fouling.
- The blending of SPANi directly into polysulfone casting solution maintains the scalability of membrane fabrication.
- Increased SPANi content in the final membrane increased hydrophilicity and anti-fouling properties with nominal changes in performance and rejection of the membranes. In a fouling test with bovine serum albumin, the SPANi/PSf composite membranes all exhibited lower fouling and greater flux recovery after rinsing the membranes with DI water.

In Chapter 3, a new method to modify commercial RO membranes with hydrophilic graft polymers is explored. Utilizing perfluorophenyl azide photochemistry, polyethylene glycol terminated with perfluorophenyl azides can be applied to membrane surfaces under ambient conditions, maintaining the roll-to-roll manufacturing of RO membranes. Several PFPA-terminated PEG macromolecules were synthesized with varying molecular weight to determine the effect of molecular weight on anti-fouling ability. Static membrane fouling tests using *E. coli* were conducted to demonstrate reduction in bacterial adhesion.

- The successful modification of commercial RO membranes as demonstrated with a new method. PFPA-PEG derivatives were dipped into a solution of water containing the photoactive molecules, dried, and exposed to a low power UV lamp for 60 seconds. The modified membrane surfaces exhibited lower sessile drop contact angles, confirming the hydrophilic modification. Additionally, ATR-IR and XPS measurements confirm the existence of PEG and PFPA covalently bound to the surface of the RO membranes, respectively.
- The presence of PEG grafted to the membrane surfaces caused slight changes to the membrane performance. When grafting with higher molecular weight PEG, the water permeability decreased due to increased hydraulic resistance of the PEG chains. However, there was a slight increase in NaCl rejection with increased molecular weight PFPA-PEG graft polymers.
- In a static bacterial adhesion test, membrane coupons grafted with higher molecular weight PEGs experience lower adhesion of *E. coli*. Using ImageJ software, the

membrane surface with the highest molecular weight PEG grating (MW = 5000), exhibited less than 1% surface coverage of *E. coli* after incubation overnight.

Chapter 4 discusses utilizing PFPA chemistry with UF membranes used for membrane bioreactors. First, modeling data indicate that foulant-membrane interactions rely heavily on Lewis acid-base interactions. A membrane with greater electron-donating functionality will possess increased repulsive interactions with foulants leading to lower fouling. To impart greater electron-donating functionality to commercial membranes, perfluorophenyl azide chemistry is implemented once again.

- The synthesis of new, water-soluble PFPA small molecules is presented. Several small molecules were synthesized containing electron-donating functionalities and different ionic groups to impart water-solubility. The PFPA derivatives were covalently bound to commercial polyethersulfone flat sheet membranes, as confirmed by XPS.
- Contact angle measurements with several liquids indicate that the electron-donating functionalies of the modified membranes increased after the modification. A zwitterionic PFPA derivative exhibited the greatest electron-donicity and was considered the most hydrophilic.
- In short-term fouling tests with sodium alginate (the "stickiest" foulant), the modified membranes demonstrated lower fouling rates in comparison to an unmodified commercial membrane. The zwitterionic PFPA exhibited the lowest fouling rate and could be operated for longer periods of times without cleaning.

Supporting Information

Appendix A

Instrumentation. Fourier Transform Infrared (FT-IR) spectroscopy was performed on a JASCO FT/IR-6300. X-ray Photoelectron Spectroscopy (XPS) was performed on a Kratos AXIS Ultra DLD with a monochromatic Al Kα X-ray source operating at 10 mA and 15 kV. Spectra have been charge corrected to the main line of the carbon 1s peak set to 284.6 eV.

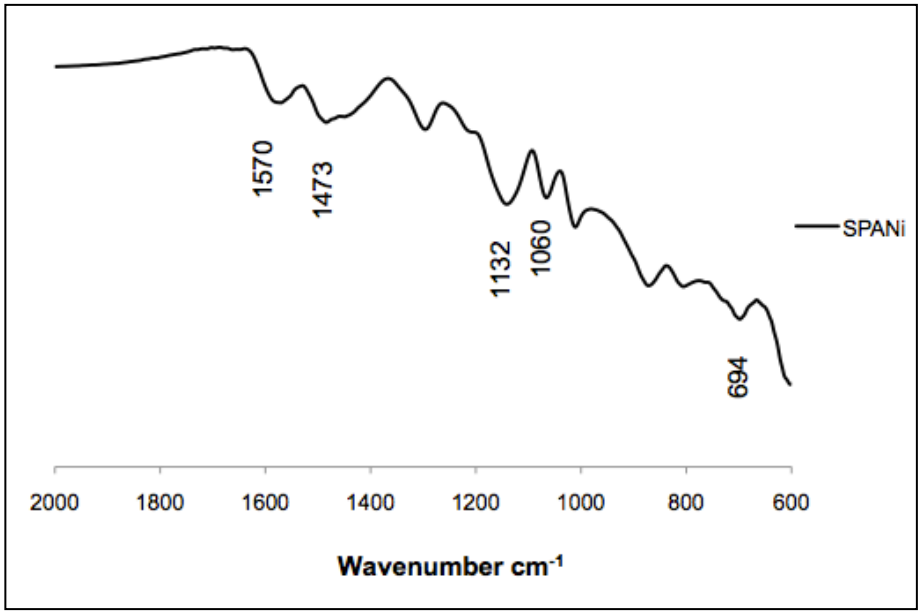

Figure A.1. FT-IR spectrum of SPANi produced via sulfonation with fuming sulfuric acid. Strong S=O stretching at 1132 cm^{-1} and 1060 cm^{-1} and S-O stretching at 694 cm^{-1} confirm the existence of sulfonic acid groups along the backbone of the polymer.[1]

Table A1. Elemental Analysis Results Obtained from XPS after Sulfonation

C% (1s)	O% (1s)	N% (1s)	S% (2p)	S:N Ratio
69.48	17.88	8.52	4.11	0.482

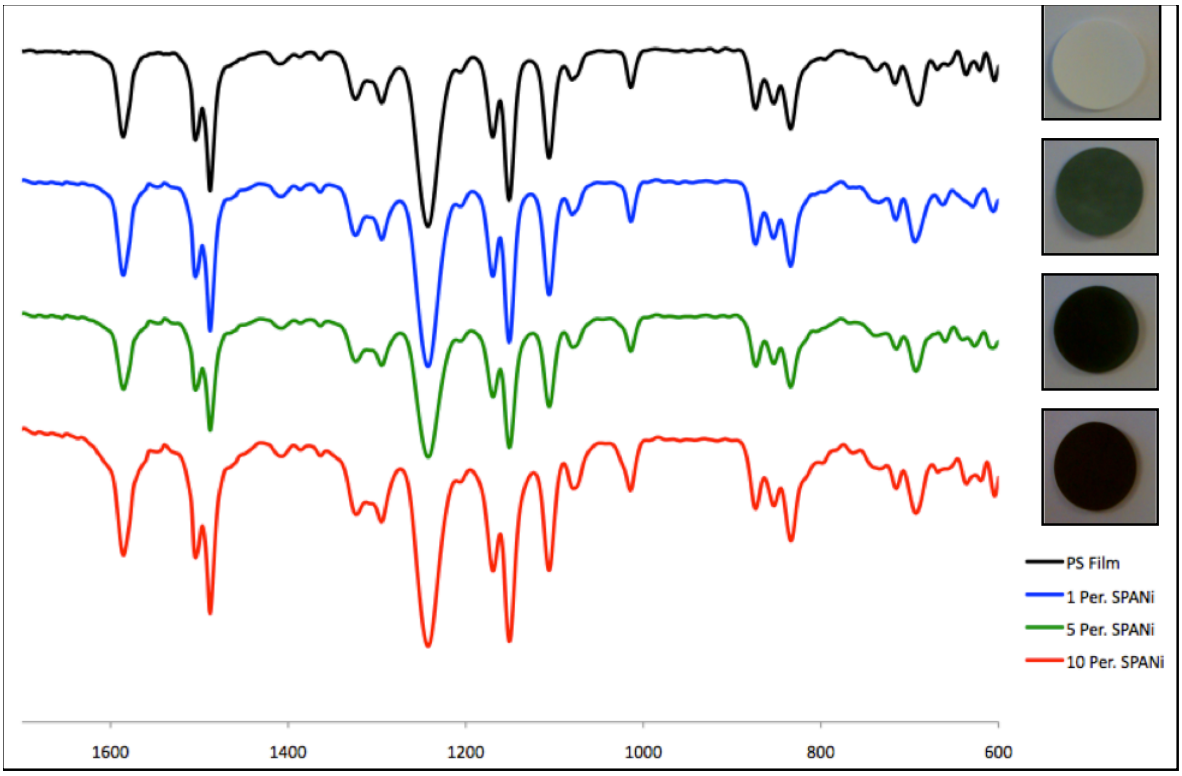

Figure A.2. FT-IR spectra of the PS pure membrane and SPANi/PS composites. No variance in the spectra is seen because of the dominance of PS within the membrane films. However, a strong color change with increasing amounts of SPANi is observed (inset).

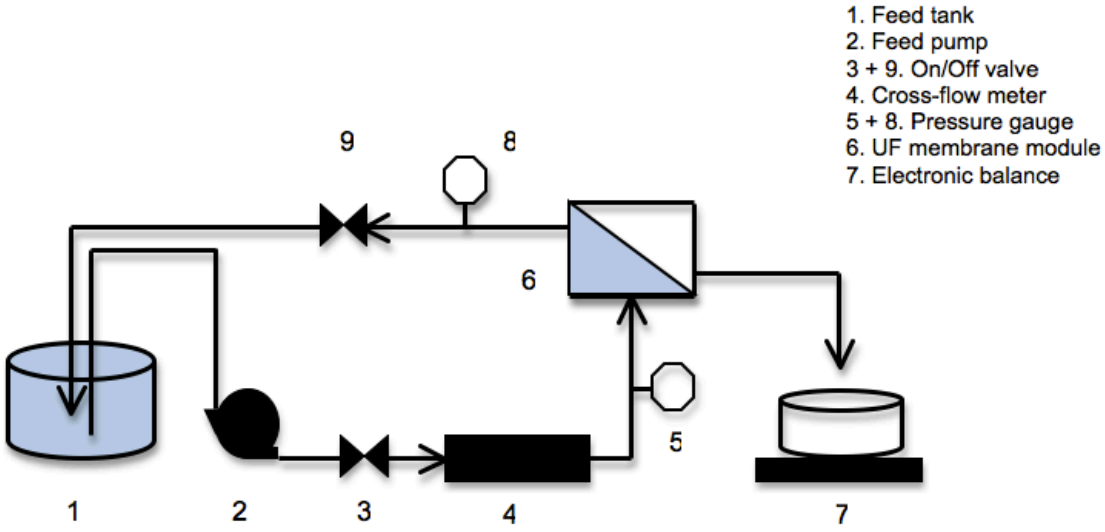

Figure A.3. Cross-flow apparatus used to conduct permeability, flux decline, and flux recovery experiments.

Supporting Information

Appendix B

Materials. Methoxypolyethylene glycol amine MW = 5000 g/mol was purchased from Sigma Aldrich (Milwaukee, WI), Methoxypolyethylene glycol amines MW = 550, 1000 g/mol were purchased from Laysan Bio (Arab, AL), *N*-Hydroxysuccinimidyl 2,3,5,6-tetrafluorobenzoate was prepared according to Keana and Cai.[1] Diethyl ether and methanol was purchased from Fisher Scientific (Pittsburgh, PA). Dow FILMTEC XLE brackish water flat sheet membranes were donated by Dow Water & Processes Solutions (Edina, MN). All materials were used as received.

Membrane Characterization. 3x1 cm membrane coupons used for FT-IR, contact angle measurements, and atomic force microscopy (AFM) were dried before use overnight in a dessicator. The modified and unmodified membranes were characterized with FT-IR on a JASCO FT/IR-6300 spectrometer. Sessile drop contact angle measurements were observed using a Krüss DSA 10 goniometer. AFM was conducted on a Bruker Dimension 5000 scanning probe microscope (in tapping mode) using a silicon tip. The average surface roughness and surface area difference percentage were determined from the surface topography for each sample.

Performance. Performance testing on the RO membranes was conducted in a stainless-steel dead-end filtration stirred cell (Sterlitech Corp., Kent, WA) with an active membrane area of approximately 0.011m^2. The stirred cell was filled with Milli-Q water, and pressurized until water flow through the membrane was first observed. The water flow rate was then recorded using a digital flow meter (FlowCal 5000, Tovatech LLC, South Orange, NJ). The system was continually pressurized at increments of 50 psi (689kPa) up to 400 psi (2758 kPa) while measuring the water flow rate at each increment. The membrane was then allowed to compact at 400 psi until the flow rate stabilized, which took approximately 3 hours for each membrane. The

salt rejection of the membrane was characterized by filling the stirred cell with 2g/L NaCl solution and pressurizing the cell to 200, 300 and 400 psi. Approximately 10 mL of the permeate solution was collected at each pressure and the conductivity was measured using a calibrated conductivity meter (Accumet XL30, Fisher Scientific). The salt rejection, R, was calculated by $R = 1 - c_p/c_b$, where c_p is the permeate concentration and c_b is the bulk feed solution concentration. The pure water permeability was determined as the slope of the linear regression line on the plot of membrane water flux (flow rate normalized by membrane area) against the pressure up to 400 psi after compaction.

PFPA-PEG$_{5000}$: H_2N-PEG_{5000} (750 mg, 0.15 mmol) was dissolved in 10 mL of $CHCl_3$. *N*-Hydroxysuccinimidyl 2,3,5,6-tetrafluorobenzoate (60 mg, 0.18 mmol) was added to solution and the reaction was allowed to stir in the dark overnight at room temperature. The resulting solution was poured into 20 mL of diethyl ether and the product was extracted 3 times with 20 mL DI water. A grey solid product (745 mg, 0.14 mmol, yield: 93%) was obtained via evaporation under reduced pressure and stored in a dessicator in the dark before use. ^{1}H NMR: (CDCl3, 300 MHz) δ= 3.63 (m) ^{19}F NMR: ($CDCl_3$, 300 MHz) δ= -140.94, -150.87. IR: 2876, 2102, 1933, 1460, 1337, 1275, 1233, 1101, 950, 836 cm^{-1}

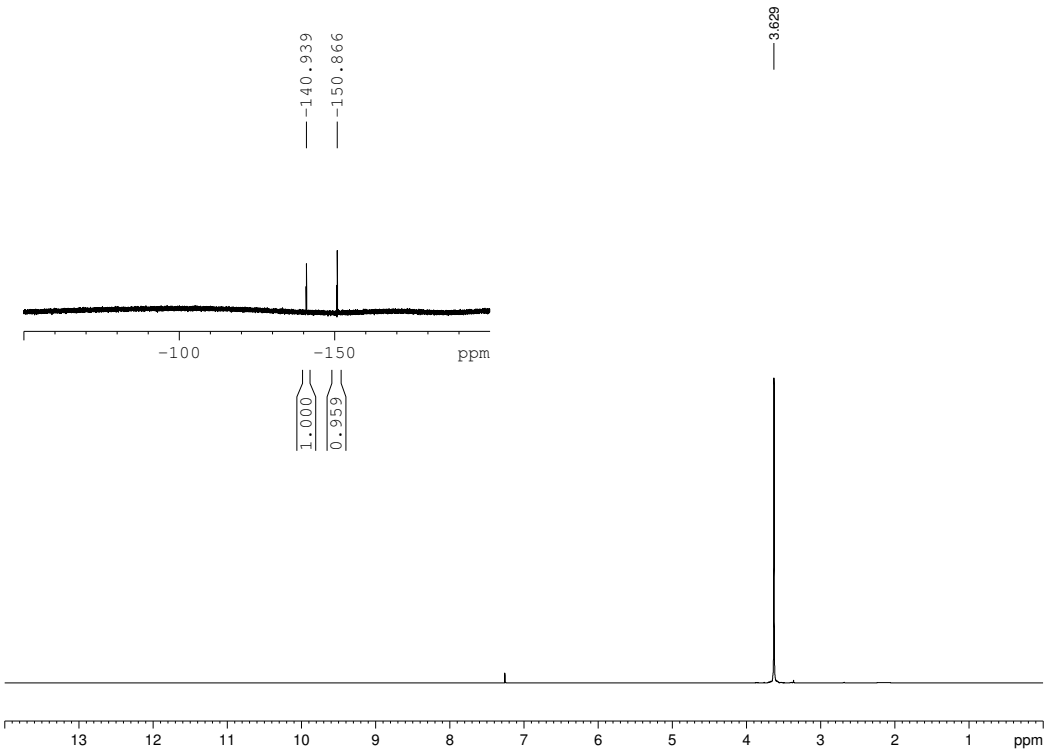

Figure B.1. ^{1}H NMR spectrum of PFPA-PEG5000 (^{19}F NMR Inset).

PFPA-PEG$_{1000}$: H_2N-PEG$_{1000}$ (820 mg, 0.82 mmol) was dissolved in 10 mL of $CHCl_3$. *N*-Hydroxysuccinimidyl 2,3,5,6-tetrafluorobenzoate (302 mg, 0.91 mmol) was added to solution and the reaction was allowed to stir in the dark overnight at room temperature. The resulting solution was poured into 20 mL of diethyl ether and the product was extracted 3 times with 20 mL DI water. A white wax (981 mg, 0.8 mmol, yield: 97%) was obtained via evaporation under reduced pressure and stored in a dessicator in the dark before use. ^{1}H NMR: (CDCl3, 300 MHz) δ= 3.64 (m), 3.38 (s), 2.72 (s) ^{19}F NMR: ($CDCl_3$, 300 MHz) δ= -140.94, -150.87. IR: 2860, 2120, 1714, 1484, 1342, 1276, 1210, 1090, 990, 940, 839 cm^{-1}.

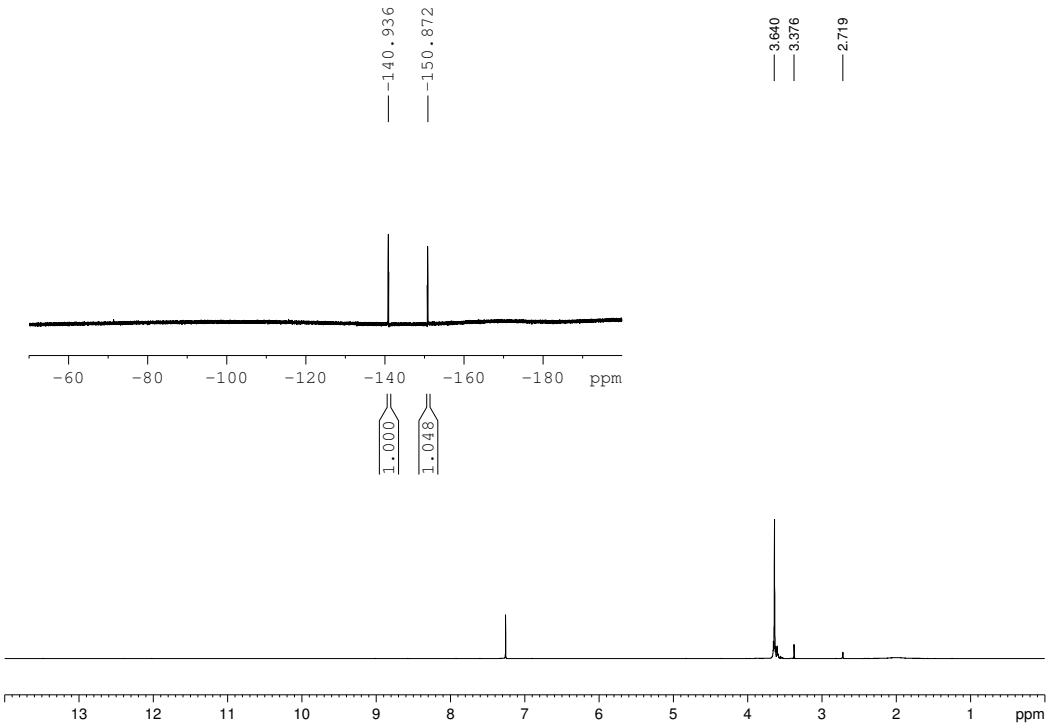

Figure B.2. ^{1}H NMR spectrum of PFPA-PEG1000 (^{19}F NMR Inset).

PFPA-PEG$_{550}$: H_2N-PEG$_{550}$ (270 mg, 0.5 mmol) was dissolved in 5 mL of $CHCl_3$. *N*-Hydroxysuccinimidyl 2,3,5,6-tetrafluorobenzoate (180 mg, 0.54 mmol) was added to solution and the reaction was allowed to stir in the dark overnight at room temperature. The resulting solution was poured into 20 mL of diethyl ether and the product was extracted 3 times with 20 mL DI water. A light yellow oil (373 mg, 0.47 mmol, yield: 94%) was obtained via evaporation under reduced pressure and stored in a dessicator in the dark before use. ^{1}H NMR: (CDCl3, 300 MHz) δ= 3.68 (m), 3.42 (s), 2.77 (s) ^{19}F NMR: ($CDCl_3$, 300 MHz) δ= -140.92, -150.79. IR: 2861, 2122, 1771, 1482, 1316, 1254, 1205, 1085, 988, 821 cm^{-1}.

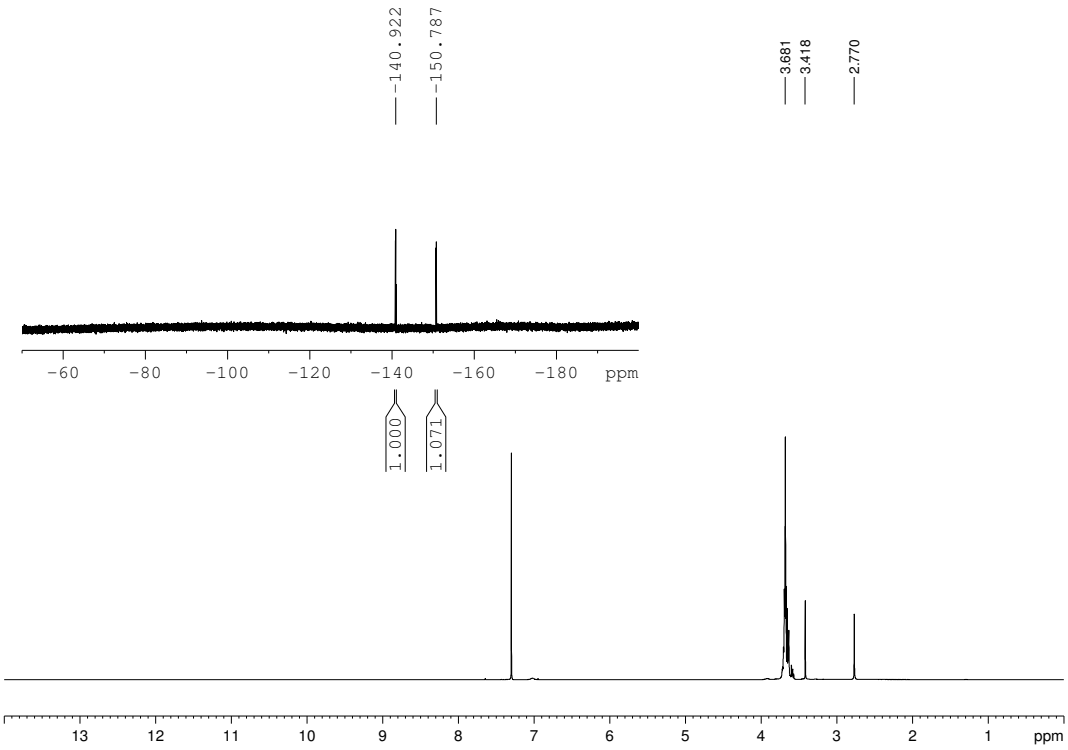

Figure B.3. ^{1}H NMR spectrum of PFPA-PEG550 (^{19}F NMR Inset).

Cell Adhesion Test. Adhesion test were performed for the membranes following a modified procedure reported by Gleason and co-workers.[19] *Escherichia coli* was used as the model bacteria for this test; pure bacterial cell cultures were suspended in Luria-Bertani (LB) broth and grown at 35ºC, shaken at 150 rpm and incubated until mid-exponential phase was reached, at which time cells were harvested by centrifugation at 3800×g for 8 min. Then cells were then resuspended with fresh LB medium to the concentration of $4x10^{7}$ cells/mL. Samples coupons, of approximately 1 cm^{2}, were incubated in this bacterial suspension for 24 hrs at 25 rpm and 35 ºC. The coupons were then removed from the suspension and gently rinsed with fresh LB broth using a Pasteur pipette. Once rinsed, the coupons were immersed in a dye solution (SYTO 9 live/dead Baclight Bacterial Viability Kit L13152, Molecular Probes) for 15 min. The SYTO 9

solution was prepared by dissolving the contents of component A in 30 mL of sterile distillated water. After the staining was complete, the coupons were gently rinsed with fresh LB broth and imaged using a microscope (Olympus BX51 microscope) equipped with a fluorescent lamp and green/red fluorescence filters and a 4x CCD camera attachment (FVIEW-II, Soft Imaging System, USA). Surface coverage estimates were calculated using ImageJ software.

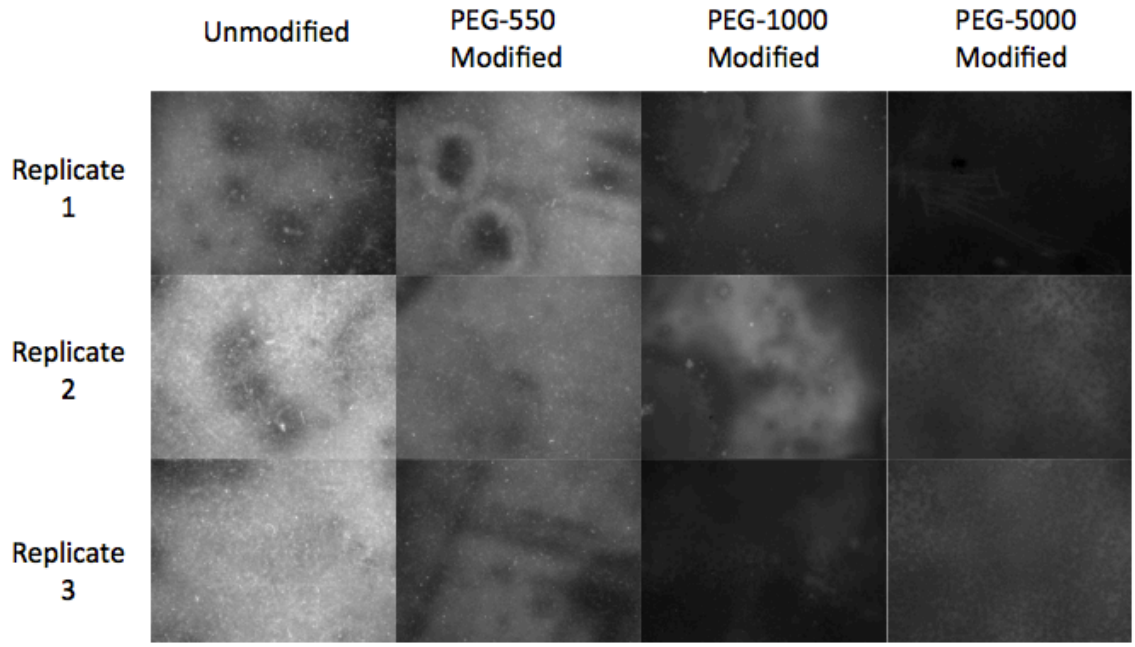

Figure B.4. Fluorescent microscopy images.

Supporting Information

Appendix C

General Procedures. Unless stated otherwise, reactions were performed under an argon atmosphere in flame-dried glassware. Tetrahydrofuran (THF), methylene chloride (CH_2Cl_2), diethyl ether (Et_2O), toluene (C_7H_8), and acetonitrile (CH_3CN) were passed through activated alumina columns prior to use. Chemical reagents were obtained from commercial sources and used without further purification. Reaction temperatures were controlled using an IKA magnetic temperature modulator. Procedures were performed at room temperature (~23 ºC) unless otherwise indicated. Column chromatography was performed on E. Merck silica gel 60 (240-400 mesh). Thin layer chromatography and preparative layer chromatography utilized pre-coated plates from E. Merck (silica gel 60 PF254, 0.25 mm or 0.5 mm).

Instrumentation. Nuclear Magnetic Resonance (NMR) spectra were recorded on either Inova-400 or Bruker-500 spectrometers. ^{1}H, ^{13}C, and ^{19}F NMR chemical shifts are given in parts per million (δ) relative to the internal standard, i.e. tetramethylsilane for ^{1}H and ^{13}C NMR spectra, or trifluoroethanol (-77.03 ppm) for ^{19}F NMR spectra. Electrospray mass spectrometry data were collected with a Waters LCT Premier XE time of flight instrument controlled by MassLynx 4.1 software. Samples were dissolved in methanol and infused using direct loop injection from a Waters Acquity UPLC into the Multi-Mode Ionization source. The flow injection solvent was 50/50 MeOH/MeCN (LCMS Grade, VWR Scientific). The lock mass standard for accurate mass determination was leucine enkephalin (Sigma L9133). UV-vis experiments were performed on a Shimadzu UV-3101PC Spectrophotometer.

Scheme C.1. General Synthesis of Small Molecule PFPAs

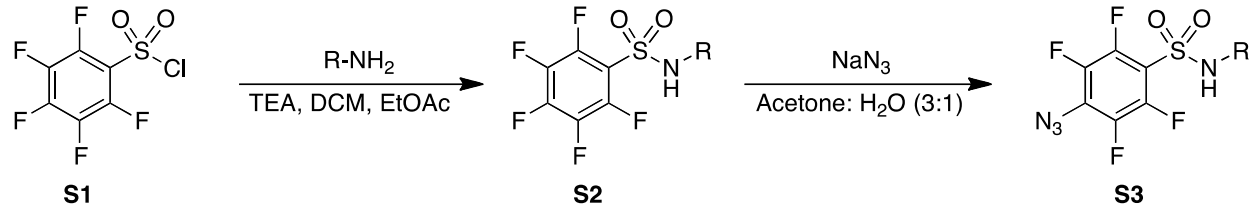

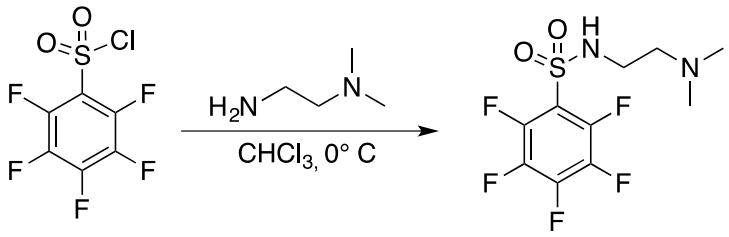

Synthesis of compound 2: *N,N*-dimethylethylenediamine (417 µL, 3.82 mmol, 1 eq) and 520 µL of triethylamine was dissolved in 5 mL of $CHCl_3$ and cooled to 0 ºC in an ice bath. Separately, pentafluorobenzenesulfonyl chloride (1.018 gram, 3.82 mmol, 1 eq) was dissolved in 5 mL $CHCl_3$ and cooled to 0 ºC. The two solutions were slowly combined by adding the solution containing the pentafluorobenzenesulfonyl chloride drop wise to the *N,N*-dimethylethylenediamine solution at 0 ºC. The ice was replaced every 15 minutes for 1 hour. After 1 hour, the reaction was removed from the ice bath and was allowed to stir at room temperature. After 2 hours, the crude mixture was partitioned between $CHCl_3/H_2O$ and washed 3x with DI water. The organic layer was concentrated under reduced pressure to give product **2** **(**875 mg, 72%) as a white solid.

Spectral data: ^{1}H NMR (400 MHz, $CDCl_3$): 2.17 (6H, s), 2.44 (2H, t), 3.19 (2H, t), 5.15 (1H, br s); ^{13}C NMR (100 MHz, $CDCl_3$): 40.6, 44.8, 57.5, 116.7 (m), 137.9 (dm, $^{1}J_{CF}$ = 257.5 Hz), 143.7 (dm, $^{1}J_{CF}$ = 262.0 Hz), 144.5 (dm, $^{1}J_{CF}$ = 257.8 Hz); ^{19}F NMR (375 MHz, $CDCl_3$): -135.2 (2F,

m), -144.8 (1F, m), -157.1 (2F, m); MS (TOF-ESI+): calculated for $C_{10}H_{12}F_5N_2O_2S$ (MH^+): 319.0540; measured: 319.0550.

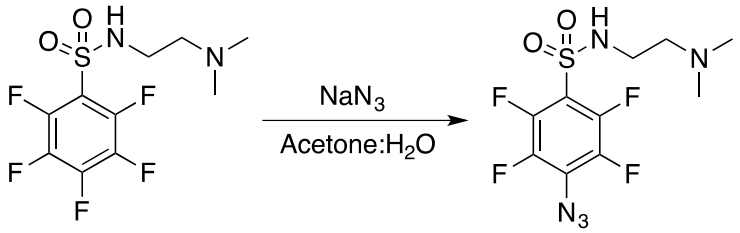

2 **3**

Synthesis of compound 3: To a solution of **2** (711 mg, 2.23 mmol, 1 eq) in an acetone/H_2O mixture (24 mL acetone, 8 mL H_2O) was added 524 mg of sodium azide (524 mg, 8.34 mmol, 3.75 eq). The cloudy reaction mixture was allowed to stir overnight in the dark. The crude mixture was diluted with $CHCl_3$ and partitioned between $CHCl_3$/H_2O, then washed 3x with copious amounts of H_2O. The organic layer was concentrated under reduced pressure to give product **3** (612 mg, 80%) as an off-white solid.

Spectral data: ^{1}H NMR (400 MHz, $CDCl_3$): 2.17 (6H, s), 2.43 (2H, t), 3.17 (2H, t), 5.19 (2H, br s); ^{13}C NMR (100 MHz, $CDCl_3$): 40.5, 44.8, 57.2, 115.9 (m), 124.4 (m), 140.2 (dm, $^1J_{CF}$ = 252.7 Hz), 144.4 (dm, $^1J_{CF}$ = 257.0 Hz); ^{19}F NMR (375 MHz, $CDCl_3$): -138 (2F, m), -149.7 (2F, m); MS (TOF-ESI+): calculated for $C_{10}H_{12}F_4N_5O_2S$ (MH^+): 342.0648; measured: 342.0654; UV–vis (EtOH): λ_{max} = 260 nm.

Synthesis of compound **4a**:

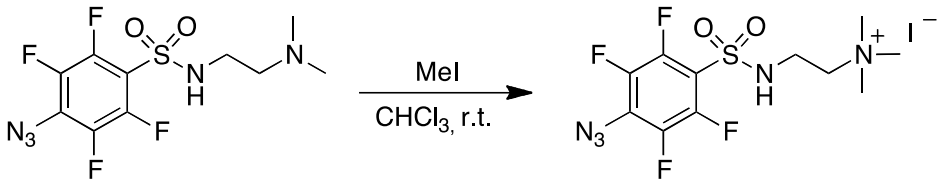

3 **4a**

Synthesis of compound 4a: To a solution of the **3** (300 mg, 0.88 mmol, 1 eq) in $CHCl_3$ (4 mL, 0.2 M) at room temperature was added methyl iodide (110 µL, 1.7 mmol, 2 eq) in one portion. The mixture was allowed to stir overnight at room temperature. In the morning the mixture was concentrated to dryness (bath temperature below 45 ˚C) to give the product **4a** (410 mg, 96%) as an off-white solid.

Spectral data: ^{1}H NMR (500 MHz, DMSO-d_6): 3.10 (9H, s), 3.46 (4H, m), 9.04 (1H, br s); ^{13}C NMR (125 MHz, DMSO-d_6): 36.9, 53.2, 64.2, 114 (m), 124.9 (m), 140.9 (dm, $^{1}J_{CF}$ = 248.5 Hz), 144.0 (dm, $^{1}J_{CF}$ = 253.4 Hz); ^{19}F NMR (375 MHz, DMSO-d6): -147.6 (2F, m), -136.7 (2F, m); MS (TOF-ESI+): calculated for $C_{11}H_{14}F_4N_5O_2S$: 356.0804; measured: 356.0797; UV–vis (H_2O): λ_{max} = 264 nm.

Synthesis of compound **4b**:

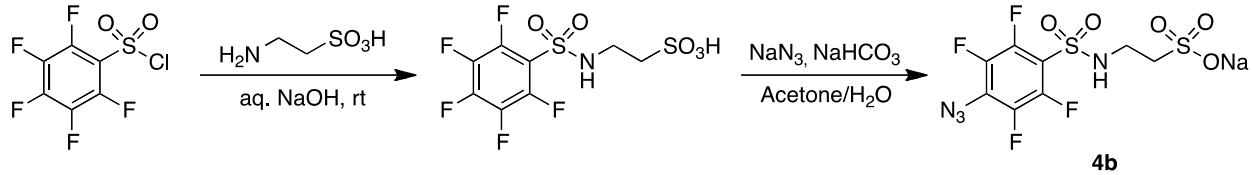

4b

Synthesis of compound 4b: Taurine (426 mg, 3.4 mmol, 1 eq) was added to a round bottom flask and dissolved in water (4 ml, aprox. 1M). 2M NaOH was added to reach a pH of 10-11. Then the sulfonyl chloride (0.55 mL, 3.75 mmol, 1.1 meq) was added in one portion. The

mixture was allowed to stir at room temperature with periodic addition of 2M NaOH to maintain a pH of 10-11. The mixture was allowed to stir overnight. In the morning upon addition of 2M NaOH no pH change occurred over 2 h. Concentrated HCl was added to a pH of 1 and the mix placed in a 0 °C freezer to precipitate. Solids were removed by filtration, washed quickly with ice-water, dissolved in MeOH, concentrated and dried to give the sulfonic acid as a white solid (653 mg, 53%). The sulfonic acid (100 mg, 0.28 mmol, 1 eq) was added to a round bottom flask followed by addition of acetone/water (3:1, 8 mL, 0.05 M). Solid $NaHCO_3$ (24 mg, 0.28 mmol, 1 eq) was added in one portion followed by solid NaN_3 (22 mg, 0.34 mmol, 1.2 eq) in one portion. After stirring overnight the mixture was filtered and the filtrate concentrated to afford the compound **4b** as a white solid (103 mg, 89%).

Spectral data: ^{1}H NMR (500 MHz, DMSO-d_6): 2.55 (2H, m), 3.16 (2H, m), 8.4 (1H, br s); ^{13}C NMR (125 MHz, DMSO-d_6): 51.4, 79.6, 117.0 (m), 123.8 (m), 140.7 (dm, $^1J_{CF}$ = 250.7 Hz), 143.7 (dm, $^1J_{CF}$ = 252.6 Hz); ^{19}F NMR (375 MHz, DMSO-d_6): -150.3 (2F, m), -139.6 (2F, m); MS (TOF-ESI-): calculated for $C_8H_5F_4N_4O_5S_2$: 376.9637; measured: 376.9635; UV–vis (H_2O): λ_{max} = 263 nm.

Synthesis of compound 4c:

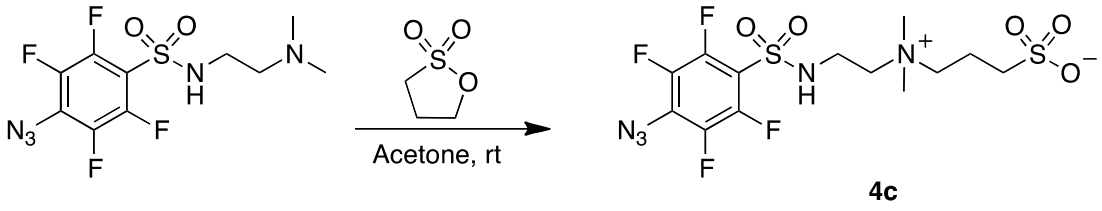

4c

To a solution of the amine (800 mg, 2.3 mmol, 1 eq) in anhydrous acetone (16 mL, 0.15 M) was added 1,3-propane sultone (343 mg, 2.8 mmol, 1.2 eq) in one portion. The mix was allowed to stir overnight in the dark. In the morning the mixture was filtered and the filtrate returned to the

initial reaction vessel, covered and allowed to continue stirring. The filtered product was washed 3x with acetone and dried. This process was repeated 3x over the course of the next 4 days to provide a total of 600 mg (52%) of the product as a white powder after drying under high vacuum.

Spectral data: ^{1}H NMR (500 MHz, DMSO-d_6): 1.96 (2H, m), 2.46 (2H, m), 3.06 (6H, s), 3.45 (6H, m) 9.00 (1H, br s); ^{13}C NMR (125 MHz, DMSO-d_6): 19.3, 36.5, 47.9, 51.0, 61.7, 63.1, 114.8 (m), 125.0 (m), 140.8 (dm. $^{1}J_{CF}$ = 250.8 Hz), 143.9 (dm, $^{1}J_{CF}$ = 254.3 Hz); ^{19}F NMR (375 MHz, DMSO-d_6): -145.4 (2F, m), -134.5 (2F, m); MS (TOF-ESI+): calculated for $C_{13}H_{18}F_4N_5O_5S_2$ (MH^+): 464.0685; measured: 464.0684 ($M+H^+$); UV–vis (H_2O): λ_{max} = 264 nm.

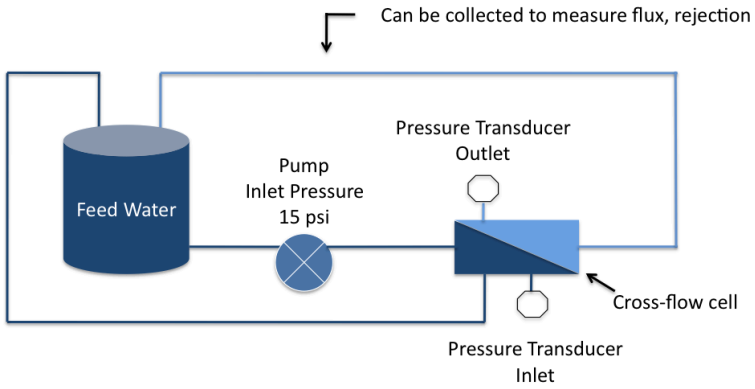

Figure C.1. Lab-built cross-flow system to monitor transmembrane pressure (TMP), flux, and rejection of sodium alginate. The pressure transducers are connected to a computer that simultaneously plots TMP during operation.

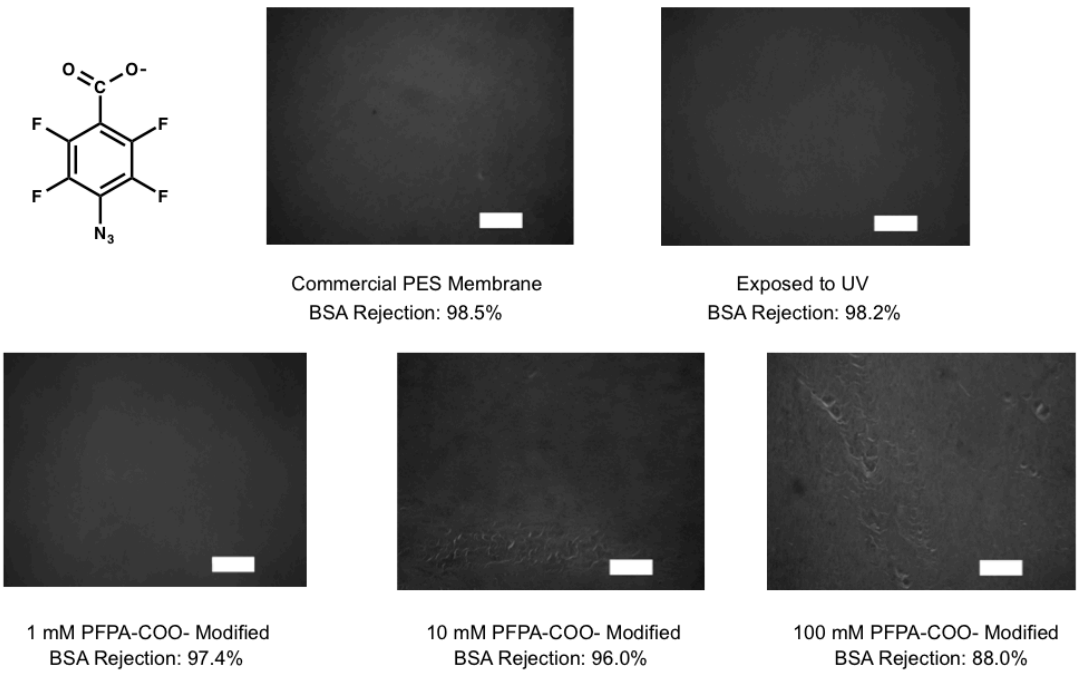

Figure C.2. Optical microscope images demonstrating visible membrane degradation at higher concentrations of a PFPA derivative (scale bar = 100 μm). Rejection of bovine serum albumin (BSA) is shown below each image. The 4-azidotetrafluorobenzoate (PFPA derivative) is shown (upper left) following the synthesized of 4-azidotetrafluorobenzoic acid by Keana *et al.*[2] To impart high water solubility, the benzoic acid was converted to the sodium benzoate by dissolution in an equimolar aqueous solution of NaOH.

Appendices References

(1) Chen, S., Hwang, G., *Macromolecules*. **1996,** 29, 3950-3955

(2) Keana, J. F. W., & Cai, S. X. *The Journal of Organic Chemistry*, **1990,** *55*(11), 3640–3647